University of Washington
Seattle, Washington 98195

DEPARTMENT OF ASTRONOMY
UNIVERSITY OF WASHINGTON

NAG8-433

THE X-RAY PROPERTIES OF HIGH REDSHIFT, OPTICALLY SELECTED QSOs

Scott F. Anderson

A dissertation submitted in partial
fulfillment of the requirements for the degree of
Doctor of Philosophy
University of Washington
1985

University of Washington

Abstract

THE X-RAY PROPERTIES OF HIGH REDSHIFT,
OPTICALLY SELECTED QSOs

by Scott Frederic Anderson

Chairperson of the Supervisory Committee: Professor Bruce Margon

Department of Astronomy

In order to study the X-ray properties of high redshift QSOs, I have taken grism/grens plates covering 17 deg.^{2} of sky previously imaged to very sensitive X-ray flux levels with the *Einstein Observatory*. Following optical selection of the QSO, the archived X-ray image is examined to extract an X-ray flux detection or a sensitive upper limit.

Two samples of grism/grens selected QSOs are emphasized. The first, sample "C", is a $\approx$ 80% complete sample of 37 QSOs with $1.8 \leq z \leq 3.0$, and $B \leq 19.5$. Using two statistical approaches that also incorporate information contained in X-ray non-detections ("survival analysis" and "stacking"), I infer from sample C data that such QSOs contribute < 3% to the diffuse X-ray background (XRB). The contribution of all QSOs with $B \leq 19.5$ to the XRB is found to be 21 ± 8%. Through the use of complete samples, very few uncertain parameters or extrapolations are used in these determinations.

The second sample, sample "N", includes 78 QSOs that occupy a narrow region of redshift (z) and optical luminosity ($L_{\rm opt}$) space. The X-ray to optical luminosity ratio is parameterized by a hypothetical power law slope, α_{ox}, connecting the two wavebands, and is thought to depend on $L_{\rm opt}$ and/or z. Sample N occupies a sufficiently narrow region of $L_{\rm opt}$-z space that ensemble mean parameters such as $\alpha_{ox}^{\rm eff}$ can be directly determined without the need to correct for such dependences. For sample N QSOs ($< z >= 2.1$, $< \log(l_{2500\,\mathring{A}}) >= 31.44$), I find $\alpha_{ox}^{\rm eff} = 1.50 \pm 0.03$ in excellent agreement with the model of Avni and Tananbaum (A-T) for the evolution of $\alpha_{ox}^{\rm eff}$. However, the width found here for the α_{ox} distribution is narrower than that found by A-T; this narrow width potentially resolves some conflicts between inferences derived from X-ray versus optically selected QSOs, but it may also result from an interaction between survival analysis and α_{ox} thresholds.

Combining sample N data with recent QSO optical counts, I show that if $\alpha_{ox}^{\rm eff}$ were independent of $L_{\rm opt}$ and/or z, QSOs probably could not dominate the XRB. However, with the suggested evolution of $\alpha_{ox}^{\rm eff}$, QSOs can contribute $\sim$ 70% to the XRB, the typical contributor being a moderate redshift ($z \approx 1 - 1.5$) QSO with $B \approx 19 - 21$.

TABLE OF CONTENTS

LIST OF TABLES

LIST OF FIGURES

LIST OF PLATES

1. INTRODUCTION AND OVERVIEW

1.1 Introduction

When observed at most wavelengths of the electromagnetic spectrum, the radiant constituents of the Universe are found to be clumped into such objects as stars and galaxies, with the intervening "background" space very dark by comparison. However, there are two regions of the electromagnetic spectrum in which the Universe (at least at current instrumental resolutions and sensitivities) looks very different: at microwave and X-ray wavelengths, the celestial sphere appears uniformly bright, with the intensity of the diffuse backgrounds overwhelming that due to discrete sources such as stars and galaxies. The research of this dissertation has relevance to the origin of the diffuse X-ray background.

The circumstances surrounding the first detection of extrasolar X-rays and the recognition of the existence of a diffuse X-ray background are well known parts of astronomical lore (*e.g.*, the reader is referred to an interesting historical account by Giacconi 1974). With the stated intention of detecting X-radiation from the Moon, in June 1962 a rocket was flown with an X-ray sensitive thin window Geiger counter aboard: it was thought that such X-radiation might arise from either bremsstrahlung interactions of the (then poorly understood) solar wind electrons and the lunar surface, or alternatively from flourescence of solar X-rays on the lunar surface. The Moon was not detected, but an isolated extrasolar source of X-rays (later identified as Sco X-1) was observed, and the presence of a non-zero X-ray flux (not strongly direction dependent) was also noted; this latter isotropic component is now called the cosmic diffuse X-ray background (frequently abbreviated in this thesis as XRB). Results from this experiment were reported by Giacconi *et al.* (1962).

Studies of the diffuse X-ray background (here I mean the background above

an energy of about 1 keV) have shown it to be bright (its energy density exceeds that due to X-ray sources within the Galaxy), and highly isotropic ($\delta I/I < 2\%$ over scales of ~ 25 square degrees: *e.g.*, Shafer 1983, Shafer and Fabian 1983). Its spectrum is well known over a broad energy range from a few to ~ 100 keV, and in the 2–10 keV band fits a thermal bremsstrahlung model quite well (*e.g.*, Marshall *et al.* 1980). These latter two points, high isotropy and spectral shape, have suggested one possible "cosmological" origin for the diffuse XRB. It could arise (see *e.g.*, Field and Perrenod 1977) from a low density but all pervasive hot intergalactic medium filling the Universe with a ~ 500 million degree gas: the temperature can be estimated from the observed X-ray spectrum. Such a low density, highly ionized intergalactic medium would be hard to detect in any other fashion.

Under the assumption that the background arises from a cosmological distribution of matter all-pervasive throughout the Universe, the observed intensity of the background can be used to estimate the energy density in the XRB ($\sim 10^{-36}\,\mathrm{erg/cm^3/sec}$ in the 2–10 keV band: *e.g.*, Schwartz and Gursky 1974). This value can then be equated with the energy density expected from of a hot intergalactic gas emitting X-rays via bremsstrahlung. This bremsstrahlung energy density is proportional to (for a temperature inferred from the X-ray background spectrum) the electron density squared, and thus the density of the intergalactic medium may be estimated. The inferred density, associating one electron with one proton, *i.e.*, a gas of ionized hydrogen, is $n \sim 10^{-6}/\mathrm{cm^3}$, and is quite close to that required to close the Universe. That is, the X-ray background is potentially a signature of a cosmologically significant intergalactic medium. Thus, while the microwave background, widely interpreted as remnant radiation from the big bang, tells us about origins of the Universe, the X-ray background may tell us of its ultimate fate (note,

however, that fluctuations in the X-ray background may also constrain the extent of clumping in the early Universe: *e.g.*, Fabian 1981).

At nearly the same time as that first detection of extrasolar X-rays, however, quasars were (quite independently from X-ray studies) being discovered: during the course of identification of the 3C radio source survey, two "quasistellar" radio sources (3C48 and 3C273) were shown to have broad emission lines in their optical spectra, emission lines showing very substantial redshifts (Schmidt 1963, and Greenstein and Matthews 1963). Having been demonstrated to be be powerful emitters in the optical (assuming the cosmological interpretation of redshifts), the potential for QSOs to be luminous X-ray sources was also soon demonstrated through (again) observations of 3C 273 (Bowyer *et al.* 1970).

One of the most exciting findings of the Einstein Observatory is that many QSOs are powerful X-ray sources (*e.g.*, Tananbaum *et al.* 1979, Ku, Helfand and Lucy 1980, Zamorani *et al.* 1981, and other references in Maccacaro 1984); prior to the launch of Einstein only three QSOs had been detected in X-rays. The inferred X-ray fluxes were such that given the then available very scanty (and, in hindsight, overoptimistic) estimates for the surface densities of QSOs at very faint magnitude limits, it was realized that the superposition of the combined X-ray flux from the QSO population as a whole could easily account for the entire XRB (*e.g.*, Setti and Woltjer 1979, Zamorani *et al.* 1981). Indeed, such considerations even suggested that the optical counts of very faint QSOs must begin to flatten at magnitudes a little fainter than $B = 20$, if the X-ray background were not to be exceeded (*e.g.*, Setti and Woltjer 1979, and Zamorani *et al.* 1981). By now it was clear that the presence of a hot intergalactic medium of closure density was far from firmly established.

Broadly, three approaches are used to investigate the two leading explanations for the origin of the XRB (thermal bremsstrahlung from a hot intergalactic medium, perhaps of cosmological density, and the superposition of point X-ray sources, especially QSOs). One is through investigation of the XRB spectrum (*e.g.*, Marshall *et al.* 1980), with subsequent comparison to the spectra expected from thermal bremsstrahlung and that expected from a superposition of point sources. The second is through fluctuations in the diffuse X-ray background (*e.g.*, Shafer 1983). The third approach is that of this dissertation, to attempt to add up the X-ray flux contribution from discrete sources (QSOs) and compare it to the observed X-ray flux from the XRB.

Initially two approaches were employed to investigate the X-ray properties of QSOs: (1) Einstein observations of heterogenous samples of previously known QSOs (*e.g.*, Tananbaum *et al.* 1979; Ku, Helfand, and Lucy 1980; Zamorani *et al.* 1981), many of which were "famous" because they are rather atypically over-luminous in the optical and/or radio wavebands; and, (2) optical identifications of serendipitous Einstein X-ray sources (*e.g.*, Margon, Downes, and Chanan 1985; Gioia *et al.* 1984; recent review by Maccacarro 1984, and references therein), objects which by selection are necessarily X-ray bright and are at low redshift ($< z > \sim 0.5$).

The former approach is potentially heavily biased towards radio or optically over-luminous objects, and the latter by X-ray bright objects, and/or nearby objects. Given such potential biases, it might be dangerous to infer that the X-ray properties of such objects necessarily can be extrapolated to apply to more typical QSOs as well. Thus, it is important to directly obtain X-ray information on more typical samples of QSOs. Steps forward in this direction have been taken through X-ray observations of optically selected samples by Marshall (1983) and Kriss and

Canizares (1985), Tananbaum *et al.* (1985), and in the current dissertation.

Tananbaum *et al.* (1985) have obtained X-ray observations of 66 of the "PG" or Bright Quasar Survey (BQS) QSOs of Schmidt and Green (1983). Because these objects are quite bright, Tananbaum *et al.* obtained a very large ($\sim$ 86%) fraction of X-ray detections in this sample, and for this reason alone it is an extremely important sample (other optically selected samples commonly have X-ray detection fractions of $< 50\%$). The objects are typically at quite low redshifts ($z < 1$). However, at the time of this writing, data from this sample had not yet been published. It should also be pointed out that the QSOs in this sample, which has a limiting completeness magnitude of $B = 16$, are so rare that they make a negligible contribution to the diffuse X-ray background.

Marshall (1983) obtained deep Einstein X-ray images of fields which contain the "Braccesi Faint" (hereafter, "BF") sample of QSOs (Formiggini *et al.* 1980). The "BF" is a sample of UV-excess selected QSOs and is largely complete to $B < 19.8$ and $z < 2.2$; the sample has a modest mean redshift of $< z >= 1.1$. Both the PG and BF samples (based on color selection criterion) are incomplete at redshifts > 2.2.

Kriss and Canizares (1985) similarly obtained deep X-ray images of two fields in which Hoag and Smith (1977) and Sramek and Weedman (1978) had previously grism selected 22 QSOs, most at high redshift ($z > 1.8$, where $L\alpha$ falls onto the F or J-emulsion). For X-ray observing efficiency, the particular grism fields chosen were ones rich not only in the surface density of grism selected QSOs, but also having a high fraction of optically bright QSOs (when compared with the entire grism samples). Unfortunately, such special qualities of these fields prohibit consideration of these objects as a complete sample.

Thus, although there is currently extensive X-ray information on fairly typical QSOs at low to moderate redshifts, prior to this study such a data base did not exist for a complete sample of high redshift QSOs. This is one of the primary motivations for the research of this dissertation. Complete samples can be used in with very few additional assumptions to estimate the contribution of such QSOs to the XRB, and I do so for high redshift QSOs ($B \leq 19.5$, $1.8 \leq z \leq 3.0$) in this dissertation.

Luminosity correlations have been found between X-ray emission and that in other wavebands. For example, it is widely held that radio bright QSOs emit (for a given optical luminosity) about three times as much in X-rays as do their radio quiet counterparts (*e.g.*, Zamorani *et al.* 1981, Tananbaum *et al.* 1983). Further, it has been generally established that within the data analyzed thus far, there is strong evidence for a nonlinear relation between X-ray luminosity and optical luminosity (*e.g.*, Avni and Tananbaum 1982, Reichert *et al.* 1982, Zamorani 1983, Kriss and Canizares 1985), although observational selection works so that it is difficult to distinguish between luminosity and redshift dependences within some samples. The sense of this relation is that in terms of luminosities, roughly $L_x \propto L_{opt}^{\gamma}$ with $\gamma \approx 0.7$. Generally, this relation has been expressed in terms of a parameter α_{ox} which is related to the ratio of X-ray to optical luminosity (and therefore can be determined independent of cosmology). Whether or not this relationship is physical (*e.g.*, Tucker 1983, Shull 1983, Netzer 1985), or a spurious correlation due to joint observational threshold effects in the optical and X-ray (Chanan 1983), remains controversial, and this point will also be investigated here.

Because of such correlations with L_{opt} and/or redshift, such parameters as the mean ratio of X-ray to optical luminosity, $< L_x/L_{opt} >$, for a sample of QSOs or the distribution of luminosity ratios, are directly interpretable quantities only for a

sample that occupies a narrow region of optical luminosity and/or redshift space. That is, in samples that have a wide range of optical luminosity and/or redshift, one must apply the proper corrections for such dependences in order to get at the intrinsic underlying distribution. With a sample that includes only a narrow range of these parameters, such corrections are not needed (or are small), and thus such a sample can be used to test the viability of models for these dependences. This is a second primary motivation for this dissertation. The optical selection technique employed here (grism selection) is well suited for obtaining such a narrow sample of objects: in particular, the technique is highly efficient at selecting out QSOs in the redshift range of $1.8 < z < 2.5$, and at $B \sim 19.5$ (so that many objects also have comparable optical luminosities). No other such large ("narrow") sample of optically selected QSOs with X-ray information is currently available.

1.2. Overview of This Dissertation

As noted above, the dependence of QSO X-ray luminosity on such other parameters as optical luminosity is relevant to studies of QSO physics as well as to the contribution of QSOs to the diffuse cosmic X-ray background radiation. Although there have been many previous X-ray studies of QSOs , the X-ray properties of typical high redshift QSOs have been largely unstudied.

In order to probe the X-ray properties of high redshift QSOs, I have, in an "after the fact" fashion, taken grism/grens plates covering $\sim$ 17 sq. deg. of sky which were previously imaged to very sensitive X-ray flux levels with the Imaging Proportional Counter on the Einstein Observatory. Grism/grens selection is a highly efficient manner in which to optically select high redshift QSOs, and I have used this technique to obtain a largely (> 80%) complete sample of QSOs to $B \leq 19.5$ and for $1.8 \leq z \leq 3.0$, as well as a sample of high redshift QSOs which occupy

narrow regions in redshift and optical luminosity space. Following optical selection, the appropriate X-ray image is examined ("after the fact") to obtain an X-ray flux detection, or more frequently a sensitive X-ray flux upper limit.

The current approach should be contrasted with studies aimed at the optical identification of serendipitous X-ray sources (*e.g.*, Margon, Downes, and Chanan 198?, Gioia *et al.* 1984). In the latter approach, the X-ray image is first examined for X-ray sources that happen by serendipity to lie within the field of view of the X-ray image, and then such sources are subsequently optically identified (frequently with a low redshift, low luminosity QSO), forming an X-ray selected sample of objects. In the current approach, however, I proceed from the optical to the X-ray data, and thus my grism/grens selected samples have no *a priori* X-ray biases, while it is clear that X-ray selection (proceeding from the X-ray to the optical) can find only those QSOs which are in fact strong X-ray sources. Because my sample is X-ray unbiased, it would, for example, be sensitive to "X-ray quiet" QSOs if indeed such a population exists.

The archived *Einstein* X-ray data used includes the roughly 50 Image Proportional Counter fields (and a few High Resolution Imager fields) with the longest integration times (> 10,000 sec) that are also at high galactic latitude ($|b^{II}| > 20°$). The new optical data (obtained at the 4m-class telescopes at CTIO, KPNO, and CFHT) include at least one "blue-grism/grens" plate on a baked IIIaF emulsion centered on each of these same deep X-ray fields. In this fashion, I have optically selected more than 400 previously uncataloged QSO candidates for which the most sensitive available X-ray flux information is already extant. In this thesis I will concentrate on a subsample ($\sim$ 90 objects) of this larger data base, where grism/grens selection is highly efficient and reliable.

A general outline of the organization of this thesis is as follows: In Chapter 3, details are given on the optical selection of the high redshift QSOs whose X-ray properties are to be studied in subsequent chapters. Keeping in mind the motivations discussed above, I have defined two optical samples: a complete sample, and a narrow sample. Chapter 3 presents a discussion of the X-ray flux data for the optically selected QSOs of Chapter 2. Because many of the optically selected QSOs are not detected in X-rays, it is necessary to use techniques that can incorporate information contained in X-ray non-detections as well as that contained in X-ray detections; two such techniques and some cautions about their use are presented in Chapter 4. Finally, with X-ray information available, the optically selected high redshift QSOs are employed in Chapter 5 to investigate the ensemble X-ray properties (*e.g.*, contribution to the diffuse X-ray background, luminosity correlations) of high redshift QSOs, and the QSO population in general.

Each chapter ends with a summary of important results. The reader might first want to skim through these for a more complete overview of the investigations conducted in the course of this dissertation.

2. THE OPTICAL SAMPLE OF QSOS

In the last chapter I discussed the need for obtaining more typical (or better yet, complete) optically selected samples of QSOs with X-ray information available. In particular, I noted that complete samples were particularly lacking at high redshift, and also that currently there are no such samples which occupy a sufficiently narrow region of optical luminosity and redshift space to test in a model independent fashion the proposed nonlinear dependence of X-ray luminosity on optical luminosity (*e.g.*, Avni and Tananbaum 1982).

Grism/grens selection is a highly efficient method for optically selecting high redshift QSOs, and also for selecting a sample occupying a narrow range of optical luminosity and redshift space, and will be the technique employed here to obtain such samples.

This chapter is concerned primarily with the optical definition and characterization of two grism/grens selected samples of high redshift QSOs. The 90 objects in these two samples are a subset of a larger data base of 400 grism/grens selected QSO candidates discoverved in the course of this thesis; these 90 QSOs occupy regions of optical luminosity/redshift space where grism/grens selection is highly efficient. The archived X-ray data applicable to these objects and to be employed in later chapters includes about 55 *Einstein Observatory* fields (50 taken with the Image Proportional Counter and 5 with the High Resolution Imager), with very long integration times (see Chapter 3), which are also at high galactic latitude ($|b^{II}| > 20^{\circ}$). The new *grism* plates were obtained at prime focus at the 4m telescopes at Kitt Peak National Observatory (KPNO) and Cerro Tololo Interamerican Observatory (CTIO), and the new *grens* plates at the 3.6m Canada-France-Hawaii Telescope (CFHT); these plates are centered on the 55 deep *Einstein* fields. This

chapter begins with a brief introduction to the techniques of slitless spectroscopy; for a more complete discussion, the reader is referred to several excellent reviews by Malcolm Smith: Smith (1978), Smith (1981), Smith (1982), Smith (1983).

2.1 Grisms and the Grens

The grisms and the grens are similar instrumental solutions to obtaining low dispersion (≈ 1000 Å/mm) spectra of all objects in a wide field of a large telescope. These instruments are particularly well suited to discovery surveys for strong emission line QSOs (*e.g.*, Hoag and Smith 1977; Sramek and Weedman 1978; Koo and Kron 1980; Crampton, Schade, and Cowley 1985). For a 4m class telescope, there would be obvious difficulties in constructing a sufficiently large objective prism; the largest current objective prisms (*e.g.*, on the U. K. Schmidt.) are $\sim$ 1 meter in diameter. Alternatively, placing a solitary grating inside the converging beam of a fairly fast telescope (f2.7 and f4.2, at the prime foci of, respectively, the 4m's and the CFHT), introduces considerable coma into the resulting spectra (di Francia, 1949). In order to correct for this coma, the transmission *grating* is coupled either with a *prism* to create a *grism* (Hoag and Schroeder 1970, Bowen and Vaughn 1973, Buchroeder 1974), or with a wedged *lens* to create a *grens* (Fourere *et al.* 1982); the coma introduced by the wedged prism or lens cancels that introduced by the transmission grating. For the grisms, the prism is quartz, and the grating has 150 grooves/mm. In the case of the CFHT, the glass lens is also the same optical element which serves as the telescope's wide field corrector, and the 43 g/mm grating is replicated on its final (flat) surface.

For all objects in the field simultaneously, the grisms/grens transmits a zero-order image object (slightly dispersed by the wedged prism or lens), as well as disperses the light into several higher order spectra symmetrically positioned about

this zero order image. The blaze (and hence most of the light) falls into one of the first order spectra. The reciprocal linear dispersion (*e.g.*, in Å mm) is approximately constant over the wavelength coverage of each individual spectrum, and this allows relatively simple direct estimation (to a typical accuracy of ± 100 Å) of wavelengths of spectral features; one simply measures the displacement of the spectral feature from the zero-order image in (for example) millimeters and then converts to wavelength using the linear reciprocal dispersion. However, there is a small ($\leq 1\%$) linear variation in the plate scale and reciprocal dispersion across the plate in the direction of dispersion (caused by the introduction of the wedged prism/lens); this change can be accounted for by measuring in millimeters (as a function of plate position) the displacement between the zero order image and the red emulsion cutoff in the first order spectra. To push to the desired faint optical limits needed in the current application, the spectra are not (at least purposefully!) trailed.

The field of view of the grisms (CTIO and KPNO) are about $34' \times 34'$, and they employ a square (in cross-section) prism/grating combination which gives good images (spectra) over almost the entire field. The CFHT grens field is about $54' \times 54'$ (the field is actually round, but the photographic plate is square); however, there is considerable degradation of image quality near the field edges, and combined with vignetting, and guide and calibration probe obscuration also near the field edges, the grens plates have an effective useful area of order 0.5 sq. deg. (*e.g.*, Weedman 1985a; Crampton, Schade, and Cowley 1985). Such optical fields of view are ideally matched to those of the Einstein X-ray images: for the IPC, the field is $\approx 1^\circ \times 1^\circ$ (but with $38' \times 38'$ inside the "ribs"), and it is $27' \times 27'$ for the HRI. The grism and grens plate scales are, respectively, 18.5"/mm and 13.6"/mm.

At both KPNO and CTIO there are two grisms available, each with reciprocal

dispersion of order 1500 Å/mm: the choices are a "blue grism" with blaze at 3550 Å, and a "red grism" with blaze at ≈ 6000 Å. At the CFHT, the grens of choice was the "blue grens" with blaze at 4300 Å and reciprocal dispersion of 1000 Å/mm; a green grens with dispersion 2000 Å/mm and blaze at 5000 Åis also available on the CFHT. The blue grens was chosen over the green grens for two reasons: (1) the blue grens more closely matches the blue grism in its wavelength response; and, (2) for the available limiting X-ray sensitivities, QSOs optically fainter than those reachable with the blue grens will not have very interesting (i.e., sensitive) X-ray flux limits or detections, and so for this study the higher dispersion of the blue grens is, by far, the more desirable feature than the capability of the green grens to push to fainter limiting magnitudes.

2.2 Grism/Grens Photographic Plates

For the wide field coverage (≈ 1 sq. deg.) needed here, photographic plates must serve as the detectors. Many possible choices of grism/grens and emulsion combinations are possible. The most commonly used emulsions in previous grism/grens surveys have been the fine grained emulsions: IIIaJ, IIIaF, and IV-N (with the overwhelming majority of the plates taken on the two former emulsions). For each of the 55 fields, I took a IIIaF+blue grism (or grens) plate combination as the primary plate for selection of the QSO sample. The desirability of obtaining redshifts directly from the plate material was a primary motivation for choosing the IIIaF (with its wide wavelength coverage of 3200 Å-6900 Å) rather than the the IIIaJ emulsion (with its more limited coverage of 3200-5500 Å). A second motivation for this choice is the availability of a detailed quantitative analysis of factors affecting limiting completeness magnitudes for the blue grism+IIIaF combination (Clowes 1981). Plate I shows a portion of one of the new IIIaF+blue grism plates, high-

lighting a discovery spectrum of a high redshift QSO. Flagged are the zero-order image, the corresponding first-order spectrum, and a prominent emission features (Lα at $z = 2.4$). The price paid for using the IIIaF emulsion is that it has (compared with the IIIaJ emulsion) a very non-uniform response as a function of wavelength, especially redward of 4800 Å, creating peaks which can mimic emission lines; note, for example the ≈ 6800 Å sensitivity peak in the spectra of stars in Plate I. However, these response irregularities appear in all spectra at the same wavelength, and it is relatively easy to guard against their spurious identification as lines by careful measurement of the wavelength of the putative features.

The blue-blazed grism/grens are, of course, less sensitive toward the red end of the spectrum, and so to extend sensitivity to redder wavelengths, I also took red grism plates on either a IIIaF emulsion (once again, 3200 Å-6900 Å) or on a IV-N emulsion (wavelength coverage of 6100-8900 Åwith a blue-cut Wratten 29 filter) whenever time permitted. Thus, for about 20 of these fields I have not only a blue grism plate, but also a red grism plate. In order to maintain as uniform a sample as possible for the current study, these red grism plates are (for the bulk of this study) used only as additional confirmation of the candidate as a QSO, or to confirm the redshift, but not for selection; however, both these sorts of red grism plates have applications to searches for very high redshift QSOs ($z \geq 3.0$) (*e.g.*, Osmer 1982; and Koo and Kron 1980) , and such candidates selected from these plates will be discussed in future publications. Typically, sky-limited exposures are ≈ 45 – 60 min on the IIIaF plates baked in forming gas, and reach a limiting continuum magnitude of B ≈ 21.0; exposure times are typically 60-90 min on the IV-N plates hypersensitized in silver nitrate, and reach a similar limiting magnitude in V

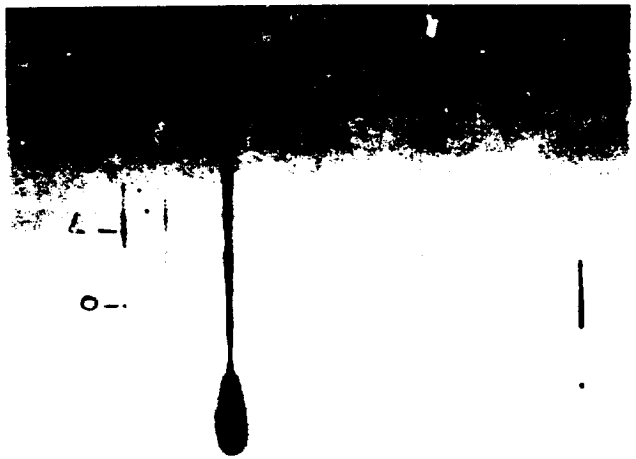

Plate I. Portion of new IIIaF blue grism plate, highlighting a discovery spectrum of a high redshift ($z = 2.4$) QSO. Flagged are the zero-order image, "O", and a strong emission line "L" ($z = 2.4$ if Lyman-α).

2.3 Selection of QSO candidates

The plates are scanned visually using a binocular microscope (typically at 7X magnification), and an "underlay" grid to systematize the search. To B$\approx$ 21, there are $\sim$ 1000 objects on each plate. Both emission line QSO candidates (the main thrust of this paper) and UV excess objects are searched for, and in the $\approx$ 17 sq. deg. (effective area) of sky surveyed approximately 400 QSO candidates were selected from these plates.

To insure thoroughness, each plate was searched several times at separate sessions. Table 2.3.a lists the 44 previously known QSOs/AGN from the catalog of Veron-Cetty and Veron (1985) which lie within the area surveyed by my new high quality plates (all grens plates, and 38 grism fields), and which have B> 17.0: brighter than this, spectra on the plates are normally overexposed, and only *extremely* strong features are detectable.

Many of these previously known QSOs are the famous QSOs which were the *Einstein* targets, and others are earlier X-ray serendipitous source identifications. Objects recovered in my search of the plates have an entry in the first column ("OBJECT") as well as in the second. Twenty-nine objects (from this list of 44) were successfully recovered in "double blind" fashion, while searching the plates. Almost all the "failures-to-recover" are QSOs/AGN at low redshift ($z < 1.8$) and/or very faint (B$\geq$ 20.5). A typical (observed) limiting continuum magnitude for a blue grism+IIIaF plate taken at the 4m in better than 2″ seeing is B$\approx$ 20.5 (*e.g.*, Clowes, 1981). For the 30 previously known objects (of *all* redshifts) listed in Table 2.3.a which are brighter than this limiting magnitude of B< 20.5 (assuming, B-V$\geq$ 0.3 for the objects with no B magnitude estimates), only eight, or 27%, were not recovered in my search of the plates.

Table 2.3.a Previously known QSOs in Grism/Grens Fields with High Quality Plates

OBJECT	PREVIOUS NAME	B	V	U-B	Z
$z > 1.8$:					
Obj. 5	1 E 0438 − 166	18.0	17.65		1.96
09385 + 119	0938 + 119	20.3	19.5	3.19	
12071 + 398	1207 + 39W3	19.65	19.4	−0.12	2.334
12079 + 397	1207 + 39W4	20.87	20.3	−0.77	1.84?
12333 + 260	WEE 58	20.6	20.5		2.04
	WEE 59		21.0		2.09
	WEE 72		21.6		2.30
12354 + 264	WEE 73	19.4	20.2		2.50
16010 + 182	1601 + 182	20.1		3.28	
16017 + 184	1601 + 184	19.1		1.94	
21204 + 168	3C432	18.18	17.96		1.805
$z < 1.8$:					
0044 − 209	PHL 6625	18.6	18.8		0.380
0111 − 015	1 E01119 − 015		19.2		0.120
	1E01129 − 017		20.3		0.284
0112 − 017	PKS 0112 − 017		17.4		1.365
0307 + 169	3C 79.0	19.54	18.75	−0.27	0.256
	1 E 0438 − 165	20.0	19.8		0.5
0833 + 654	3C 204.0	18.76	18.21	−0.99	1.112
0835 + 580	3C 205.0	18.10	17.62	−0.48	1.534
	1 E08386 + 134		19.6		0.723
0849 + 287	B2 0849 + 28		20.5		1.273
	1 E08492 + 284		20.5		0.209
	1E08498 + 283		18.5		0.197
	1 E08500 + 284		20.0		1.273
0850 + 284	1 E08502 + 284		17.7		0.922
0903 + 169	3C 215.0	18.48	18.27	−0.66	0.411
0937 + 118	1 E09378 + 118		18.6		0.783
1018 + 201	1 E1018 + 2010		18.54		0.250
1227 + 024	1 E 1227 + 024			0.5	
	U 1229 + 115		18.5		1.027
1234 + 262	WEE 67		20.2		0.02
1234 + 262	WEE 68		20.4		1.55
	3C 295#52		20.2		0.467
	3C 295#48		20.2		0.461
1409 + 574	3C 296#6		20.31		0.473
1415 + 252	1 E14150 + 252		20.5		1.057
	1 E14151 + 254		20.0		0.560
1416 + 254	1 E1416 + 254		18.7		0.674
	3C 318.0	21.93	20.9		0.752
1614 + 055	1 E16148 + 055		18.47		0.855
1726 + 499	EX 1726 + 499	18.7	19.3		0.815
	PKS 1756 + 237		18.0		1.721

	1 E2125 − 1456	18.13	0.304
2141 + 039	1 E 1416 + 040	19.2	0.410

Notes to Table 2.3.a:

(1) References to individual objects may be found in Veron-Cetty and Veron (1985), except for 0044 − 209 = PHL 6625 which is from Margon, Downes, and Chanan 1985, *Ap. J. Suppl.*, 59, 23.

(2) Two digits to the right of the decimal point in the magnitude columns generally implies that the quoted values are more reliable.

(3) Objects with an entry in the column "Object" are those recovered in double blind fasion from the new grism/grens plates. Objects with no entry in this column were "missed".

More importantly, in the redshift regime where grism/grens selection is most successful ($z \geq 1.8$) the search technique proved even more efficient. Such previously known, high redshift objects are listed as the first 11 entries in the Table. Seven of these have B< 20.5; *all* seven were not only recovered in a double blind search of the plates, but also were correctly assigned the proper redshift. However, the four very faintest (B≥ 20.5) high redshift objects were not completely recovered: Wee 58, Wee 59, Wee 72, and 1207.9 + 3945. The two objects Wee 58 and 1207.9 + 3945 were nevertheless recovered in my sample as UV excess selected QSOs, but not correctly interpreted as "Lyman-α" QSOs. An additional complication in assessing the significance of the "missing" 1207.9 + 3945 is that the strength of its lines may well be highly variable: lines of MgII, CIV and CIII were detected by Arp, but not seen later by Stocke *et al.* (1983); indeed this AGN sometimes has been classified as a BL Lac (Veron-Cetty and Veron 1985). The two high redshift objects completely missed, Wee 59 and Wee 72, are very faint (B> 21) QSOs discovered by Weedman (1985a) using the more sensitive green grens. It is to be emphasized that all four of these "missed" objects are considerably fainter than the completeness magnitude (B= 19.5) for which I will argue below. And, the ($\approx$ 100%) success with which the high redshift objects of Table 2.3.a to B< 20.5 were recovered, provides considerable confidence in the thoroughness of the search technique, to $\approx$ 1 magnitude fainter than this limit. The question of "completeness" as distinct from "thoroughness" is addressed below in section 2.3.2.1.

The previously known QSOs that are the targets of the some of the Einstein X-ray images, will be excluded (even if successfully recovered) from the optically selected samples to be defined below. This is necessary to avoid potential X-ray biases of the sort discussed in Chapter 1.

A problem commonly encountered in searching grism/grens plates is that of spectral overlap: the zero-order image of object B overlaps the first order spectrum of object A, and the zero-order image from B is spuriously interpreted as an emission line in spectrum A. At surface densities of objects on the plate, $\approx$ 1/sq. arc min., a few percent of the spectra will be affected by overlap. Overlap of this sort is easy to decipher on the grism/grens plate when the spectrum of object B is prominent. To avoid spurious identification of such overlaps as emission features when the spectrum of object B is not so prominent, a careful comparison is made between the grism/grens plate and the Palomar Observatory Sky Survey (hereafter, the "POSS"); one looks for any evidence of the presence of object B on the POSS at the location of the putative line feature in A. Further, in fields with more than a single plate, it was often the case that a subsequent plate was purposefully taken with the dispersion direction perpendicular to that of a previous plate; this is an excellent way to guard against overlap, since the putative feature will not appear in the spectrum of A on both plates if indeed it is due to spurious overlap.

2.3.1 The UV Excess Selected Sample

Searches for ultraviolet excess objects from U and B direct plates have proved an effective way of finding QSOs at low to moderate redshifts (*e.g.*, Formiggini *et al.* 1980; Marshall *et al.* 1984); above z= 2.2, Lα is redshifted into the B band, and hence higher redshift QSOs fail to show an ultraviolet excess in U-B. The blue grism/grens plates are suitable not only for selecting out emission line QSOs, but also for selecting out such UV excess objects which do not also show emission lines (see, *e.g.*, Crampton, Schade, and Cowley 1985; Weedman 1985b). However, this generally is done (and this shortcoming is also true for my sample) in an extremely unquantitative fashion, relying mainly on the judgment of the eye of the person

scanning the plate to determine whether or not an object has an ultraviolet excess. Obviously, such QSO candidates do not in any way constitute an *a priori* complete sample of UV-excess selected QSOs, although some observers (*e.g.*, Weedman 1985b) are able to establish *a posteriori* completion estimates. Further, all such objects lacking strong emission features must be followed up with slit spectroscopy before they can be confidently classified as QSOs.

In examining my plates, I have found 180 QSO candidates which have strong UV excess (UVX), but which lack any strong emission features. Marshall *et al.* (1984) in their spectroscopic follow up the "Bracessi faint" (Formiggini *et al.* 1980) sample, have found that $\approx$ 50% of the UV excess selected candidates to B= 19.2, and nearly 100% in the range 19.2 to 19.8 are subsequently confirmed to be QSOs. In my sample, I find, 100 QSO candidates to B$\leq$ 19.2 which are UV excess selected and lack strong emission lines; I find an additional 50 such candidates in the range B= 19.2 to 19.8, and yet another 30 at still fainter magnitudes. Assuming the above selection efficiency of 50% to B= 19.2, and keeping track of the low redshift QSOs ($z<$ 2.2) which *do* have emission lines detectable on the grism/grens plates, I estimate that $\approx$ 40 of the UV excess selected candidates to B$\leq$ 19.2 are indeed QSOs. Then to B$\leq$ 19.8 there should be $\approx$ 90 UVX selected candidates in my sample which are actually QSOs. With the addition of a few more QSOs from the UVX candidates fainter than B= 19.8, I therefore roughly estimate that $\approx$ 100 of the 180 UV excess selected candidates are indeed low redshift QSOs at $z<$ 1.8; fewer than 10 of these are rediscoveries of the Einstein target QSOs.

Further confirmation that $\approx$ 100 of these UV excess selected candidates are likely to be low redshift QSOs is the following: 50 of my UV excess QSO candidates are probably (based on positional coincidence) the optical identifications of Einstein

serendipitous X-ray sources. The X-ray study of the Braccesi faint sample by Marshall (1983), yielded an X-ray detection rate of $\approx$ 50% to B$<$ 19.8. Thus, for the X-ray sensitivities available for my sample (which are comparable to those available for the Braccesi sample) it is not inconsistent to expect $\sim$ 50 X-ray detections from a sample of $\sim$ 100 UV excess selected QSOs to B$\leq$ 20.

Comparison of the surface density counts of UV excess selected QSOs from *e.g.*, the Bracessi sample, shows that there is probably significant ($>$ 60%) incompleteness in my sample for UV excess selected objects to B$\leq$ 19.8. However, similar arguments to B$\leq$ 19.2, suggest that my UV excess selected sample might be as much as 80% complete. At the bright end there are too many objects (by a factor of $\approx$ 5 - 10 at B= 17.0) in my candidate list when compared with other surface density estimates for bright UV excess QSOs. The main sorts of objects likely to be contaminating the bright end of the UV excess selected sample are white dwarfs, subdwarf O stars, etc. Indeed, I have taken slit spectra at the KPNO 84" with the Intensified Image Disector Scanner (IIDS) of several of the brightest such objects, and these in fact turned out to be white dwarfs.

It is likely that future spectroscopic follow up of my new UV-excess selected sample will yield an additional $\sim$ 100 (most, previously uncatalogued) optically selected QSOs with very sensitive X-ray information available, and with $\sim$ 50 objects detected in X-rays. Although such a sample would be very incomplete, it nevertheless potentially provides an additional large optically selected sample of QSOs for studying the X-ray conditional luminosity function (*i.e.*, the dependence of QSO X-ray luminosity on redshift and optical luminosity: Avni and Tanabaum 1982). However, pending follow up spectroscopy these UV excess objects must be de-emphasized in the present study.

2.3.2 The Emission Line Candidates

There are, however, redshift and magnitude regimes where grism/grens selection is quite efficient and the plates themselves can, with reasonable confidence be used (at least in a statistical sense) to classify the candidates as QSOs, and estimate redshifts. From this high efficiency redshift/magnitude regime I have established two emission line selected samples which will be used in subsequent chapters to investigate the X-ray properties of high redshift optically selected QSOs.

The efficiency with which emission line objects are selected from grism/grens plates depends strongly on the intrinsic strength of the emission line under scrutiny and the seeing, as well as on the continuum magnitude. The dependence on intrinsic line strength highly favors the selection of "Lyman-α" QSOs at redshifts $\geq$ 1.8, where the strong Lα line is redshifted onto the wavelength response of the IIIaF emulsion. At the low grism/grens dispersions, the spectral resolution is determined by the seeing. For the CFHT plates, virtually all of which were taken in $< 1''$ seeing, the resolution is $\sim$ 70 Å. Through generous allocations of observing time, I was able to obtain a blue grism plate in $\leq 2''$ seeing for almost all the grism fields, retaking plates initially taken in poor seeing; thus, the resolution is typically better than $\sim$ 150 Å in the grism fields. The frequently excellent seeing at the CFHT, coupled with the higher dispersion of the grens, allows somewhat weaker-lined objects to be detected than with the grism (*e.g.*, Crampton, Schade, and Cowley 1985).

The non-uniform response as function of wavelength of the IIIaF emulsion can be seen in Figure 1 of Carswell and Smith (1978) which displays the response curve for the blue grism +IIIaF combination. The response has a broad maximum near 3500 Å with smoothly decreasing sensitivity to 4800 Å. Redward of 4800 Å there are peaks in the response at 5300 Å, 6100 Å, and 6800 Å. Because of these response

non-uniformities, a conservative approach is followed for the emission line samples emphasized in this thesis: henceforth, I concentrate only on those emission line QSOs selected from blue grism/grens plates on the IIIaF emulsion, and having a strong feature blueward of 4800 Å, corresponding to z< 3.0 for Lα QSOs. The additional spectral information redward of 4800 Å is used in the current application only to look for confirming spectral features (*e.g.*, a second line at a consistent redshift). As noted before, the higher redshift QSO candidates (z> 3.0 and Lα at observed wavelength > 4800 Å) will be discussed in later publications.

2.3.2.1 The Complete Sample "C"

Clowes (1981) has given a thorough, quantitative discussion of selection effects operating in grism surveys, concentrating especially on those for emission line objects selected from IIIaF plates taken with the blue-blazed grisms. Clearly, because such objects are selected on the basis of lines, completeness limits depend on more than just apparent magnitudes; such factors as line strength and the seeing (hence resolution) are also quite important. Clowes' models predict, for example, a selection curve for the IIIaF+blue grism plates which provides a description of how the limiting (observed) equivalent width of Lα+NV varies as a function of seeing and continuum magnitude. Clowes demonstrated that his models are quite successful at reproducing the appropriate data from the Hoag and Smith grism survey (Hoag and Smith 1977; Osmer 1980).

From Clowes' Figure 1, it can be seen that for the blue-blazed grism +IIIaF plate combination, taken in 2" seeing, the limiting detectable (observers frame) equivalent width of Lα+NV is $\sim$ 200 Å for a continuum magnitude at 1475 Å in the QSO rest frame of m(1475) = 19.8; this corresponds to a continuum B magnitude of B(cont)= 20.0 for z= 1.8, and B(cont)= 20.2 for z= 3.0. Brighter than these

limiting magnitudes, of course, weaker features can be detected.

Lyman-α equivalent widths are available for a sample of radio-selected QSOs (Richstone and Schmidt 1980). Their data suggest that for $z \geq 2$, fewer than $\sim 25\%$ of QSOs will have observed Lα-NV equivalent widths of less than ~ 200 Å. A radio selected sample is appropriate for this comparison because radio selection is the only efficient (*a priori*) line-strength-independent technique of finding high-redshift objects. Thus, taking account of the flux contribution of lines, grism selection should be $\geq 80\%$ complete for Lα QSOs to at least an *observed* magnitude of $B \leq 19.5$, provided the seeing is $\leq 2''$. As noted above, blue-blazed IIIaF plates were obtained in 2" seeing or *better*, for almost all fields.

Further confirmation that $B < 19.5$ is an appropriate completeness limit for grism/grens selection is provided in Figure 2.3.2.1.a. Plotted here is the distribution of apparent magnitudes (see § 2.4 for a discussion of these magnitude estimates), for the high confidence (mainly high redshift) emission line QSOs in my sample. The surface densities of grism selected QSOs per unit magnitude interval are known to increase, or at least not decrease, with fainter limiting magnitudes at least to $B \sim 20.5$ (Gaston 1983). Thus the paucity of QSOs to the faint side of the peak in the distribution shown in Figure 2.3.2.1.a. is generally attributed to the onset of incompleteness around $B \approx 19.5$.

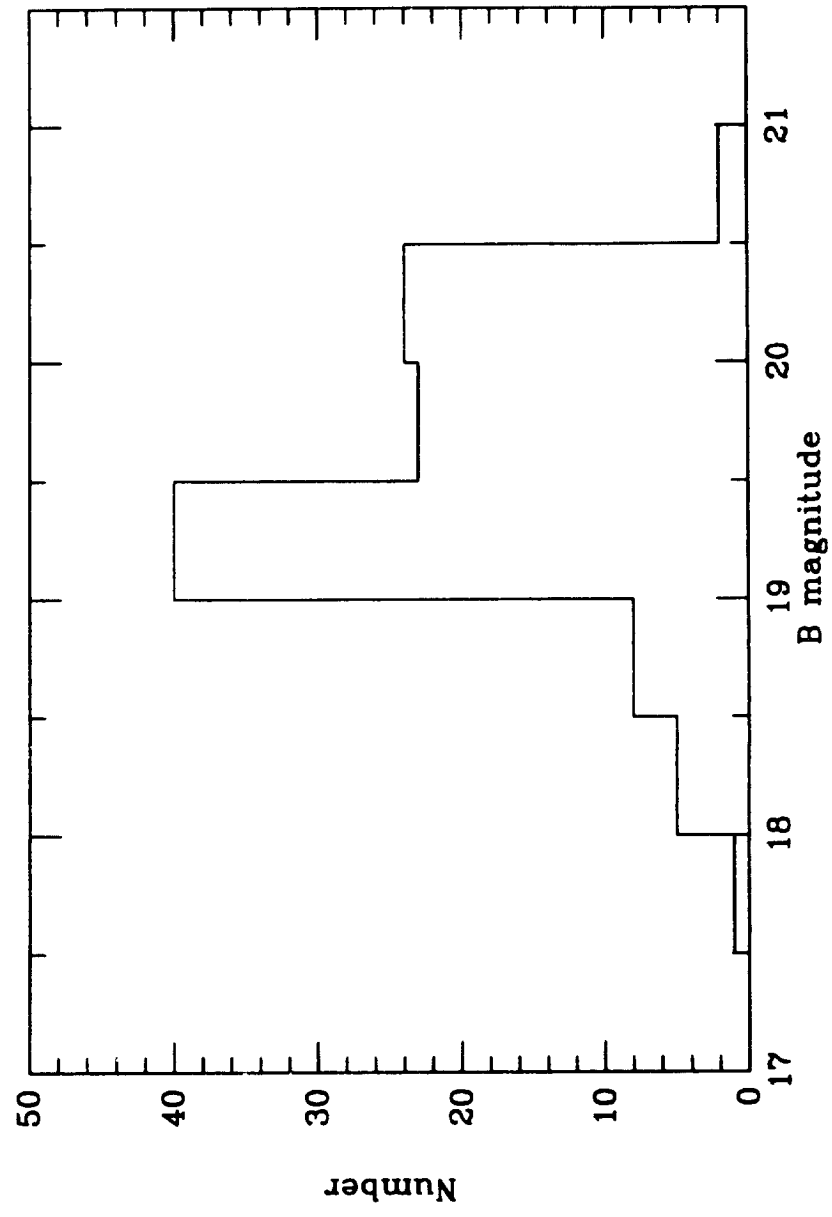

Figure 2.3.2.1.a. The distribution of apparent B magnitudes for the high confidence grism/grens emission line selected QSOs (mainly at high redshift). Note that the decrease at magnitudes fainter than the peak is generally interpreted as due to the onset of incompleteness at $B \sim 19.5$.

Following the arguments above, I have established a subsample (hereafter, sample "C") of my emission line selected QSOs which should constitute a reasonably complete ($\geq$ 80%) sample. Sample C consists of all (high confidence) blue grism selected emission line QSOs with $1.8 \leq z \leq 3.0$ and B$\leq$ 19.5. When only a single line is detected on the plate (true for about half the cases in Sample C), I have assumed the line identification to be Lα; other workers (*e.g.*, Osmer 1980) have found that $\sim$ 80% of such strong-lined grism objects indeed turn out to be Lα QSOs. It will be argued later that this assumption is also a conservative approach (in the current application) when interpreting the X-ray data. For uniformity in optical selection biases, I exclude from sample C those QSOs selected on other plate/grism combinations (*i.e.*, objects selected on the red grism plates), and, again taking a conservative approach, exclude even those selected from CFHT blue grens +IIIaF plates. The CFHT plates are excluded for several reasons. First, the complete follow-up slit spectroscopy needed to produce "Clowes-type selection curves" is currently unavailable for any large sample of blue-grens+IIIaF selected QSOs, although such follow-up spectroscopy is in progress by Crampton and associates. Second, even if such curves were available, it would be difficult to combine the results of grism and grens surveys: the grens is less UV sensitive than the grisms; this, for example, means that QSOs in the range $z\approx$ 1.8 to $z\approx$ 2.0 are not found as efficiently on the grens plates as they are on the grism plates.

There are 38 fields for which a high quality blue grism+IIIaF plate is available. These 38 fields cover an area of 12.9 sq. deg.; 40 sample C objects were found in these fields, yielding a surface density of 3.10+-0.049 QSOs/sq. deg to B= 19.5 and with redshifts $1.8 \leq z \leq 3.0$. The 40 QSOs of sample C are listed in Table 2.3.2.1.a. Note that not all 38 fields actually yielded any QSOs which satisfy the parameters of sample C, but that these fields must be included in calculating the surface density

of such objects.

The surface density found here is in good agreement with that found by other workers; for example, there were 14 high redshift objects selected in the 5.2 sq. deg. covered by the Hoag and Smith survey using the same grism/emulsion combination (see discussion in Schmidt and Green 1983): yielding a surface density of $\approx$ 2.7 per sq. deg. This good agreement in surface densities adds further confidence that my sample is largely complete, and my search technique thorough. Further in this regard, it is important to stress again that to B= 20.5, all seven previously known high redshift ($z>$ 1.8) QSOs were were recovered in double-blind fashion (§ 2.3).

The "complete" sample C will be used in Chapter 5 for a direct estimation of the contribution of high redshift QSOs to the diffuse X-ray background. This direct approach requires the use of complete samples.

Table 2.3.2.1.a The Complete QSO Sample "C" (B≤ 19.5 and 1.8 ≤ z < 3.0)

Object	R.A. (1950)	Dec (1950)	B	log (l_{2500})	z
Obj. 5			18.3	31.91	1.96[3]
Obj. 6			19.3	31.67	2.20
Obj. 7			19.2	31.66	2.2
Obj. 8			19.1	32.23	3.00
08366+654	08 36 37.5	+65 24 01	19.0	31.57	1.9
08388+131	08 38 48.4	+13 10 00	19.1	31.53	1.88
08388+133	08 38 50.5	+13 19 42	19.0	31.52	1.80
08500+283	08 50 03.6	+28 18 32	19.3	32.11	2.90
09038+167	09 03 52.6	+16 46 15	18.2	32.14	2.4
09379+121	09 37 56.8	+12 09 33	19.0	31.98	2.7
09388+117	09 38 50.8	+11 42 54	18.6	31.87	2.2
09392+121	09 39 14.5	+12 07 24	19.0	31.46	1.80
11131+183	11 13 08.4	+18 21 18	18.6	31.83	2.20
11156+180	11 15 33.3	+18 02 39	18.1	31.85	1.90[3]
12071+398[1]	12 07 11.6	+39 53 24	19.4	31.61	2.33[3]
12076+399	12 07 38.6	+39 56 17	17.5	32.39	2.4
Obj. 10			19.3	31.53	2.06
Obj. 11			19.1	31.47	1.90
12302+120	12 30 11.0	+12 02 59	19.1	31.45	1.90
12336+264	12 33 28.7	+26 29 54	19.1	31.75	2.40
12354+264[1]	12 35 25.8	+26 27 30	19.4	31.68	2.5
Obj. 12			19.2	31.41	1.90
Obj. 15			19.1	31.60	2.0
Obj. 16			18.2	32.32	2.7
14149+251	14 14 59.5	+25 06 02	18.7	31.63	1.87
14151+254	14 15 08.3	+25 28 45	19.3	31.64	2.31
15181+201	15 18 07.6	+20 07 50	19.2	31.62	2.1
16017+184[1]	16 01 47.0	+18 25 34	19.1	31.51	1.94[3]
Obj. 17			19.0	31.93	2.6
17272+502	17 27 12.5	+50 15 07	19.1	31.67	2.1
17272+499	17 27 17.0	+49 56 41	19.3	31.44	1.9
17274+503	17 27 28.1	+50 21 03	19.2	31.66	2.2
Obj. 19			19.4	31.63	2.10
20382-012	20 38 16.6	-01 16 21	19.1	32.21	2.9
21260-150	21 26 01.0	-15 03 02	19.3	31.60	2.2
Obj. 21			19.4	31.57	2.10
21342-149	21 34 13.1	-14 55 56	18.3	32.00	2.20
21556-302	21 55 40.4	-30 14 27	18.9	31.75	2.20
21470-302	21 57 05.9	-30 14 52	18.4	31.77	1.9

Notes:

(1) Previous cataloged objects (see references in Veron-Cetty and Veron 1985):
12071+398 is previously cataloged as 1207+39W3,
12354+264 is previously cataloged as Wee 73,
16017+184 is previously cataloged as 1601+184.

(2) Redshifts are based on identification of strongest feature as Lα; when more than a single line on the grism/grens plate is detected at a consistent redshift (usually CIV), two decimal places are listed for the redshift (although redshift is still uncertain to ~ 0.1 in z).

(3) Slit spectrum confirms redshift.

(4) See Appendix A for explanation of nomenclature "Obj. 5".

2.3.2.2 The Narrow Sample "N"

The second subsample of objects to be defined, hereafter sample "N", includes 82 very high confidence emission line QSOs selected from *both* grenses and grisms which also fall within the following parameter ranges: $1.8 \leq z \leq 2.5$ and $31.0 \leq \log l_{2500} \leq 32.0$; l_{2500} (in units of erg/sec/Hz) is the monochromatic luminosity at 2500A in the QSO frame. The estimation of these optical luminosities are discussed below in § 2.4. Sample N does not constitute a complete sample, but merely represents those QSOs candidates for which the plate material alone is deemed adequate to confidently classify the object as a QSO, and which lie in a narrow redshift and magnitude (and hence, luminosity) range where grism/grens selection is highly efficient. The choice of the allowed range of redshift and optical luminosity parameters is a somewhat arbitrary choice, but in the present work is motivated, in part, by the high efficiency of grism/grens selection within these parameter ranges, but also by the desirability (see discussion below in this section) of having a large sample of QSOs with X-ray information available which occupy a *narrow* region of redshift-optical luminosity space.

As above, when only a single strong line is detected (about half the time), it is assumed to be Lα; this assumption may lead to contamination of the sample by lower redshift objects. Follow-up spectroscopy of earlier grism samples (*e.g.*, Osmer 1980), suggests that such contamination should be $\leq 20\%$. Crampton, Schade, and Cowley (1985) have found that the greater sensitivity of the grens to weak features allows them to find lower redshift objects with considerably greater efficiency: $\sim 2/3$ of their grens selected sample may be at $z < 1.8$. However, unlike Crampton *et al.*, in the current application, I am not trying to push the plates to extremely faint magnitude limits; such very faint QSOs will not have very sensitive X-ray flux

detections or upper limits. Further, lacking follow-up spectroscopy for most of my candidates, I include in Sample N only my very high confidence grens QSOs (*i.e.*, those with very strong lines). Even in Crampton *et al.*'s grens sample, their highest confidence (their "Class 1") QSOs are mainly at $z \geq 1.8$: only two of the eight previously uncataloged objects in their Table III which have follow-up spectroscopy are confirmed to be at $z < 1.8$. Further, for the very high confidence grens QSOs in my sample, I find a surface density ≥ 2.0/sq. deg to $B \leq 19.5$ for objects with probable redshifts $z \geq 1.8$, a value quite similar (but a little lower) than that I found in § 2.3.2.1 for my grism sample; a somewhat lower surface density is in fact expected from the grens because of its lower efficiency in the redshift range $z = 1.8$ to 2.0. Finally, we note that for *both* grism and grens selected candidates included in sample N, more than 50% of the QSC candidates have more than one single strong line detected on the plate at a consistent redshift. Therefore, it seems likely that there is no dramatic difference between the redshift distributions of the grism-selected QSOs and the relatively bright, high-confidence, strong-lined grens QSOs considered here, and I estimate $\leq 20\%$ contamination from lower redshift objects. In any case, contamination of the high redshift samples by lower redshift objects should tend to overestimate such quantities as the mean X-ray flux, contribution to the diffuse X-ray background, etc., for high redshift objects (see Chapter 5 for a more detailed discussion). In later chapters, I will argue for relatively small upper limits for such X-ray quantities anyway, and so this small uncertainty in the precise redshift distribution of the sample merely makes the derived X-ray upper limits more conservative ones.

In addition, I have also included in sample N another 10 QSOs from the Hoag and Smith and Sramek and Weedman surveys which also lie within the parameter ranges defined for sample N ($1.8 \leq z \leq 2.5$ and $(31.0 \leq \log(l_{2500}) \leq 32.0)$. These

surveys were carried out with the identical blue grism used in the current study, and they found similar magnitude and redshift distributions, surface densities, etc.; so there is every reason to believe that these are quite similar objects to those in my sample. The X-ray emissions from these 10 objects have been studied in quite deep Einstein IPC images discussed by Kriss and Canizares (1985). Note that for observing efficiency, the particular grism fields chosen by Kriss and Canizares for X-ray observations were not only abnormally high in surface density of QSOs, but also fields with an overabundance of optically bright objects; such special qualities of these particular fields preclude consideration of the objects studied by Kriss and Canizares as a complete sample.

Sample N, then, includes a total of 92 objects which occupy a narrow region of optical luminosity and redshift space ($1.8 \leq z \leq 2.5$, and $31.0 \leq \log(l_{2500}) \leq 32.0$). Although this sample is incomplete, it is well suited for empirically testing models for the dependence of QSO X-ray luminosity on such other parameters as optical luminosity and redshift, *i.e.*, for studying the X-ray conditional luminosity function (see, *e.g.*, Avni and Tanabaum 1982, and later chapters). Because it has been found by several workers that there is a strong dependence of the mean X-ray to optical luminosity ratio $< l_{2\,keV}/l_{2500} >$ on optical luminosity and/or redshift, a measured value of $< l_{2\,keV}/l_{2500} >$ for a sample of QSOs is a directly interpretable quantity only when it can be determined within a narrow range of optical luminosity/redshift space (or for a complete sample like sample C). Sample N will be used to empirically test models (*e.g.*, Avni and Tananbaum 1982) for the evolution of the ratio $< l_{2\,keV}/l_{2500} >$ with l_{2500} and z; the narrow regime of redshift-optical luminosity covered by sample N, allows this measurement to be made in a model independent fashion.

Shown in Figure 2.3.2.2.a and 2.3.2.2.b are the distributions in redshift and optical luminosity for sample N; the distributions have means of $< \log(l_{2500}) >= 31.44$, and $< z >= 2.1$. The QSOs of sample N are listed in Table 2.3.2.2.a, and finding charts are given in Appendix B. Note that there are 30 objects in common between the samples N and C, *i.e.*, many sample C objects are also within the parameter ranges of sample N.

Figure 2.3.2.2.a. Distribution of redshifts in sample N.

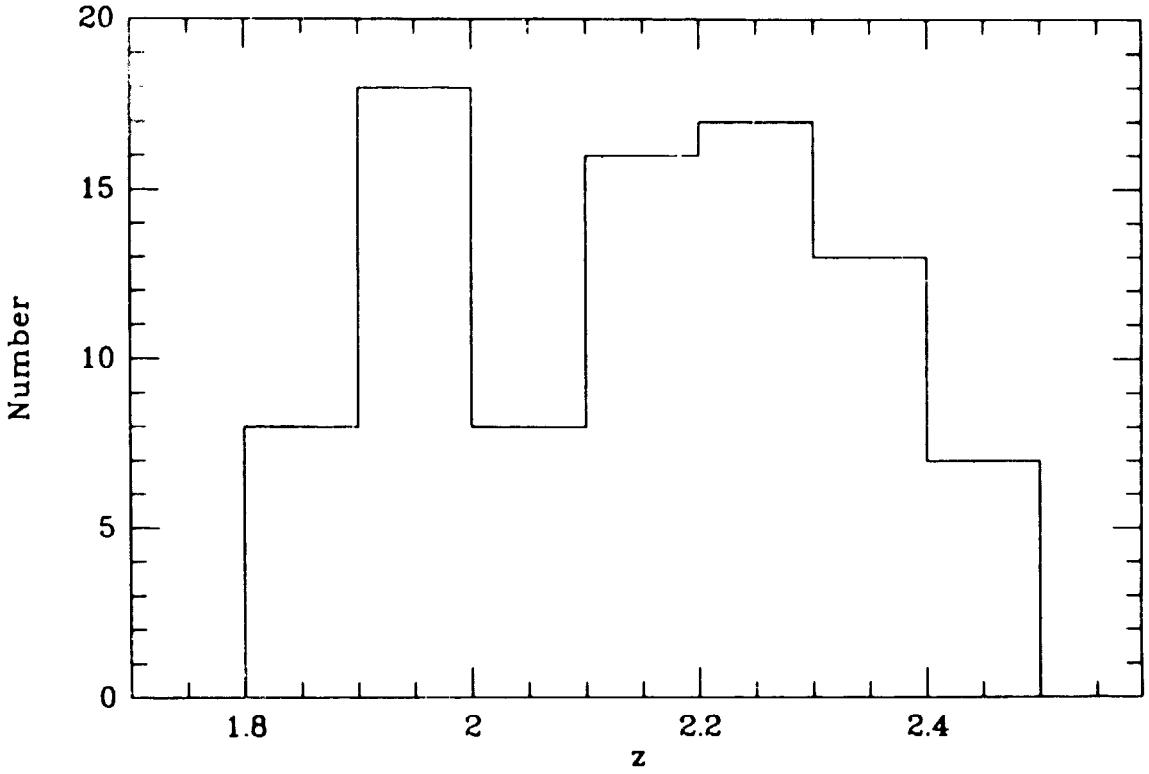

Figure 2.3.2.2.b. Distribution of optical luminosities in sample N.

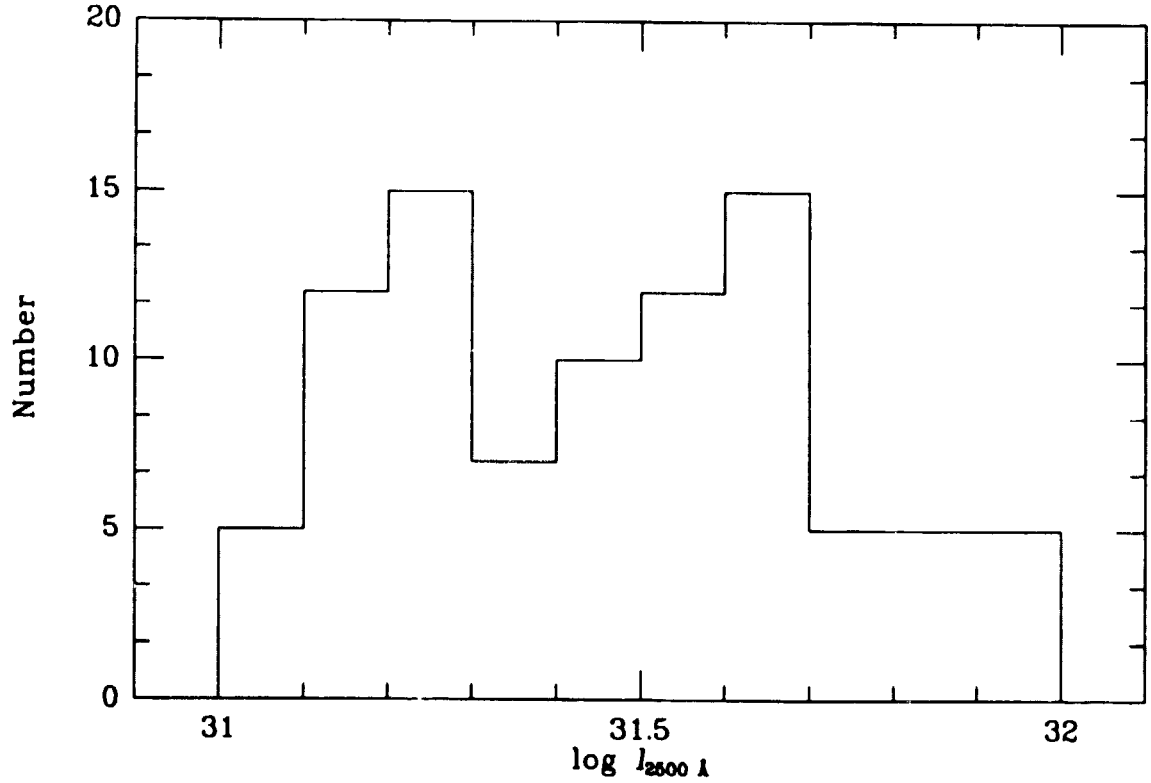

Table 2.3.2.2.a: The "Narrow" Sample "N"
($31.0 \leq \log (l_{2500}) \leq 32.0$ and $1.8 \leq z \leq 3.0$)

Object	R.A. (1950)	(Dec (1950)	B	log (l_{2500}'	z
Obj. 1			20.4	31.13	2.20
00151 + 160	00 15 09.9	+16 03 13	19.9	31.33	2.20
00159 + 155	00 15 54.8	+15 35 48	20.6	31.07	2.30
01121 − 014	01 12 06.6	−01 26 45	20.3	31.17	2.20
02031 + 151	02 03 07.3	+15 09 07	20.3	31.10	2.00
02031 + 152	02 03 08.4	+15 17 04	19.7	31.50	2.38
Obj. 2			18.7	31.97	2.5
02036 + 150	02 03 38.4	+15 01 05	19.9	31.32	2.10
Obj. 3			20.3	31.20	2.30
02057 + 150	02 05 44.8	+15 00 41	20.5	31.20	2.40
03057 + 172	03 05 45.9	+17 12 12	20.4	31.27	2.40
03061 + 169	03 06 06.7	+16 54 23	20.3	31.21	2.14
Obj. 4			19.1	31.61	2.0
03074 + 172	03 07 28.9	+17 16 37	19.2	31.66	2.28
Obj. 5			C		
Obj. 6			C		
Obj. 7			C		
08366 + 654			C		
08388 + 131			C		
08388 + 133			C		
09382 + 117	09 38 13.9	+11 45 32	19.9	31.37	2.30
09382 + 120	09 38 14.7	+12 05 45	19.5	31.42	2.00
09383 + 120	09 38 23.9	+12 05 58	20.2	31.32	2.4
09388 + 117			C		
09392 + 121			C		
09392 + 117	09 39 17.2	+11 46 02	19.8	31.21	1.9
Obj. 9			20.2	31.18	2.1
11131 + 183			C		
111366 + 182	11 13 41.9	+18 12 53	19.5	31.29	1.9
11143 + 184	11 14 19.2	+18 28 38	20.3	31.15	2.20
11156 + 180			C		
11147 + 183	11 14 46.6	+18 19 42	19.7	31.21	1.9
12071 + 398			C		
Obj. 10			C		
Obj. 11			C		
12275 + 024	12 27 35.3	+02 28 47	20.2	31.12	2.0
12292 − 116	12 29 12.4	+11 37 48	19.7	31.14	1.80
12302 + 120			C		
12336 + 264			C		
12354 + 264			C		
Obj. 12			C		
Obj. 13			20.1	31.22	2.1
Obj. 14			20.2	31.20	2.2
Obj. 15			C		
14144 + 256	14 14 29.9	+25 36 42	19.6	31.22	1.80
14148 + 252	14 14 49.7	+25 13 34	19.7	31.20	1.83

14151 + 254			C		
14149 + 251			C		
15090 − 092	15 09 03.4	−09 17 09	19.9	31.18	1.9
15100 − 089	15 10 00.5	−08 57 48	20.4	31.17	2.1
15184 + 202	15 18 25.9	+20 17 33	19.9	31.34	2.10
15181 + 201			C		
16016 + 184	16 01 38.3	+18 24 08	20.2	31.24	2.31
16017 + 184			C		
17252 + 499	17 25 14.1	+49 57 46	19.9	31.20	1.90
17257 + 503	17 25 43.4	+50 18 15	20.4	31.15	2.1
17264 + 504	17 26 25.3	+50 28 30	19.9	31.20	1.9
17272 + 502			C		
17272 + 499			C		
17274 + 503			C		
17449 + 206	17 44 59.1	+20 36 05	19.0	31.91	2.41
17465 + 201	17 46 33.3	+20 10 58	19.0	31.64	1.90
Obj. 18			18.9	31.81	2.0
Obj. 19			19.4	31.55	2.10
Obj. 20			20.2	31.35	2.3
20374 − 007	20 37 25.8	−00 44 39	19.9	31.47	2.3
20381 − 011	20 38 10.9	−01 09 10	20.4	31.25	2.26
21189 + 168	21 18 59.9	+16 51 26	19.5	31.64	2.30
21259 − 148	21 25 57.4	−14 51 02	19.9	31.38	2.30
Obj. 21			C		
21265 − 150	21 26 34.1	−15 02 39	20.3	31.18	2.1
21342 − 149			C		
21354 − 145	21 35 27.8	−14 32 11	19.9	31.18	1.90
21357 − 147			C		
21416 + 037	21 41 40.5	+03 45 07	20.2	31.05	1.8
21431 + 040	21 43 10.8	+04 03 59	19.2	31.57	2.0
21558 + 034	21 55 51.2	+03 29 33	19.0	31.56	1.9
21556 − 302			C		
21570 − 302			C		
1624 + 266			18.1	31.95	2.20
1623 + 270			19.6	31.51	2.44
0131 − 402			20.2	31.08	2.11
0132 − 405			19.4	31.43	2.15
0130 − 403			19.1	31.56	2.16
0132 − 402			19.4	31.45	2.18
0131 − 404			20.4	31.08	2.25
0131 − 405			19.7	31.41	2.36
0130 − 404			18.9	31.74	2.39
0132 − 405			20.7	31.08	2.46

Notes to Table 2.3.2.2.a

(1) A "C" in the B magnitude column denotes that the object is also a sample C object; information on these objects can be found in Table 2.3.2.1.b.

(2) The final 10 objects in the table are the relevant objects (from the grism surveys of Hoag and Smith, and Sramek and Weedman) whose X-ray properties have been studied by Kriss and Canizares (1985).

(3) Objects with two or more lines detected on the grism/grens plates have two digits to the right of the decimal place in their listed redshifts; this convention does not, in general, mean that the redshifts are determined as accurately as indicated.

(4) See Appendix A for an explanation of nomenclature "Obj. 1".

2.4 Optical Magnitudes and Monochromatic Luminosities at 2500 Å

In many of the later applications, a relevant quantity will be the mean $l_{2\ keV}/l_{2500}$ ratio of a sample of QSOs, and thus it is necessary to estimate l_{2500} for these QSOs. Optical B magnitudes are estimated using image diameter measurements from the POSS O print. Image diameters are measured with a 50X microscope, and converted to B magnitudes using the approach outlined in Hayman, Hazard, and Saniitt (1979). In order to avoid any sytematic biases (personal or instrumental), I recalibrated the image-diameter/magnitude relation (using the same Plaut photometric sequence used by Hayman *et al.*) for my own eye/50X microscope combination. The relationship I found was

$$B = 21.87 - (0.043d) - [0.3\sec(\delta - 33)] \qquad (2.4a)$$

where d is the image diameter in microns, and δ the declination of the object; the last term is intended to correct for the differential atmospheric extinction between the Plaut photometric sequence and the object.

Two "photometric" standard fields were used to test the reliability of this recalibrated image diameter-magnitude relation: the first includes 47 photoelectrically calibrated standards from a field in M15 (Sandage and Katem 1977), while the second included the 53 grism selected (Sramek and Weedman 1978) QSOs with magnitudes determined from spectrophotometry and microdensitometry (Vaucher and Weedman 1980). These latter QSO magnitudes are continuum magnitudes at 4500 Å, and thus the test here for the Sramek and Weedman sample requires that POSS image diameters (which include flux contributions from emission lines), be converted into optical continuum magnitudes. This is exactly the sort of process required for my new grism/grens selected samples. For both these photometric test samples the rms differences between my POSS estimates and the photometric

ones are ≤ 0.5 magnitudes for B< 20.5. These reliability test results are displayed graphically in Figure 2.4.a, and clearly show that any systematic errors should be quite small in the mean (≤ 0.1 magnitude).

As is clear from this plot, our estimates are considerably more uncertain (rms~ 1 magnitude) at magnitudes fainter than B= 20.5. This results from at least two factors. The first is that near the POSS limiting magnitude (B~ 20.5 – 21), the image diameter does *not* change with magnitude; instead, only the "hardness" of the image changes (see, *e.g.*, Hayman, Hazard, and Sanitt 1979). A second cause of this degradation in the validity of the image-diameter/magnitude relation in the "photometric" QSO sample is the following: the Vaucher and Weedman magnitudes plotted in Figure 2.4.a are *measured* continuum magnitudes, while my POSS estimates are *predicted* continuum magnitudes using magnitude corrections for the equivalent width of the "average" lines (*e.g.*, ~ 90 Å(1+z) for Lα: Richstone and Schmidt 1980). However, because of the obvious selection effects, the grism selected test sample is dominated at the faint end by objects that have anomalously strong emission (this effect also can be seen in Clowes' Figure 1): thus at the faint end, my assumed "average" line will tend to assign too little flux to the actual emission line strength, and my POSS magnitude (including flux from the line) will overestimate the continuum magnitude. Such faint end effects will certainly affect my new grism/grens objects in a similar fashion, and therefore, in sample N (and, of course, sample C as well), only those objects with B≤ 20.5 are included.

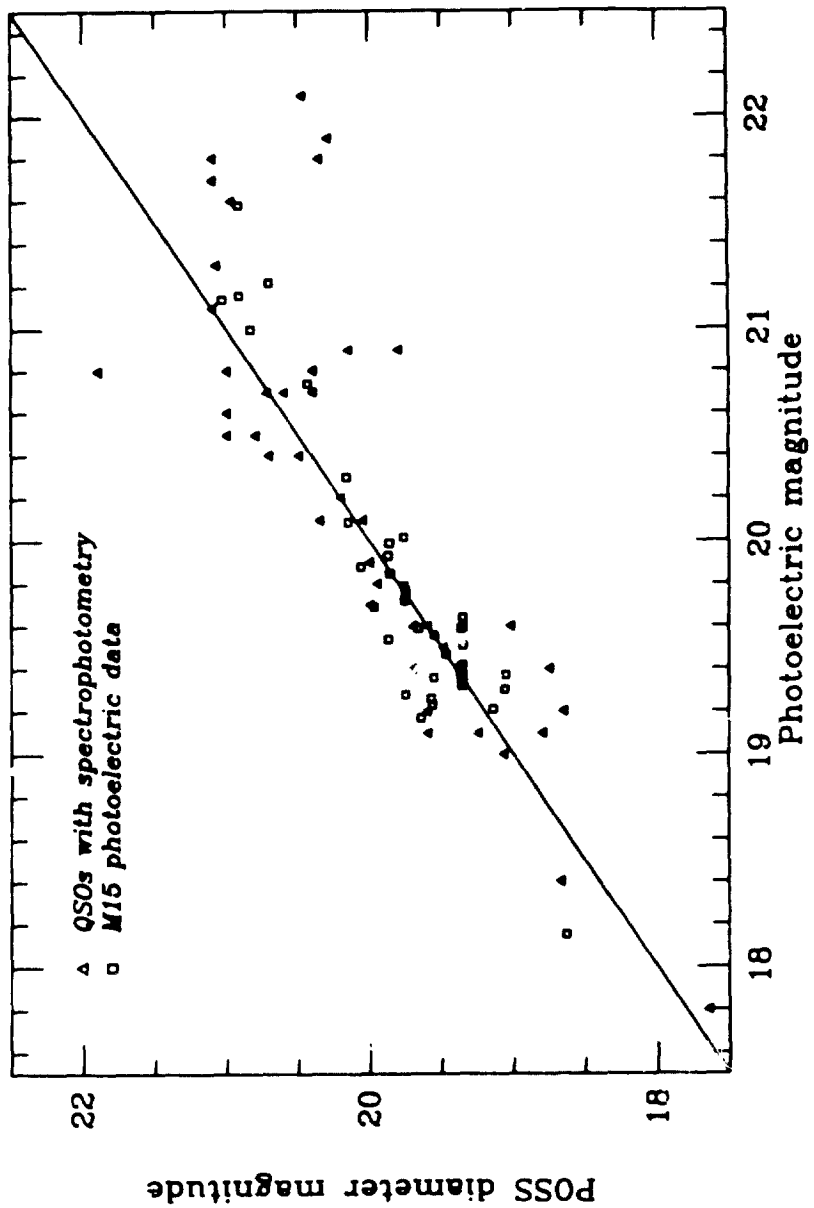

Figure 2.4.a. Tests of reliability of magnitudes estimated from POSS. Plotted are the measured magnitudes at 4500 Å for a QSO sample with spectrophotometrically calibrated magnitudes available. The points represent B magnitudes for a photoelectric sequence in M15.

The POSS B magnitudes are corrected to continuum magnitudes using the data in Veron (1985). He estimates the line correction ΔB(line) as a function of redshift calculating contributions from Lα, CIV, CIII, etc. Throughout the redshift range of interest, the average line correction is ~ 0.3 magnitudes. The POSS B magnitudes are further corrected for extinction within the Galaxy according to

$$\Delta B(\text{ext}) = -0.24 \csc |b^{II}| \qquad (2.4.b)$$

Finally, corrected B magnitudes (corrected for extinction and the presence of emission lines) are converted to monochromatic luminosities at 2500 Å in the QSO rest frame using the following relations (see, *e.g.*, Schmidt 1968; Schmidt and Green 1983):

$$B_c = B + \Delta B(\text{line}) + \Delta B(\text{ext}) \qquad (2.4.c)$$

$$\log (l_{2500}) = -\frac{B_c}{2.5} - 19.38 \qquad (2.4.d)$$

$$\frac{S\nu_1}{S\nu_2} = \left(\frac{\nu_1}{\nu_2}\right)^{-\alpha_o} \qquad (2.4.e)$$

$$\frac{S_\nu \left(2500\text{Å}(1+z)\right)}{S_\nu (4410\text{Å})} = \left[\frac{4410\text{Å}}{(1+z)2500\text{Å}}\right]^{-\alpha_o} \qquad (2.4.f)$$

$$A(z) = z \left\{1 + \frac{z(1-q_o)}{[(1+2q_o z)^{1/2} + 1 + q_o z]}\right\} \qquad (2.4.g)$$

$$D_l = \frac{c}{Ho} A(z) \qquad (2.4.h)$$

$$l_{2500} = \frac{4\pi D_l^2 S_\nu(2500\text{Å}(1+z))}{1+z} \qquad (2.4.i)$$

where $S_\nu(2500\text{Å}\,(1+z))$ is the flux density (erg/sec/cm^2/Hz) at an observed frequency corresponding to $\lambda_{\text{obs}} = 2500\text{Å}(1+z)$, and D_l is the luminosity distance. Note that I have assumed a power law spectral form for the optical continuum.

Throughout this dissertation, the following values are assumed: $q_o = 0$, $H_o = 50$ km/sec/Mpc, and $\alpha_o = 1.0$. These values are chosen mainly for ease of comparison with previous studies of the X-ray properties of QSOs (*e.g.*, Zamorani *et al.* 1981) in which such values were adopted. The optical characteristics (B, and log 2500 Å) of samples C and N are shown in Tables 2.3.2.1.a. and 2.3.2.2.a.

2.5 Optical Coordinates

Optical coordinates were measured from the POSS prints using the University of Washington Digitizer, or the two-axis measuring machines at KPNO and CfA. Although coordinate accuracies differ among theses various machines, all optical coordinates should be accurate to at least 10″. Such accuracy is more than adequate for the IPC fields with their X-ray error circles $\sim 60''$ in radius, but for the HRI with its $\sim 3''$ X-ray error circles, some of these optical coordinate uncertainties are somewhat larger than optimum. Optical coordinates for sample N and C QSOs are also listed in Tables 2.3.2.1.a and 2.3.2.2.a.

2.6 Summary

A sample of ~ 400 QSO candidates with the most sensitive available X-ray data already extant has been optically selected. Two high redshift subsamples of this large data base have been defined for subsequent study in later chapters; these two samples include ≈ 90 objects from regions of optical luminosity-redshift space where grism selection is highly efficient. Sample C is a largely (> 80%) complete sample to B$\leq$ 19.5 and $1.8 \leq z \leq 3.0$, and will be used in Chapter 5 for a direct estimation of the contribution of such high redshift QSOs to the diffuse X-ray background. Sample N is a sample occupying a narrow region of redshift and optical luminosity space that makes it ideal for testing models of the evolution of X-ray luminosity with optical luminosity and redshift.

3. THE X-RAY DATA FOR THE GRISM/GRENS SELECTED QSOS

The previous chapter discussed the selection of a new optical sample of high redshift QSOs from grism/grens plates taken in regions of the sky for which the most sensitive available X-ray flux information is already extant. In this chapter, the archived *Einstein* X-ray data for these optically selected QSOs is discussed and presented.

Throughout this chapter, information from the following references are used frequently, and the reader desiring more details is referred to these useful publications on X-ray astronomy: Gursky and Schwartz (1974) for an introduction to X-ray observational techniques; Giacconi *et al.* (1979a, 1981) for an introduction to the Einstein Observatory; Einstein Observatory Revised User's Manual (or EORUM) (1984), and Harnden *et al.* (1984) for details on obtaining X-ray fluxes from Einstein images.

3.1 The *Einstein Observatory* and the Archived X-ray Images

The *Einstein Observatory* (Giacconi *et al.* 1979a; Giacconi *et al.* 1981) which operated in earth orbit from November 1978 through April 1981, is a grazing incidence, focusing optics, Wolter type I (Wolter 1952) X-ray telescope; originally, the observatory was known as the High Energy Astronomical Observatory-2, or HEAO B. For the Einstein telescope, X-rays are reflected by total external reflection (index of refraction less than unity) first by a paraboloidal surface which focuses axial rays into an annulus, and then brought to a final (point) focus by a second reflection off a hyperboloidal surface. Because of the grazing incidence angles employed, such mirrors have a small ratio of effective collecting area to polished surface; to provide greater collecting area, four such confocal mirrors are nested in the Einstein Observatory.

Among the four available focal plane instruments (Giacconi *et al.* 1979a, 1981) there are two imaging instruments, which provide both spatial resolution and flux information for X-rays of energy a few keV. The Imaging Proportional Counter (hereafter, the "IPC"), has a field of view of $60' \times 60'$ (but with $\sim 38' \times 38'$ inside the window support "ribs"), spatial resolution of $\sim 1.5'$ at 1.5 keV, and an effective detector/telescope area at 1.5 keV of ~ 110 cm^2. The High Resolution Imager (hereafter, the "HRI"), provides higher spatial resolution of 2", but with relatively low quantum efficiency: at 1 keV, the effective area is ~ 10 cm^2.

The archived *Einstein* X-ray data to be used in constraining the X-ray emissivities of the grism/grens QSOs consist of high galactic latitude ($|b^{II}| > 20°$) X-ray images with very long integration times: 50 IPC images with integration times of 10,000-45,000 seconds, and 5 HRI images with integration times of 40,000-100,000 sec. By comparison, the so-called Deep Survey fields (the handful of the very deepest Einstein X-ray images) have exposure times of 30,000-60,000 sec in the IPC, and 10,000-50,000 sec in the HRI (Giacconi *et al.* 1979b, Griffths *et al.* 1983). Thus, the Einstein fields employed in the current study overlap even the X-ray flux sensitivities of the Deep Survey fields, and are thus among the most sensitive of any currently available.

It is to be emphasized that these X-ray fields were initially imaged in X-rays for reasons not directly related to the current study. Instead, these images originally had as their respective primary targets a wide range of potential X-ray sources, including bright stars, cataclysmic variables, clusters of galaxies, normal galaxies, and even a few AGN/QSOs. However, the X-ray information on the target (even if detected) commonly is contained within only the central few 10s of square arc min of the IPC, and within less than 1/3 square arc minute in the HRI. Thus, within

the large fields of view ($\sim$ 0.2 to 1 square degree) of these X-ray images there is a great deal of information available on the X-ray sky which is not associated with the target objects.

In an "after the fact fashion" (*i.e.*, after the X-ray data had already been acquired, I took grism/grens plates centered on 55 deep Einstein images. The QSOs whose optical selection was described in Chapter 2 (and, in particular, samples C and N) constitute the samples whose X-ray properties are investigated here using the previously "unused" portions of these X-ray images.

The approach used here is to be contrasted with programs aimed at the optical identification of serendipitous X-ray sources (*e.g.*, Margon, Chanan, and Downes 1985, Gioia *et al.* 1984, Maccacaro, T. 1984, Reichert *et al.* 1982). In the latter approach, previously uncataloged X-ray sources which by serendipity lie within the X-ray image are noted and ***subsequently*** optically identified, thus forming an *X-ray* selected sample of objects (many of which indeed turn out to be low redshift QSOs). On the other hand, the QSOs investigated here are first ***optically*** selected from the grism/grens plates, and then the archived Einstein images are used to derive a sensitive X-ray flux detection, or more frequently, an X-ray flux upper limit. The optically selected grism/grens samples described here have no *apriori* X-ray biases, while at the risk of stating the obvious, X-ray selection tends to pick out only the X-ray bright objects.

3.2 The IPC and the HRI X-ray Data

With the list of optically selected QSOs (and coordinates) from Chapter 2 in hand, the corresponding position in the appropriate X-ray image is now examined to extract either an X-ray detection or flux upper limit. Several tests for source reality (*i.e.*, whether or not the QSO is detected in X-rays) are made. The definition

of an X-ray detection, and the estimation of X-ray count rates and fluxes for the optically selected QSOs detected in X-rays, and upper limits for the non-detections are now discussed in some detail. Because most of the objects in the grism/grens sample have X-ray information derived from the IPC rather than the HRI, most of the current discussion emphasizes the former instrument.

3.2.1 The Imaging Proportional Counter (IPC)

The IPC (Giacconi *et al.* 1979a, Giacconi 1981) is a position sensitive gas proportional counter allowing for two dimensional X-ray imaging with moderate angular resolution of order 1'; it has non-negligible response to X-rays of energy 0.2-0.28 and 0.5-4 keV. A proportional counter (*e.g.*, Gursky and Schwartz 1974) detects electrons via the photoelectric effect. An incident X-ray photoionizes an atom of the confined gas, ejecting an electron having an energy equal to the difference in energy between that of the incident X-ray and the appropriate ionization potential. An applied high voltage field accelerates the photoionized electron, which in turn collisionally ionizes further gas atoms, producing a cascade of electrons which are collected on the anode wires, and detected as a pulse. The total charge in the pulse (the "pulse height"), is approximately proportional to the number of ion-electron pairs created, which in turn is approximately proportional to the energy of the incident X-ray. Thus, "pulse height analysis" can provide (in principle) some spectral resolution (currently, actual spectra can be obtained only for very strong on axis sources), and is provided for in the IPC by 32 pulse height channels covering the 0.1-6 keV range. Rise times in the multiwire anodes provide two dimensional spatial information on the location of the incident X-ray. Thus, information is provided on the X-ray flux (arrival rate of pulses), spatial location (their rise time), and energy (pulse height).

In practice, the objects of interest here (QSOs at faint apparent optical magnitudes) have such low X-ray fluxes that the IPC must be used in broadband fashion, combining the counts from a number of contiguous pulse height channels. In the IPC, the X-ray background includes contributions from (in roughly decreasing order of importance) the Galactic and extragalactic diffuse X-ray backgrounds, particle induced background (*e.g.*, cosmic rays, trapped radiation), on-board calibration sources, solar X-rays scattered by the earth's atmosphere, and atmospheric X-rays during days of strong solar activity (*e.g.*, Harnden *et al.* 1984). At energies $\leq 0.5\,\mathrm{keV}$, the soft X-ray background (mainly from the interstellar medium in the Galaxy) dominates all but the strongest sources, making the lower energy pulse height channels of limited use in the current application. Further, the gas confining window fails to transmit between 0.28 and 0.5 keV. Above $\approx 3.0\,\mathrm{keV}$, where the optics have low efficiency, hard photons from a typical source are generally overwhelmed by the background contribution from the on-board calibration system. Thus, for the present study, X-ray count rates and fluxes will generally be estimated using the IPC as a broadband detector in the 0.5–3.0 keV range; however, several other broad band energy ranges are also used for establishing the existence of sources.

The field of view of the IPC is about 1 square degree, but the gas-confining window of the proportional counter is supported by a "Tic-Tac-Toe" pattern of aluminum structural members. These "ribs" obscure X-rays in the same pattern, so that the useable area inside the central sqaure of the Tic-Tac-Toe pattern is about 38'x38'. The unobscured edges of the image are also useable but less sensitive, due to vignetting.

3.2.1.1 Automated Source Detection Algorithms in the IPC

Each IPC (and HRI) image, has been transformed into a user-useful form by the Einstein Observatory staff at the Center for Astrophysics. The standard IPC production reprocessing (EORUM, Harnden *et al.* 1984) has been applied to almost all the relevant IPC fields, and includes an automated search technique (in several broad energy bands) to locate X-ray sources within the image. A square "detect cell" consisting of 25 square subcells (5 subcells by 5 subcells) is slid across the X-ray image. At the location of the cell center, a source is tested for by comparing the number of broadband counts within the central 9×9 subcells (hereafter, the "detect window") with the expected number of background counts. Two algorithms for estimating the background are available: the first, called LDETECT, estimates the background from the 16 perimeter subcells (hereafter, the "frame") of the detect cell and is optimized for the detection of point sources; the second, called MDETECT, predicts the background by comparison with a "background map", constructed by scaling images of Deep Survey fields (long exposures on fields free of strong X-ray sources) to the exposure time of the relevant image in question. While MDETECT is superior for finding non-point sources or sources in confused regions, the LDETECT mode is generally adequate for isolated point sources, and is the algorithm most commonly applied in the images relevant to the current study. Lists of possible X-ray sources from such automated searches are compared for positional coincidence (X-ray centroid within $\sim 1'$ of the optical position) with the optically selected QSOs from Chapter 2. The automated source finding algorithms commonly are applied using the counts in three different broadband energy ranges: the "soft" band (0.2–0.8 keV), the "hard" band (0.8–3.50 keV), and the "broad" band (0.2–3.5 keV). Note that the energy band (0.5–3.0 keV) used here for estimation of X-ray count rates and fluxes is most similar to the "hard" band in the automated detection finding

algorithms.

The X-ray point response function in the IPC is energy dependent: as the pulse height decreases (softer photons), the signal to noise ratio for assigning a location to the X-rays also decreases. Thus, the area of the IPC that must be included in determining the broadband count rate for a source of X-ray photons actually depends on the *apriori* unknown (at least in the current application) X-ray spectrum of the object. For a "typical QSO spectrum", the FWHM of the Gaussian core of the point response function at 3.5 keV might be only 60% of that at 0.5 keV (e.g., see EORUM). Thus, the optimal size of the detect window of the detect cell is also energy dependent, and in turn dependent on the (*apriori* unknown) X-ray spectrum of the source. For a QSO (called here an "optimal QSO") with an intrinsic X-ray power law spectrum with (energy) index $\alpha_x = 0.5$, passing through a absorbing column of gas of solar composition characterized by $N_H = 2.0 \times 10^{20}\,\mathrm{cm}^2$, the optimal detect window size is $\sim 2.4' \times 2.4'$ for the "hard" X-ray band (Harnden *et al.* 1984). Such a window will include $\sim 85\%$ of the broadband counts from such a point source. However, note that a QSO with a softer spectrum than the optimal QSO will have a smaller percentage of its counts falling within this detect window.

For the present study, an optically selected QSO is considered to have been detected in, for example, the IPC "hard" energy band by the automated detection algorithms if the total number of counts in the detect window equals or exceeds that 5σ (assuming Poisson statistics) above that predicted for the background; that is, source counts/background counts$^{1/2} \geq 5$. The reason for requiring such a high significance is discussed in a subsequent paragraph. Note, however a non-detection here is really only a 5σ non-detection of the optimal QSO. In the current discussion, I have emphasized the hard energy band for concreteness, and for its similarity to

the 0.5–3.0 keV band for which fluxes will be derived; however, detections found in soft and broad bands by the automated source finding algorithms are also checked for positional coincidence with the grism/grens selected QSOs, and the same 5σ criterion is applied.

9.2.1.2 Source Existence from "IXLUM"

In an analogous approach to the LDETECT algorithm, I have done a second test for source existence using a circular detect window of radius 3' centered on the optically selected QSO position, and estimating a (normalized to 3' radius circle) background from a concentric annular frame extending radially from 3' to 5'; counts in pulse height channels corresponding to the 0.5–3.0 keV band are used. The use of this large-sized circular detect window has a distinct advantage: it is sufficiently large that, unlike the optimally sized window, the determination of the broadband source counts can be done without a detailed *a priori* knowledge of the source's (or non-detection's!) X-ray spectrum; the 3' circular detect window is sufficiently large that more than 99% of the counts in the 0.5–3.0 keV band will fall within the 3' circular detect window for a wide range of reasonable possible QSO X-ray spectra. For simplicity in later discussions, let us call the approach described in the current paragraph "IXLUM", after the Einstein/CfA offline software routine which implements this algorithm (see EORUM).

However, a price is paid for using the large 3' detect window, instead of the optimally sized window: extra background noise is introduced into the determination of the source counts (and count rates or fluxes as well). For example, a 5σ detection of an optimal QSO in an optimally sized $2.4' \times 2.4'$ window, would register only as a $\approx 2.6\sigma$ detection in the 3' circle. Thus, in addition to the 5σ automated detection algorithm criterion, I also count as possible detections QSOs which show a $\geq 2.6\sigma$

detection in the larger 3' circle.

3.2.1.3 X-Ray Contour Maps

However, an LDETECT/IXLUM algorithm like those described above can also fail to find real sources in confused regions with other X-ray sources nearby. For example, suppose a weak source of interest (call it source A) lies within the detect window, while other strong sources B and C fall, by bad luck, in the frame. The contamination of the frame from B and C will cause an overestimation of the local background, and the real source A might be missed. To guard against such circumstances I also made X-ray contour maps of $17' \times 17'$ portions of the IPC images which included the location of the optically selected QSO: the X-ray data are first smoothed by convolving the data with a two-dimensional gaussian of full width half maximum (FWHM) of 64". A background again is estimated here, but now it is done so over a much larger portion the image allowing better averaging over small scale fluctuations in the background such as that which might be caused by B and C. Making these contour maps proved to be an appropriate precaution: a few of the grism/grens selected QSOs not established as X-ray detections in the LDETECT/IXLUM algorithms were found, through examination of these contour maps, to be, in fact, X-ray sources in confused regions. Further, for the IXLUM detection tests and flux determinations, these contour maps allowed me to look for portions of 3'–5' annular frame that might be contaminated by nearby unrelated sources, and cause an overestimation of the local background.

3.2.1.4 Detection Criteria in the IPC

In summary, a QSO in an unconfused region is accepted as a detection if it satisfies any two of the following: (1) $\geq 5\sigma$ detection in LDETECT/MDETECT; (2) $\geq 2.6\sigma$ detection in IXLUM; (3) $\geq 3\sigma$ detection in smoothed contour map.

For a QSO in a confused X-ray region, source reality is mainly determined (and sometimes the count rate estimated from) the X-ray contour maps.

3.2.1.5 Fluxes in the IPC

Beyond establishing source reality, the same advantage of not needing to know *a priori* the source X-ray spectrum in IXLUM approach is also of utmost importance when estimating broadband count rates (and hence fluxes). For example, assuming the canonical value of 85% of the source counts lying within a $2.4' \times 2.4'$ box (true for the optimal QSO only), would underestimate the (hard) broadband count rate for a QSO with a spectrum softer than that of the optimal QSO. Thus, for all optically selected QSOs (with one exception), the X-ray count rate (and flux) in the broadband 0.5–3.0 keV is determined using IXLUM with a 3' circle. Again, not using an optimally sized detect cell in this circumstance adds considerable background noise to the calculation, and thus a few of the weaker sources (even though they are 5σ detections in LDETECT/MDETECT) have rather large (to $\sim$ 50%) uncertainties in their count rates (and hence fluxes). Indeed, for one detection (Obj. 2), the count rate was so poorly determined in the 3' radius window, that its count rate was estimated directly from the smaller $2.4' \times 2.4'$ window. The desirability of not introducing grossly uncertain X-ray fluxes (or upper limits) into the grism/grens selected QSO samples discussed here is the motivation for requiring such a high 5σ detection threshold in the automated flux detection algorithms. For objects not detected in X-rays, a 2.64σ IXLUM upper limit, corresponding approximately to an LDETECT/MDETECT 5σ upper limit, is derived using the background from the 3'-5' annular frame.

The observed broadband flux $F_{\rm obs}$ (0.5–3.0 keV) is related to the observed source count rate $S_{\rm obs}$ (0.5–3.0 keV)/t through the proportionality (Tananbaum

et al. 1979):

$$F_{\rm obs}(0.5-3.0\,{\rm keV}) = \frac{S(0.5-3.0\,{\rm keV})}{t}\,\frac{\int_{0.5}^{3.0} E^{-\alpha_x} e^{-a(E)N_H}\,dE}{\int_{0.5}^{3.0} A(E)E^{-(1+\alpha_x)}e^{-a(E)N_H}\,dE} \quad (3.2.1.5.a)$$

where $a(E)$ is the photoelectric absorption cross-section as a function of energy (E) for a gas of solar composition (Brown and Gould 1970) but expressed per hydrogen atom, N_H is the column density of absorbing gas in the Galaxy (assuming no intrinsic absorption in the source), α_x is the (energy) slope of an assumed X-ray power law spectrum in the 0.5–3.0 keV band, and $A(E)$ is the effective energy of the IPC/telescope as a function of energy.

The IXLUM algorithm actually includes in A(E) corrections for vignetting (loss of mirror reflection efficiency off-axis), scattering (correction for counts scattered outside the 3′ circle by small scale mirror imperfections), and source photons that fall outside the 3′ circle because of the pulse height (*i.e.*, energy) dependence of the point response function. These corrections are much less critically dependent on the assumed input X-ray spectrum than they would be for the optimally sized detect cell. Also, it is important to note that, for the grism/grens selected QSOs discussed here, a recent recalibration of the IPC effective area has been used which causes the X-ray fluxes listed here to be systematically $\sim$ 10% higher than the values which would have been found using the earlier calibration; most results in the literature published prior to $\sim$ 1983 used the old calibration and this systematic offset must be kept in mind when comparing results.

Note from Eq. 3.2.1.5.a that in converting a broadband count rate into a broadband flux, it has now become necessary to assume an X-ray spectrum. Following the usual practice (*e.g.*, Zamorani *et al.* 1981), it is assumed that the average QSO spectrum (at least in the 0.5–3.0 keV range) is a power law with spectral (energy)

index of 0.5. This spectrum has been traditionally assumed for it is similar to the value, $\alpha_x = 0.4$, found for the spectrum of the diffuse X-ray background in the 3-20 keV band (Schwartz 1979), and that of the famous QSO 3C 273, also ~ 0.4 as well (Worrall *et al.* 1979). However, a number of workers have since shown that for lower luminosity AGN (particularly Seyfert 1s) the mean spectrum between 0.7 and 100 keV can be adequately described by a power law of spectral (energy) index $\alpha_x \sim 0.7 - 0.8$ (Mushotzky *et al.* 1980, Rothschild *et al.* 1983, Petre *et al.* 1984). Further, recent work by Elvis and collaborators (e.g., Elvis and Lawrence 1985), indicates that the mean value for low redshift ($z < 0.2$) optically bright QSOs from the Bright Quasar Survey (Schmidt and Green 1983) may be much closer to $\alpha_x = 1.0 - 1.2$, with a wide dispersion about the mean. These results suggest that the X-ray spectra of QSOs may well be (in the mean) considerably steeper than $\alpha_x = 0.5$.

For broadband fluxes, this uncertainty is not so important: for a typical object in the sample, changing the assumed power law spectrum from 0.5 to 1.2 decreases the flux estimate by $\leq 15\%$. However, this uncertainty is compounded for a monochromatic flux determination (see Eq.3.3.b.). The diffuse X-ray background intensity is well measured only above $\approx$ 2 keV, and yet the IPC and HRI have responses such that they have an "effective" energy response (for a typical QSO spectrum) of 1–2 keV; thus, the common practice is to compare the Einstein and diffuse X-ray background data in terms of monochromatic fluxes at 2 keV. The broadband response of the IPC is such that if the actual X-ray slope is of order unity rather than 0.5, the inferred monochromatic flux at 2 keV for a QSO (or *e.g.*, the contribution of QSOs to the X-ray background at 2 keV) will be overestimated by $\sim$ 40%. Of course, if the slope is actually of order unity, not only has the percentage contribution of QSOs to the background been markedly overestimated, but it is also quite

difficult (without some very ad hoc assumptions) to reconcile the composite X-ray spectra of a superposition of QSOs with that of the diffuse X-ray background. The rationale adopted here is that, if QSOs *do* dominate the background, they must have a spectrum consistent with it, and thus for the current study, the canonical $\alpha_x = 0.5$ will continue to be assumed in this paper. (Note that this spectrum is also assumed in the definition of the optimal QSO for which the LDETECT/MDETECT algorithms are optimized in the broad and hard energy bands). Thus, an implicit assumption is made that that there is some spectral evolution (or intrinsic slope break) that accounts for the apparent difference between the X-ray spectra of *e.g.*, the Bright Quasar Survey objects, and those which could conceivably contribute substantially to the background. Note that since later I will use my new data to derive a relatively small upper limit on the contribution of high redshift QSOs to the diffuse X-ray background, the assumption of $\alpha_x = 0.5$ rather than 0.8 or 1.0 merely makes this upper limit a more conservative one. In further defense of this assumption (even though in the current application it is a conservative assumption, and therefore probably needs no further defense), it should be noted that currently there are no observations available for X-ray spectra of the sort of QSOs which might contribute substantially to the background to contradict this assumption: such QSOs are too faint for the current X-ray instrumental sensitivities.

In equation 3.2.1.5.a., a value for the column density of neutral hydrogen in the Galaxy is also required. Values of N_H as a function of sky position have been derived by Heiles (1975) from 21 cm radio observations, and these values are used here. The uncertainties of N_H have only a small effect on the broadband flux calculation of Eq.3.2.1.5.a., and indeed Tananbaum *et al.* (1979), have shown that the combined effect of varying α_x from 0 to 1, and N_H from 0 to $10^{21}\,\mathrm{cm}^{-2}$ causes only a $\pm 15\%$ uncertainty in the quoted broadband fluxes (in the mean). There

are also variations in the IPC "gain" which cause uncertainties in the relationship between energy boundaries and pulse height channels; the combination of this latter uncertainty and those associated with α_x and N_H should lead to a total uncertainty in broadband fluxes of $\sim 30\%$ (Tananbaum *et al.* 1979).

3.2.2 The High Resolution Imager (HRI)

The High Resolution Imager (Giacconi *et al.* 1979a, 1981) is also a two dimensional X-ray imaging instrument providing broadband ($\sim 0.1 - 4.5\,\mathrm{keV}$) imaging and flux information. It is constructed of two microchannel plates (*e.g.*, see Gursky and Schwartz 1974) coupled in in a cascade approach for high gain. Each plate consists of a two-dimensional array of glass tubes ("channels") with length to diameter ratio of 80 and small center to center tube spacing. The input face to the first plate is coated with MgF_2, a photoelectric converter material. An incident X-ray photon photoionizes an electron on the face of the first plate, or on the interior surface of the MgF_2 photocathode coated channels. With a high voltage applied, the photoionized electrons are accelerated and collisionally ionize further atoms along the channel walls, producing a cascade of electrons. Positional information is available, since the electrons are roughly confined to within the diameter of the channels, and the charge is collected on a fine crossed wire grid. Spatial resolution of a few arc sec is obtained over a field of $\sim 27' \times 27'$. The HRI provides high spatial resolution but at the expense of spectral information, field of view, and sensitivity compared with the IPC. In the current application, the primary interest is to push to very faint X-ray flux levels, and so only a few very long HRI fields have been included in our grism/grens survey. Note that because, the HRI lacks energy resolution, it is strictly a *broadband* device, and one does not have the luxury of excluding data from the energy ranges $\leq 0.5\,\mathrm{keV}$ and $\geq 3.0\,\mathrm{keV}$; this introduces added uncertainty

into the conversion of HRI count rates into fluxes.

The non-Xray background count rate of the HRI is $\sim$ 10 times that of the diffuse X-ray background and arises primarily from the following three causes: field emission on the microchannel plate defects; (2) UV sensitivity to geocoronal Lα; (3) cosmic rays and trapped particles, in *e.g.*, the South Atlantic Anomaly (see EORUM).

Similar considerations (*e.g.*, the point response function is again energy dependent) to those discussed above for the IPC apply to the HRI as well. For the handful of grism/grens selected QSOs with X-ray information in the HRI, I have checked for the reality of sources in a fashion similar to that described above for the IPC. Sources found by the automated source finding algorithms are checked for positional coincidence of $\leq 11''$ (note that most of this uncertainty is due to the optical uncertainty) with the grism/grens selected QSOs, and smoothed X-ray contour maps were made. Finally, I have followed the approach outlined by Marshall (1983) as a further check. At the location of each optically selected QSO, I used an optimally sized circular detect window (optimum for the optimal QSO): the size of this circle is $6.8''$ for source $\leq 7'$ off axis, and is $13.5''$ for sources $\geq 10'$ off-axis; between $7'$ and $10'$ off-axis, both sized windows were checked. The background is estimated from a nearby $4' \times 4'$ box (the background doesn't vary much over the field of view), which contains neither the optically selected QSO, nor any obvious X-ray sources. A detection is again defined as 5σ in the optimally sized circular window.

Using an HRI algorithm, HXLUM, analogous to the IPC algorithm IXLUM, count rates and fluxes (or upper limits) are again estimated using a larger than optimally sized window (again this practice helps eliminate some of the uncertainty in obtaining a broadband count rate for a source whose spectrum is not known

a priori); in this case it is an $18''$ radius circular detect window. As such, some real sources have rather large uncertainties associated with their count rates and fluxes. The broadband nature of the HRI, and is responsiveness to soft photons are such that flux determinations are considerably more sensitive to the assumed input X-ray spectral parameters. Galactic absorption effectively creates a lower energy cutoff in the HRI response, and so varying N_H from 0 to $10^{21}\,\mathrm{cm}^{-2}$, can change the count rate to bradband flux conversion factor by $\sim 40\%$; a similar uncertainty results from the uncertainty in spectral index α_x (Tananbaum *et al.* 1979). Such large uncertainties, are a further motivation for concentrating mainly on X-ray information from the IPC; whenever both HRI and IPC information of comparable sensitivity are available for an optically selected QSO, the IPC is taken to be the more reliable estimator of X-ray fluxes.

3.3 X-Ray Fluxes, Luminosities, Luminosity Ratios, etc. for Grism/Grens Selected QSOs

Observed broadband fluxes (or upper limits) are translated into broadband fluxes corrected for Galactic absorption of X-rays using the N_H data from Heiles (1975). Then, assuming the canonical X-ray spectral index value of $\alpha_x = 0.5$, these corrected broadband fluxes are converted into monochromatic luminosities at 2 keV in the QSO frame (for later comparison with the optical luminosities of the QSOs). The following relations are used:

$$F_{\mathrm{cor}}(0.5-3.0\,\mathrm{keV}) = F_{\mathrm{obs}}(0.5-3.0\,\mathrm{keV})\,\frac{\int_{0.5}^{3.0} E^{-\alpha_x}\,dE}{\int_{0.5}^{3.0} E^{-\alpha_x}\,e^{-a(E)N_H}\,dE} \qquad (3.3a)$$

$$l_{2\mathrm{keV}} = \frac{4\pi D_l^2\,F_{\mathrm{cor}}(0.5-3.0\,\mathrm{keV})}{\nu_{2\mathrm{keV}}}(1+z)^{\alpha_x-1}\left[\left(\frac{3\,\mathrm{keV}}{2\,\mathrm{keV}}\right)^{1-\alpha_x} - \left(\frac{0.5\,\mathrm{keV}}{2\,\mathrm{keV}}\right)^{1-\alpha_x}\right]^{-1} \qquad (3.3b)$$

It is useful to compare the ratio of X-ray and optical monochromatic luminosities; this ratio will be nicely independent of uncertainties in the cosmological parameters H_0 and q_0, and allows ready comparison of the relative X-ray emissivities of QSOs of a variety of optical luminosities. The traditional way of doing this (*e.g.*, Tananbaum *et al.* 1979), and the practice followed here, is to define a quantity α_{ox} which the slope of a hypothetical power law connecting optical and X-ray waveband (specifically between 2500 Å and 2 keV in the QSO frame); that is

$$\alpha_{ox} = -\frac{\log(l_{2\,\mathrm{keV}}/l_{2500})}{\log(\nu_{2\,\mathrm{keV}}/\nu_{2500})} = -[\log(l_{2\,\mathrm{keV}}/l_{2500})]/2.605 \qquad (3.3.c)$$

Note that a higher value of α_{ox} corresponds to a lower value of the ratio $l_{2\,\mathrm{keV}}/l_{2500}$ and that an upper limit on $l_{2\,\mathrm{keV}}$ corresponds to a lower limit on α_{ox}.

Presented in Table 3.3.a. are the X-ray data for the grism/grens selected sample C and N QSOs defined in Chapter 2. Listed are observed broadband X-ray fluxes (0.5–3.0 keV), X-ray luminosities at 2 keV in QSO reference frame (or upper limits), and values (or lower limits) for α_{ox}. Even at these most sensitive of any current X-ray sensitivities, only $\sim 27\%$ (21/78 for sample N, and 10/37 for sample C) of the grism/grens selected objects are detected in X-rays. Note that a few of the objects selected from the grism plates do not lie within the X-ray image; in general, the position angle of the (square) X-ray image is at some arbitrary angle with respect to that of the (square) grism/grens plate, and so the useful area of overlap between the two is reduced (by losses at the corners, for example).

Table 3.3.a: X-Ray Data for Sample C and N QSOs

Object	Sign.	$F_{obs} \times 10^{13}$ (0.5-3.0 keV)	log ($l_{2\,\mathrm{keV}}$)	α_{ox}
Obj. 1	2.7	0.493	27.59	1.36
00151 + 160	0.7	< 0.688	< 28.24	> 1.19
00159 + 155	0.2	< 0.565	< 27.70	> 1.29
01121 − 014				
02036 + 150	1.3	< 0.633	< 27.65	> 1.41
02031 + 151	−0.7	< 0.641	< 27.60	> 1.34
02031 + 152				
Obj. 2	3.0	0.689	27.90	1.56
Obj. 3	6.2	1.280	28.06	1.20
02057 + 150				
03057 + 172				
03061 + 169	2.1	< 0.645	< 27.71	> 1.34
Obj. 4	3.6	0.597	27.59	1.54
03074 + 172				
Obj. 5	4.8	0.523	27.61	1.65
Obj. 6	2.8	0.422	27.49	1.60
Obj. 7	3.4	0.925	27.86	1.46
Obj. 8	4.4	1.110	28.33	1.50
08366 + 654	0.4	< 0.728	< 27.59	> 1.53
08388 + 131	2.1	< 0.766	< 27.60	> 1.51
08388 + 133	1.7	< 0.735	< 27.53	> 1.53
08500 + 283	0.2	< 0.692	< 28.07	> 1.55
09038 + 167	0.0	< 0.882	< 27.95	> 1.61
09379 + 121	−0.2	< 0.601	< 27.91	> 1.56
09382 + 117	−0.1	< 0.670	< 27.77	> 1.38
09382 + 120	1.3	< 0.576	< 27.54	> 1.49
09383 + 120	−0.8	< 0.597	< 27.77	> 1.36
09388 + 117	2.0	< 0.683	< 27.73	> 1.59
09392 + 121	1.6	< 0.629	< 27.46	> 1.54
09392 + 117	2.2	< 0.652	< 27.54	> 1.41
Obj. 9	2.9	0.685	27.68	1.35
11131 + 183	−0.6	< 0.593	< 27.65	> 1.60
11136 + 182	−2.0	< 0.682	< 27.54	> 1.44
11143 + 184	2.1	< 0.661	< 27.70	> 1.33
11156 + 180	1.9	< 0.795	< 27.61	> 1.63
11147 + 183	1.8	< 0.692	< 27.55	> 1.40
12071 + 398	1.8	< 0.608	< 27.73	> 1.49
12076 + 399	0.1	< 0.680	< 27.81	> 1.76
Obj. 10	3.5	0.765	27.69	1.48
Obj. 11	2.8	0.265	27.60	1.48
12275 + 034	−0.5	< 2.690	< 28.20	> 1.12
12292 + 116	2.0	< 0.747	< 27.53	> 1.39
12302 + 120	−0.4	< 1.310	< 27.83	> 1.39
12336 + 264				
12354 + 264	1.1	< 0.599	< 27.81	> 1.49
Obj. 12	3.3	0.876	27.66	1.44

Obj. 13	3.4	0.914	27.79	1.32
Obj. 14	4.5	1.220	27.97	1.24
Obj. 15	2.1	< 0.648	< 28.06	> 1.56
Obj. 16	−0.2	< 0.459	< 28.27	> 1.56
14144 + 256				
14148 + 252	2.1	< 0.552	< 27.41	> 1.46
14149 + 251	−0.9	< 1.160	< 29.49	> 0.82
14151 + 254	1.6	< 0.653	< 27.86	> 1.45
15090 − 092	1.5	< 2.610	< 28.15	> 1.16
15100 − 089	0.2	< 1.250	< 28.37	> 1.07
15181 + 201				
15184 + 202	−0.9	< 0.512	< 27.56	> 1.45
16016 + 184	2.3	< 0.625	< 27.75	> 1.34
16017 + 184	1.5	< 0.578	< 27.51	> 1.54
Obj. 17	2.7	0.664	27.92	1.54
17252 + 499	−2.0	< 0.594	< 27.50	> 1.42
17257 + 503	−0.3	< 0.558	< 27.59	> 1.37
17264 + 504	1.4	< 0.564	< 27.48	> 1.43
17272 + 502	< 87.7	$< 1.53 \times 10^4$	< 30.03	> 0.63
17272 + 499	−1.2	< 0.633	< 27.53	> 1.50
17274 + 503	< 2.1	< 0.521	< 27.61	> 1.55
17449 + 206				
17465 + 201	0.3	< 0.646	< 28.56	> 1.18
Obj. 18	10.1	2.050	28.13	1.41
Obj. 19	2.9	0.693	27.70	1.51
Obj. 20	7.9	2.800	28.41	1.13
20374 − 007				
20381 − 011	1.5	< 0.643	< 27.76	> 1.34
20382 − 012	2.1	< 0.561	< 28.00	> 1.62
21180 + 168				
21259 − 148	1.6	< 0.674	< 27.79	> 1.38
Obj. 21	2.7	0.688	27.74	1.48
21265 − 150	0.6	< 0.662	< 27.67	> 1.35
21342 − 149	1.3	< 0.710	< 27.75	> 1.63
21354 − 145	1.2	< 0.787	< 27.63	> 1.36
21357 − 147	2.0	< 0.715	< 27.70	> 1.49
21416 + 037	1.2	< 0.658	< 27.52	> 1.36
21431 + 040	−1.6	< 0.836	< 27.72	> 1.48
21558 + 034	0.7	< 0.712	< 27.59	> 1.52
21556 − 302	< 2.1	< 1.130	< 27.94	> 1.46
21570 − 302	1.7	< 1.080	< 27.75	> 1.54
1624 + 266			27.50	1.76
1623 + 270			< 27.63	> 1.55
0131 − 402			27.77	1.32
0132 − 405			< 27.44	> 1.58
0130 − 403			27.97	1.43
0132 − 402			27.83	1.44
0131 − 404			< 27.54	> 1.41
0131 − 405			< 27.58	> 1.52

0130 − 404	< 27.62	> 1.64
0132 − 405	< 27.56	> 1.41

Notes to Table 3.3 a:

(1) "Sign." is the ratio of source counts/(background counts)$^{1/2}$ in 3′ circle.

(2) $F_{obs}(0.5 - 3.0\,keV)$ is the observed broadband X-ray flux or limit in units of erg/cm^2/sec. log ($l_{2\,keV}$ is the logarithm of the monochromatic X-ray luminosity at 2 keV in the frame of the QSO, in units of erg/sec/Hz. The parameter α_{ox} is defined and discussed in the text.

(3) The last 10 rows in Table 3.3.a give relevant information on the X-ray emission from 10 QSOs (also grism selected) previously studied in X-rays by Kriss and Canizares (1985).

(4) See Appendix A for an exaplanation of nomenclature "Obj. 1".

(5) Objects with incomplete X-ray information are those QSOs which lie within an optical grism/grens plate, but lie outside the usable area of the X-ray image (*e.g.*, on the "ribs in the IPC).

At the very sensitive limiting X-ray flux levels of these images, the chance of a spurious positional coincidence between a grism/grens selected QSO and a physically unrelated X-ray source is non-negligible. For example, a typical limiting sensitivity for the IPC images employed here is 5×10^{-14} erg/sec/cm^2 in the 0.5-3.0 keV band; use of the logN-logS (surface density versus limiting X-ray flux) curve of X-ray sources from the Deep Survey study of Giacconi *et al.* (1979b), predicts the order of 11 X-ray sources per square degree to such a limiting sensitivity. Then associating with each X-ray source an error circle of radius 1 arc minute, and assuming a surface density of $\sim$ 5 sample N or C QSOs per square degree, there should be approximately one chance coincidence of a grism/grens selected QSO and an unrelated X-ray source. Thus, the observed detection fraction of $\sim$ 27% given above is likely to be a small overestimate of the actual number.

Recalling (see discussion in Chapter 2) that the comparably optically faint Bracessi QSOs with X-ray information (also of comparable sensitivity) available were detected in $\sim$ 50% of the cases (Marshall 1983), gives the first qualitative indications that these high redshift QSOs might have lower ratios of X-ray to optical emissivities than their lower redshift/lower optical luminosity counterparts.

One way to parameterize the mean X-ray to luminosity ratio of a collection of QSOs is the parameter $\alpha_{ox}^{\rm eff}$ (Tananbaum *et al.* 1979). In analogy with the definition of α_{ox} above, this parameter is defined to be

$$\alpha_{ox}^{\rm eff} = -[\log < l_{2\,\rm keV}/l_{2500} >]/2.605 \qquad (3.3.d)$$

where $< l_{2\,\rm keV}/l_{2500} >$ is the (cosmology independent) mean of the $l_{2\,\rm keV}/l_{2500}$ ratio for the sample. Note that $\alpha_{ox}^{\rm eff}$ is not the same as the mean α_{ox}

$$< \alpha_{ox} > = - < \log (l_{2\,\rm keV}/l_{2500} > /2.605 \qquad (3.3e)$$

In order to determine these mean parameters for the grism/grens selected objects, and compare with other samples (*e.g.*, the Bracessi samples), it is essentail to use a statistical approach which incorporates information contained in the non-detections. These statistical techniques will be described in the next chapter.

3.4 Summary

The archived X-ray data on the QSOs of sample N and C have been presented. A detailed discussion of the definition of an X-ray detection has been given, and some of the uncertainties and difficulties associated with converting broadband X-ray count rates into fluxes and luminosities have been discussed. Even at these most sensitive of all currently available X-ray flux data, only 27% of the class N and class C QSOs are detected in X-rays.

4. TWO STATISTICAL APPROACHES FOR INCORPORATING INFORMATION IN X-RAY NON-DETECTIONS

In the previous chapter the fraction of X-ray non-detections was found to be quite high among the grism/grens selected samples C and N. In order to effectively examine the ensemble X-ray properties (*e.g.*, $\alpha_{ox}^{\rm eff}$, or contribution to the X-ray background) of these optically selected QSOs, it is necessary to use statistical approaches which incorporate information contained in the X-ray non-detections as well as that in the detections. Two such statistical techniques that deal with such "censored" data (data with some upper or lower limits) are briefly described in the current chapter.

The first approach, called "survival analysis" has been widely used in studies of the X-ray properties of QSOs, and indeed was introduced to the astronomical community primarily for its use in such studies. However, I show in this chapter that, at least in the presence of a substantial non-random censoring, the results of conventional survival analysis should be very cautiously interpreted; this point has not been stressed much in the astronomical literature thus far. Survival analysis is powerful in the sense that it allows an estimation not only of single ensemble parameters like $\alpha_{ox}^{\rm eff}$, but also of, for example, the distribution function of α_{ox} values; again, I demonstrate that it can be a rather poor estimator of the actual distribution in the presence of significant non-random censoring.

The second technique, "stacking", has not had any widespread usage in X-ray studies of QSOs, although its use is common in other areas of astronomical research. This alternate approach serves as a useful check on the results of survival analysis for the estimation of some ensemble X-ray parameters; however, it does not serve as an estimator of distribution functions.

4.1 Introduction to Survival Analysis

The first technique ("survival analysis") was introduced into widespread astronomical use for precisely the current sort of application: Avni *et al.* (1980), developed a technique (which they called "detection and bounds") for incorporating information contained in lower limits; primarily the technique was developed with the intention of investigating the distribution function of α_{ox} for the famous QSOs which were among the targets of pointed Einstein Observations. Pfleiderer and Krommidas (1982) independently developed a similar technique for astronomical application to studies of extragalactic radio sources.

More recently it has been realized that the "detections and bounds" method is a... independent redevelopment of a statistical approach known as "survival analysis" which was already in widespread use in the fields of epidemiology, actuarial science, and industrial reliability (Feigelson and Nelson 1985, Schmitt 1985). Through several decades of statistical research in such fields, survival analysis has been extensively developed so that although the detections and bounds method is a correct formulation (to the great credit of Avni *et al.* and Pfleiderer and Krommidas!), the available survival analysis literature contains more analytically elegant or computationally efficient formulations. Indeed, there are a number of monographs on survival analysis available in the statistical literature (*e.g.*, Kalbfleisch and Prentice 1980, and references in Feigelson and Nelson and in Schmitt), and even several statistical analysis packages (*e.g.*, SPSS, BMDP, and IMSL) in widespread use at large computing facilities which have routines already in place to carry out the computations.

In order to familiarize the reader with the technique and to present some examples of its limitations not previously stressed in the astronomical literature, I

give below a very brief introduction to the formulation of survival analysis that will be used extensively in the current study. For more thorough introductions to the field (with emphasis on astronomical applications), the author highly recommends the papers by Avni *et al.*, Feigelson and Nelson, and Schmitt. Much of my review below is based on material from these excellent sources.

Survival analysis derives its name from its most common (non-astronomical) applications. A typical example is the following: a biomedical researcher is interested in testing the effectiveness of a drug in prolonging life in patients with a terminal disease, and is therefore interested in the time to death (or *survival* time) of the patient undergoing treatment. The limitations of funding and the need to publish promptly require that the initial study be completed within a few years. During the course of this study, some patients die, but some do not, and thus the researcher has available a list survival times for some patients but only lower limits on the survival times for the patients who have survived to the end of the study. The researcher clearly does not want to throw away the information contained in these lower limits; these are his successes and the key to future funding. Additionally, patients may be "lost" to the study, *e.g.*, they may drop out of the research program while still alive, and again the researcher is not eager to neglect the information that these patients were alive (lower limit on survival time) when they left the study.

In the current application to QSOs, there are objects detected in X-rays for which α_{ox} is known and lower limits on α_{ox} for other objects. The survival analysis technique can readily handle the circumstance in which upper limits instead of (or even in addition to) lower limits are available, for example, when considering X-ray flux or luminosity data (rather than α_{ox}).

4.1.1. Kaplan-Meirer Product Limit Estimate for the Distribution of a Censored Variable

A simple and convenient way of estimating (in non-parametric fashion) the distribution of a random variable in the presence of "right" (lower limit) censoring has been given by Kaplan and Meirer (1958). Presented below is a intuitive plausibility argument for the result they derived more formally in a maximum likelihood formulation. The Avni *et al.* Detections and Bounds formulation is equivalent, but is analytically more complicated, making it (and associated error analysis) computationally less efficient.

Suppose it is desired to estimate the distribution function of α_{ox} values for a sample of n QSOs in the presence of censoring. That is, α_{ox} values are measured for some objects, but for some objects only a lower limit on α_{ox} is known. Assume α_{ox} to be be a random variable (*e.g.*, α_{ox}) distributed with probability density $f(\alpha)$ so that $f(\alpha_{ox})d\alpha$ is the probability that α is in the interval $(\alpha_{ox}, \alpha_{ox}+d\alpha)$. *A fundamental point, to be discussed again below, is that the implicit assumption has now been made that detections and non-detections arise from the same parent population.* Let $S(\alpha_{ox})$ be the so-called "survivor function", the probability of finding a QSO with $\alpha > \alpha_{ox}$ (in the more common down-to-earth applications of survival analysis, α's would be replaced by, *e.g.*, the times to death, so that $S(T)$ would be the probability a patient would survive a time $t > T$). Then,

$$S(\alpha_{ox}) = \int_{\alpha_{ox}}^{\infty} f(\alpha)d\alpha, \quad \text{and} \quad f = -dS/d\alpha. \qquad (4.1.1.a)$$

Let α_i be the the true value of α_{ox} for the ith QSO, and $\alpha_i^{\rm lim}$ be the corresponding detection limit (this will vary from QSO to QSO, and image to image). If $\alpha_i \leq \alpha_i^{\rm lim}$, the object is detected in X-rays, otherwise it is only known that

$\alpha_i > \alpha_i^{\rm lim}$. Then let $a_i = \min(\alpha_i, \alpha_i^{\rm lim})$ be the measurement of (or limit on) α_{ox} for the ith QSO; for simplicity assume that the measurements have been ordered so that $a_1 < a_2 < \ldots < a_i \ldots a_n$.

Let $n_i(\alpha_i)$ be the number of objects in the sample with measurements (detections or lower limits) $a > a_i$. Let $d_i(\alpha_i)$ be the number of detections at α_i, and p_i be the conditional probability that a QSO will have $\alpha_{ox} > \alpha_i$, given that it is known to have $\alpha_{ox} > \alpha_{i-1}$. Then an estimate of p_i is:

$$p_i = \frac{n_i - d_i}{n_i} \qquad (4.1.1.b)$$

From the usual multiplicative rules for conditional probabilities

$$S(\alpha_{ox}) = \Pi \left(1 - \frac{d_i}{n_i}\right). \qquad (4.1.1.c)$$

$$i : \alpha_i < \alpha_{ox}$$

This relation is the Kaplan-Meirer product limit estimator of the survival function, and it can be shown to be the maximum likelihood estimator of the survival function. In the case of a tie between a lower limit and a detection, the usual procedure is to treat the lower limit as if it is slightly larger than the detection. If the largest observation is censored then Eq. 4.1.1.c. shows that $S(\alpha_{ox})$ is finite as α_{ox} approaches infinity; to avoid this unphysical result, the usual procedure (*e.g.*, Feigelson and Nelson), is to treat the largest observation as uncensored, even when it is censored.

The mean value of α_{ox} is readily estimated from

$$< \alpha_{ox} >= \int_0^\infty \alpha f(\alpha) d\alpha = \int_0^\infty S(\alpha) d\alpha, \qquad (4.1.1.d)$$

$$= \sum_{i=1}^{n+1} S(a_i)\,(a_i - a_{i-1})$$

where $\alpha_0 = 0$, $\alpha_{n+1} = \infty$, and $0 \cdot \infty = 0$ (Feigelson and Nelson 1985). Again, if a_n is censored $s(\infty) > 0$, and $< \alpha_{ox} >$ is infinite. The usual practice is to again treat a_n as a detection even if it is censored.

Analytical estimates of the uncertainties in the mean of the sample and the survival function are available but have complicated expressions. The interested reader is referred to Feigelson and Nelson (1985) (and references contained therein) for such formulae.

Although it is straightforward to reformulate the statistics for "left" censored data (data involving upper limits), note that one also can readily handle left censored data merely by transforming it into right censored data (Feigelson and Nelson 1985). For concreteness, consider the monochromatic luminosity ratio $r = l_{2\,\rm keV}/l_{2500}$; for X-ray nondetections only an upper limit is available on this quantity. Let r_i be the ith measurement of or upper limit on this ratio for the ith QSO. Then, for some (sufficiently large) constant M, one simply makes the transformations $r_i' = M - r_i$. Then the r_i's constitute a set of right censored data. Then the mean value of r for a sample of QSOs is just $< r >= M - < r' >$. Note that this is precisely the quantity needed to obtain $\alpha_{ox}^{\rm eff}$ (see Eq. 3.3.d.).

4.1.2 Some Problems with Survival (Analysis)

4.1.2.1 Threshhold Effects

An issue of current controversy (*e.g.*, Chanan 1983, Kriss and Canizares 1985) is that of the significance and consequences of X-ray threshold and optical threshold effects in obscuring the true nature of the parent distribution of such quantities as α_{ox}. For example, Chanan has demonstrated that the combination of reasonable

optical and X-ray thresholds (coupled with a wide α_{ox} distribution) can potentially lead to to apparent but spurious relations between α_{ox} and l_{2500} of the sort found by Avni and Tananbaum (1982) (*i.e.*, a correlation between α_{ox} and optical luminosity). One hope has been that by using survival analysis and incorporating the information contained in lower limits on α_{ox}, such spurious threshold effects would be negated. The effects of non-random thresholds have not been previously emphasized in the astronomical literature from the point of view of survival analysis, although Chanan has argued from an alternate point of view that they are likely to be present. The hazards of non-random thresholds (pattern censoring) have been discussed in the statistical literature (*e.g.*, Kalbfleisch and Prentice 1980).

By Monte Carlo techniques, I have investigated some of the consequences of the interactions between survival analysis and detection thresholds. These interactions can indeed lead to misleading results especially in the presence of significant non-random censoring. Note that threshold effects in α_{ox} units correspond to joint thresholds in optical and X-ray flux sensitivities.

Using a Gaussian random number generator with input $< \alpha_{ox} >= 1.56$, and input $\sigma = 0.2$, I have generated a synthetic α_{ox} distribution with approximately Gaussian form (see Figure 4.1.2.1); the input mean is in anticipation of results discussed in the next chapter for sample N, while the input value of σ is taken from Avni and Tananbaum (1982). This Gaussian form is *not* intended to necessarily represent the actual distribution of α_{ox}, but is merely used as a convenient computational form. For the specific distribution of Figure 4.1.2.1.a, the output means are $< \alpha_{ox} >= 1.55 \pm 0.02$ and $\sigma = 0.2$, while the $\alpha_{ox}^{\rm eff}$ for this distribution is 1.45 ± 0.02.

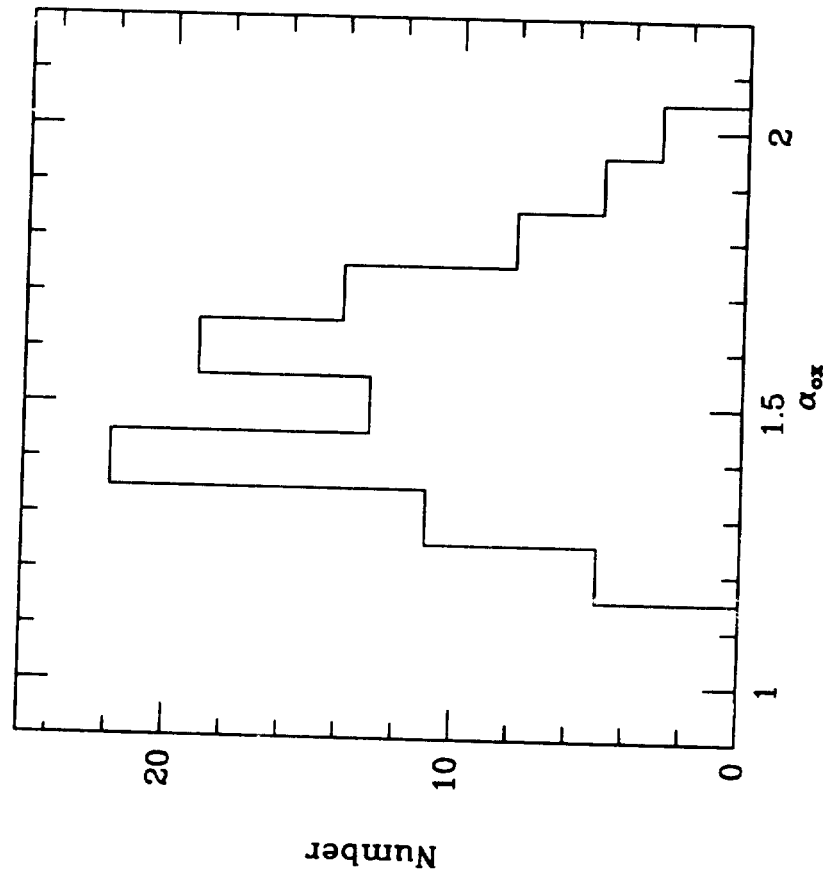

Figure 4.1.2.1.a. Gaussian synthetic distribution of α_{ox} values for use in Monte Carlo studies of the interaction of survival analysis and thresholds.

First, consider this distribution to be an idealized sample N sort of distribution; in particular, suppose it to be the α_{ox} distribution of 100 QSOs all of the same optical luminosity and redshift (sample N, it will be recalled, is a sample of objects in a narrow range of redshift luminosity space). Further, assume that all 100 QSOs in this idealized sample are imaged in X-rays to a uniform flux sensitivity limit (this is also roughly true for sample N QSOs). Then, for this idealized sample, the X-ray flux limit directly translates into a uniform lower limit on α_{ox} for the sample. Now let us impose this uniform X-ray flux (and hence α_{ox}) threshold on the idealized distribution, and subject the resulting observations to conventional survival analysis, asking what values does survival analysis yield for $< \alpha_{ox} >$ and $\alpha_{ox}^{\rm eff}$. Finally, this entire process is done for several different limiting flux thresholds to try to gain some insight into the interactions between survival analysis and flux thresholds. Again, we follow the standard procedure of treating the highest α_{ox} observation (limit or detection) as though it were uncensored.

The results are shown in Table 4.1.2.1.a. The mean α_{ox} value from survival analysis (even within the errors) is in quite serious disagreement with the true value for this very extreme censoring (threshold) pattern, even when the threshold is sensitive enough to detect $\sim 50\%$. of the objects. The $\alpha_{ox}^{\rm eff}$ value from survival analysis converges more quickly to the true value; this is due to its heavy weighting of X-ray bright objects (*i.e.*, its a geometric rather than arithmetic mean of α_{ox}). Thus, it is seen that $\alpha_{ox}^{\rm eff}$ is a somewhat more reliable parameter in the presence on significant non-random censoring.

Table 4.1.2.1a: Non-Random Threshold Effects in Survival Analysis

$\alpha_{ox}^{\rm thresh}$	$< \alpha_{ox} >$	$\alpha_{ox}^{\rm eff}$	detection fraction
1.3	1.29 ± 0.002 (13.0)	1.29(±0.01) (7.2)	11/100
1.4	1.38 ± 0.005 (8.2)	1.37(−.01, +.005) (3.6)	27/100
1.5	1.44 ± 0.009 (5.0)	1.41(−0.01, +.02) (1.4)	44/100
1.6	1.49 ± 0.013 (2.5)	1.44(−.02, +.01) (< 1)	62/100
1.7	1.52 ± 0.016 (1.2)	1.44(−.01, +.02) (< 1)	78/100
1.8	1.54 ± 0.018 (< 1)	1.45(±0.02) (< 1)	90/100
1.9	1.54 ± 0.019 (< 1)	1.45(±0.02) (< 1)	93/100
2.0	1.55 ± 0.020 (< 1)	1.45(±0.02) (< 1)	99/100
2.1	1.55 ± 0.020 (< 1)	1.45(±0.02) (< 1)	100/100

Note: numbers in the rightmost set of parentheses within the second and third columns show the significance (in σs) of the difference between the survival analysis estimate and the true value.

The reason for the systematic underestimate in the presence of thresholds is easy to understand intuitively. Survival analysis typically assumes that the survivor function $S(\alpha_{ox})$ goes to zero at the highest observation (censored or uncensored). That is, it truncates the distribution; in a non-parametric approach (without some *a priori* knowledge of the distribution function) this is the best it can do. However, such a truncation by thresholds is quite artificial, and, as demonstrated above, can lead to serious systematic underestimates of parameters such as $< \alpha_{ox} >$, or $\alpha_{ox}^{\rm eff}$. Note also that such threshold censoring changes the apparent relation between α_{ox} and $\alpha_{ox}^{\rm eff}$. Further, the error estimates on α_{ox} and $\alpha_{ox}^{\rm eff}$ are also extremely small in the presence of significant threshold censoring. This latter point is also easy to understand in terms of the premature truncation of the estimated distribution: Because of the Gaussian nature of the assumed distribution, there are very few objects at α_{ox}'s much below the truncation threshold (at least for α_{ox} thresholds less than $< \alpha_{ox} >$). Most of the objects are detected quite close to the threshold, and thus the apparent width of the distribution (*e.g.*, standard deviation of the sample, or the mean) is underestimated. In the presence of such non-random thresholds, conventional survival analysis can be a very poor estimator of the actual distribution; the approach assumes that non-detections are distributed randomly.

If one had some *a priori* knowledge of the actual distribution above the threshold, one might think that an appropriate approach is to merely choose a higher value of α_{ox} as the the truncation value of α_{ox} where $S(\alpha_{ox}) = 0$. However, this requires some knowledge which the researcher does not usually have, and indeed then such quantities as $< \alpha_{ox} >$, $\alpha_{ox}^{\rm eff}$, etc., become functions of the presumed truncation point. One approach is an extension of that followed by Avni *et al.*: take the highest observed α_{ox} (censored or not), and treat it as a detection for calculation

of the ensemble mean parameters (this is the standard approach), but estimate the uncertainty in such parameters by conservatively estimating a *(suspected)* reasonable value for the α_{ox} where $S(\alpha_{ox})$ approaches zero for the actual distribution. For the idealized distribution of Figure 4.1.2.1.a, we have the luxury of knowing that an appropriate 3σ limit is ~ 2.1. Following the suggested procedure and using 2.1 for the truncation points in estimating the uncertainty, yields the results for the idealized distribution shown in Table 4.1.2.1.b. (compare with the previous table).

Note that the approach outlined here (and see Avni *et al.* 1981), at least leads to no inconsistencies within the errors between the true and survival analysis estimated values for the parameters α_{ox} and $\alpha_{ox}^{\rm eff}$. However, note that the error bar so defined is not obviously interpretable as the usual 1-sigma uncertainty estimate.

When the nature of the distribution beyond the detections threshold is so uncertain that a reasonable (and conservative!) guess cannot be made as to where the α_{ox} distribution may be considered truncated, then formally, the uncertainties (in $< \alpha_{ox} >$ in the positive direction approach $+\infty$ in the presence of significant threshold censoring. For $\alpha_{ox}^{\rm eff}$, one can obtain a strict limit, by assuming that $l_{2\,\rm keV}/l_{2.00}$ is zero for all non-detections. Then, (and this is also clear from an examination of the previous two tables), it is more appropriate in the presence of significant threshold censoring to consider survival analysis parameter estimates to be good estimates only of a lower limit on $< \alpha_{ox} >$ and $\alpha_{ox}^{\rm eff}$. This also is an intuitive notion: in the presence of significant threshold censoring with many limits near the threshold, the best one can do is also obtain limits on the ensemble parameters.

Table 4.1.2.1.b: Error Estimate with Increased Truncation Value of α_{ox}

α_{ox}^{thresh}	$< \alpha_{ox} >$	α_{ox}^{eff}	detection fraction
1.3	$1.29(+0.748, -0.002)$	$1.29(+0.37, -0.01)$	11/100
1.4	$1.38(+0.546, -0.005)$	$1.37(+0.20, -0.01)$	27/100
1.5	$1.44(+0.377, -0.009)$	$1.41(+0.09, -0.01)$	44/100
1.6	$1.49(+0.164, -0.013)$	$1.44(+0.03, -0.02)$	62/100
1.7	$1.52(+0.089, -0.016)$	$1.44(+0.03, -0.01)$	78/100
1.8	$1.54(+0.054, -0.018)$	$1.45(\pm 0.02)$	90/100
1.9	$1.54(+0.042, -0.019)$	$1.45(\pm 0.02)$	93/100
2.0	$1.55(\pm 0.020)$	$1.45(\pm 0.02)$	99/100
2.1	$1.55(\pm 0.020)$	$1.45(\pm 0.02)$	100/100

Note that in the case of astronomical applications, a detection is generally only a probabilistic statement, *i.e.*, a 3σ detection, or a 4σ detections, etc. The above example of the interaction between thresholds and survival analysis shows that indeed as one changes the definition of a detection, one is, of course, changing the threshold, and thus the parameter estimates from survival analysis will actually change, depending on whether one defines a detection to be 3σ, 4σ, etc. This is true even if there are no further objects detected in the range 3–4 σ. Thus, a conservative approach is to require a high level of statistical significance in defining a detection and treat the results of survival analysis as estimates for limits on the actual distribution parameters.

Now suppose that there are two idealized QSO samples with the identical parent distributions of Figure 4.1.2.1.a, both at the same redshift, but with different optical luminosities. That is, suppose that sample A, composed of objects at optical luminosity l_{2500}^{a} and with redshift z, has the identical parent distribution of α_{ox} values as sample B, consisting of objects with optical luminosity l_{2500}^{b} and also at redshift z; assume that $l_{2500}^{a} > l_{2500}^{b}$. Thus, for these hypothetical idealized samples, I have assumed no dependence of α_{ox} on optical luminosity. Now a uniform X-ray flux threshold is applied to both samples; since sample A is a collection of more luminous objects, it has a more sensitive α_{ox} threshold than sample B, *i.e.*, $\left(\alpha_{ox}^{lim}\right)_A > \left(\alpha_{ox}^{lim}\right)_B$. From the results of Table 4.1.2.1.a (which conceptually also apply to the current hypothetical situation) it is seen that the standard survival analysis would lead to the spurious conclusion that sample B (the lower luminosity sample) with its less sensitive α_{ox} threshold, has lower values for $< \alpha_{ox} >$ and α_{ox}^{eff} than sample A, *i.e.*, that the ratio of X-ray to optical luminosity is higher in the lower optical luminosity sample than in the higher optical luminosity sample. This

result is clearly spurious, since the initial assumption was that both samples had identical α_{ox} distributions. This sort of spurious correlation caused by the introduction of joint optical and X-ray thresholds was discussed by Chanan (1983), and here it is demonstrated that survival analysis is not free from such spurious threshold effects. This same result, of course, applies to any number of samples, with differing (mean) optical luminosities, but at the same redshift; for a given redshift, only the optically (and hence X-ray) moreluminous objects are detected at sufficiently high α_{ox} values that the shape of the actual distribution function is well sampled. The α_{ox} flux thresholds confine the detection of lower optical luminosity objects to lie on the low α_{ox} side of the distribution, and survival analysis spuriously interprets this as implying that the lower luminosity objects have systematically lower α_{ox} values (higher relative X-ray to optical luminosities) than in the high optical luminosity QSOs.

Such possible spurious effect due to the interaction of flux thresholds and survival analysis are cause for special concern. For example, as argued by Chanan and confirmed here for survival analysis, qualitatively such spurious threshold effects could mimic the sort of inverse dependence of α_{ox} on optical luminosity discussed by Avni and Tananbaum (1981), and given physical interpretation by, for example, Tucker (1983). In practice, this sort of spurious threshold effect competes against another sort of observational selection: most high luminosity QSOs are at high redshift, and apparently faint in the optical. This type of optical observational selection factor tends (for a given X-ray flux sensitivity) to make the α_{ox} threshold for high optical luminosity objects systematically smaller than for lower redshift objects. Thus, in practice, one must carefully consider the censoring *pattern* to qualitatively assess the potential influence of threshold effects. I will return to this point in more detail in Chapter 5.

Note that the above sort of sharp cutoff threshold pattern can apply (approximately) to other types of samples as well as to the N-like samples. For example, the surface density of QSOs per unit magnitude is known to increase with limiting magnitude to optical magnitudes fainter than B$\sim$ 20. Thus, in flux limited samples like sample C, where greatest number of objects are close to the optical flux threshold, and where most objects at the flux threshold are at similar redshift, most objects in the sample will be of similar optical luminosity. If such a sample is imaged in X-rays to a uniform flux sensitivity, then for most objects in the sample there will be a common α_{ox} threshold as well. Secondly, consider a set of planned targeted X-ray observations of a collection of QSOs with a wide range of *apparent* optical fluxes. It may be the case that the X-ray observer will scale his planned exposure times to be just sufficiently long enough to get a desired X-ray signal-to-noise ratio, *i.e.*, observation times will be planned assuming a "typical" α_{ox}. Thus, although of very different *apparent* X-ray fluxes, the objects in such a set of targeted observations might be imaged to a fairly uniform α_{ox} threshold.

4.1.2.2 The Assumption of the Identity of Parent Distributions of Detections and Non-detections

As noted above, a fundamental assumption made in survival analysis is that the detections and non-detections arise from the same parent distribution. This is certainly an Occam's razor sort of assumption in X-ray studies of QSO, since it has been demonstrated that substantial fractions (*e.g.*, 50% detection fractions in the work of Marshall (1983) and Kriss and Canizares (1985), and the 86% detection fraction in the PG sample) of QSOs are in fact X-ray emitters. However, that one has made this assumption must be constantly kept in mind. For example, survival analysis of QSOs surveyed in the radio wavebands would lead to extremely

misleading results if one made the assumption that all QSOs were radio emitters. In the latter case there is substantial evidence that there is a dichotomy between radio bright and radio quiet QSOs. If there were a substantial population of X-ray quiet QSOs (Anderson and Margon 1983), including them as non-detections in the survival analysis of a sample of X-ray bright objects could lead to quite erroneous conclusions about the X-ray properties of the QSO population as a whole. The basic point is that there are many (an infinite number of) possible *actual* distributions that can, in the presence of substantial non-random censoring, lead to the same survival analysis *estimated* distribution. For example, imagine there are two populations of QSOs, one with $< \alpha_{ox} > \sim 3$, and the other with $< \alpha_{ox} > \sim 1.5$ (for concreteness, one might imagine two Gaussian distributions, for example). Objects in the X-ray quiet group would not have been sampled given current instrumental sensitivities, and therefore would have only upper limits established in the current data; only objects from the X-ray bright sample would be detected. Thus, survival analysis, assuming that all QSOs arise from the same parent distribution of α_{ox} values, would erroneously give back a mean $< \alpha_{ox} >$ of order 1.50 for the entire QSO population. As a specific example, I have artificially generated a subsample of X-ray quiet QSOs by translating the distribution of Figure 4.2.1.1.a to a mean $< \alpha_{ox} >= 3.0$. Then I have applied survival analysis with a uniform α_{ox} threshold of 1.60 to the double peak distribution of Figure 4.1.2.2.a, but incorrectly assumed that detections and non-detections arise from the same parent population. The true mean of the actual distribution is ~ 2.25, but the value found from the incorrectly applied survival analysis is 1.54 ± 0.01 (assuming the standard truncation).

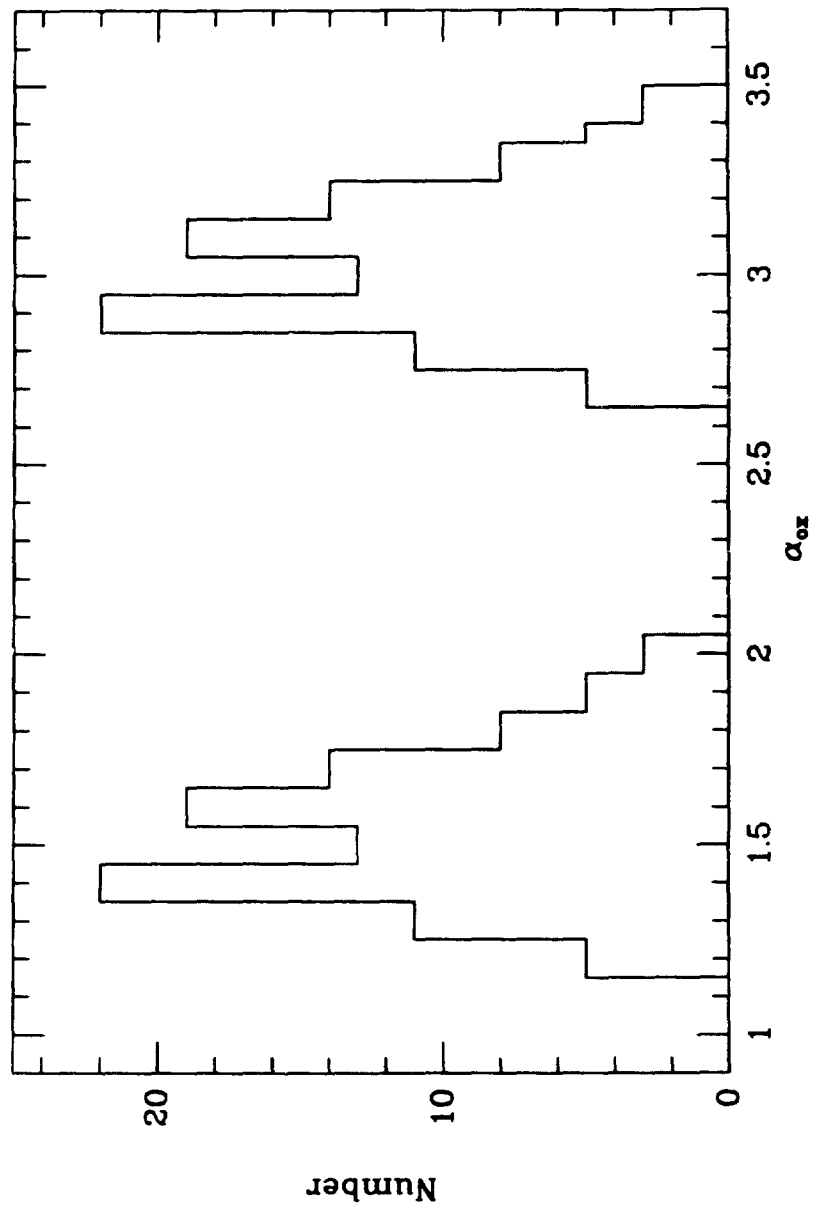

Figure 4.1.2.2.a. Synthetic double peaked distribution illustrates some potential hazards of assuming that non-detections arise from the same parent distribution as detections.

Again, the basic moral is "you don't get something for nothing", or, more properly, you don't get everything for something: in order to uniquely specify the form of the actual distribution, one must have the a very substantial number of detections, and these detections must sample the distribution over the entire range of possible α_{ox} values. In this sense again, the PG (with its $\sim$ 86% detection fraction) sample is the best hope for getting at what the actual distribution looks like (although of, course, one might still argue cogently that the PG QSOs are not very representative of typical QSOs).

4.2 Stacking

Given the sorts of uncertainties noted above for survival analysis, it is desirable to have a second technique to check the former results. Stacking of images is done commonly in optical astronomy to take very deep (*i.e.*, optically sensitive) optical pictures. Caillault and Helfand (1985) have innovatively applied stacking techniques to X-ray images of the Pleiades in order to get at the mean X-ray luminosity of Pleiades stars. At the suggestion of Helfand, I have applied this technique to the the grism/grens selected QSOs. This stacking technique will be used primarily to obtain the mean observed X-ray flux of sample C, and hence estimate the contribution of such QSOs to the diffuse X-ray background (Chapter 5).

4.2.1 Mean Flux for Complete Samples

In the X-ray image at the location of each optically selected QSO, the total counts (0.5–3.0 keV) in the 3′ IXLUM detect window (Chapter 3), and the background counts in the $3-5'$ frame are determined. These counts are summed (*i.e.*, *stacked*) for all QSOs in the sample with appropriate weighting, and the mean flux of the sample is estimated. For a sample of n QSOs with X-ray images of comparable flux sensitivity, this gives the usual $n^{1/2}$ increase in sensitivity over that in a

single X-ray image.

Let S_i be the X-ray source counts (0.5–3.0 keV) for the ith QSO, so that the X-ray flux (0.5–3.0 keV) for the ith QSO is $F_i = C_i \frac{S_i}{t_i}$, where t_i is the integration time of the appropriate X-ray image, C_i is the appropriate conversion for transforming count rates into fluxes. Let T_i and B_i be, respectively, the total (background plus source) counts on the source and background counts. Then, assuming Poisson statistics:

$$\sigma_{F_i} = C_i \frac{(T_i + B_i)^{1/2}}{t_i} \qquad (4.2.1.a)$$

(assuming that C_i is precisely known).

Then using the usual weighting by inverse of the variance, the mean flux for the sample of n QSOs is just

$$< F > \approx \frac{\sum F_i/\sigma^2_{F_i}}{\sum 1/\sigma^2_{F_i}} = \frac{\sum \frac{S_i t_i}{C_i(T_i - B_i)}}{\sum \frac{t_i^2}{C_i^2(T_i - B_i)}} \qquad (4.2.1.b)$$

Now assume that the background counting rate is constant (from image to image), and either that the source count rates are small compared to the background count rates (this is true for almost all the objects in sample C), or that the count rates for all QSOs are approximately equal. Then the term $(T_i + B_i)/t_i$ in Eq. 4.2.1.b is approximately constant. Make the further assumption that C_i is approximately constant (*e.g.*, the mean $< C >$) for all QSOs. Then from Eq. 4.2.1.b above,

$$< F > \approx < C > \frac{\sum S_i}{\sum t_i} = < C > \frac{(T - B)}{t} \qquad (4.2.1.c)$$

where T, B, and t are, respectively, the total counts, background counts, and integration time in the *stacked* image. The uncertainty in the mean flux (again assuming

no uncertainty in $< C >$) is (assuming Poisson statistics)

$$\sigma_{<F>} \approx < C > \frac{(T+B)^{1/2}}{t} \qquad (4.2.1.d)$$

Thus, the signal-to-noise ratio in the ensemble mean flux is $(T-B)/(T+B)^{1/2}$. If the individual images are of comparable sensitivity so that $T \approx nT_i$, $B \approx nB_i$, the signal-to-noise ratio for the mean flux from the stacked image increase roughly as the square root of the number of QSOs.

Thus, although the individual S_i's cannot be accurately determined (for low X-ray fluxes) from the single images, the ensemble average flux can be much more sensitively measured from the stacked image. The ensemble mean X-ray flux is the quantity required for estimating the contribution of a complete sample of QSOs to the diffuse X-ray background, and I apply the stacking technique to sample C (Chapter 5) to obtain such an estimate for QSOs to $B \leq 19.5$ and $1.8 \leq z \leq 3.0$. In Chapter 5 I note some further advantages of using complete samples in such an estimation, and in general, the use of complete samples with stacking potentially provides a powerful tool for studying the contribution of QSOs to the X-ray background; basically the only parameter that one has to assume in such an approach is the X-ray spectral slope. If one makes a conservative assumption (say $\alpha_x = 0.5$) then one has a very nice estimator of an *upper limit* on the contribution of QSOs to the X-ray background.

I have performed Monte Carlo simulations to assess the influence of threshold effects on stacking (corresponding to varying the total integration times). The model here simulates 100 QSOs, each imaged in X-rays for t_i seconds (all t_i's are assumed equal). The QSOs (again in imitation of sample N), are assumed to all be at $z = 2.1$, and have $\log(l_{2500}) = 31.44$, but with α_{ox} values distributed as in

Figure 4.1.2.1.a. For such a Gaussian distribution function and set of parameters, the ensemble mean IPC counting rate (0.5–3.0 keV) would be $< s >= 1.66 \pm 0.096 \times 10^{-3}$ counts/sec. For each QSO/image, noise is introduced into the individual S_i's B_is, and T_i's (actually Gaussian noise is assumed, but this will qualitatively approximate the expected Poisson noise) for each QSO/image. Then the 100 noise-added images are stacked and the noise-added ensemble values of T and B for the stacked image are determined as described above. Finally, this whole process is repeated for different assumed t_i's (*i.e.*, different count rate thresholds) yielding the results found in Table 4.2.1.a, where the detection fraction is the number of objects that would have been accepted as X-ray detections under the definitions spelled out in Chapter 3. Note that the Gaussian noise assumed in the S_i's is not a very good approximation to Poisson noise for the 1000, and 5000 sec integration times, but qualitatively the results are quite encouraging: even in the presence of substantial non-random censoring, stacking apparently is capable of excellent performance, and is not so strongly affected by threshold effects as is potentially true for survival analysis; compare Table 4.2.1.a with Table 4.1.2.1.a, and note that an approximate conversion between an α_{ox} threshold and an integration time threshold can inferred by comparing columns "detection fraction" in the two tables.

Table 4.2.1.a: Threshold Effects in Stacking

t_i(sec)	$< s >$ $(counts/10^3 sec)$	detection fraction
20,000	1.634 ± 0.090	38/100
10,000	1.624 ± 0.128	27/100
5,000	1.610 ± 0.179	17/100
1,000	1.551 ± 0.396	3/100

4.2.2 Stacking and α_{ox}^{eff} for Sample N

Stacking can also be used in approximate fashion for sample N to estimate α_{ox}^{eff}; and this will again serve as a useful check on the results of survival analysis. Let $r = l_{2\,keV}/l_{2500}$ be the monochromatic luminosity ratio. Then (see *e.g.*, Eq. 2.4.e.-f.),

$$r = \frac{f_{2\,keV}}{f_{2500}} (1+z)^{\alpha_x - \alpha_o} \qquad (4.2.2.a)$$

where $f_{2\,keV}$ and f_{2500} are the monochromatic fluxes (*e.g.*, erg/sec/cm^2/hz) in the observer's frame at, respectively, frequency corresponding to 2 keV and 2500 Å. Then form the following weighted ensemble average for a sample of n QSOs:

$$< r >= \frac{\sum r_i f_{2500}^i t_i}{\sum f_{2500}^i t_i} \qquad (4.2.2.b)$$

Note that the weighting factor of t_i enters in a natural fashion, since the variance in the X-ray flux is proportional to t_i (see discussion above). The weighting by optical flux is just an ansatz that works: but note that in an idealized N-type sample (all QSOs at the same z and same optical luminosity), this weighting factor cancels out, while in the actual narrow sample N this will be approximately true.

For the actual sample N, the term $(1+z_i)^{(\alpha_x - \alpha_o)}$ (see Eq. 4.2.2.a) varies by only 11% over the entire range in redshift, and thus the assumption that $z_i =< z >$ in this term should add a dispersion in α_{ox} of less than 0.02. Then, once again assuming $C_i =< C >$, so that $f_{2\,keV}^i = C_i S_i/t_i \approx < C > S_i/t_i$, one can write for the stacked image of all QSOs in the sample,

$$< r > \approx \frac{< C > (1+< z >)^{\alpha_x - \alpha_o} \sum S_i}{\sum f_{2500}^i t_i} = \frac{< C > (1+< z >)^{\alpha_x - \alpha_o} (T - B)}{\sum f_{2500}^i t_i} \qquad (4.2.2.c)$$

where T and B have the same meaning as above, but where $< C >$ is now a conversion between broadband counts and monochromatic flux. An estimate of the uncertainty in $< r >$ is (assuming counting statistics):

$$\sigma_{<r>} \approx \frac{< C > (1+< z >)^{\alpha_x - \alpha_o} (T+B)^{1/2}}{\sum f_{2500}^{i} t_i} \qquad (4.2.2.d)$$

neglecting dispersion introduce by optical flux uncertainties, $< z >$, and $< C >$. Then, as an approximate check on the survival analysis estimate of $\alpha_{ox}^{\rm eff}$ the above expression from stacking can used with $\alpha_{ox}^{\rm eff} = -\log(< r >)/2.605$. Note that the numerator in Eq. 4.2.2.c is proportional to the total number of X-ray counts emitted jointly from all the QSOs in time t, while the denominator is proportional to the total number of optical counts received in the same time. Thus, the apparently strange weighting of Eq. 4.2.2.d also leads to a natural interpretation in the stacked image.

4.3 Summary

A brief introduction to two techniques to study the X-ray properties of QSOs in the presence of X-ray censoring has been given. The first technique, survival analysis, has had widespread use in previous studies of X-ray emission form QSOs. Through Monte Carlo simulations, I demonstrate that in the presence of non-random censoring, survival analysis is subject to the same sort of threshold effects discussed by Chanan (1983); these *potentially* can lead to spurious correlations between α_{ox} and optical luminosity that are qualitatively similar to the relationship found by Avni and Tananbaum (1982) (although in the next Chapter I will argue that it is unlikely that the correlation is a spurious one). It is shown that such α_{ox} (joint optical and X-ray) threshold effects make it prudent to regard the estimates of $< \alpha_{ox} >$ and $\alpha_{ox}^{\rm eff}$ derived from survival analysis as estimates for *lower limits* on

these quantities. Further, it is shown that $\alpha_{ox}^{\rm eff}$ (rather than $< \alpha_{ox} >$) is a more reliable parameter in the presence of significant non-random censoring. The second technique, "stacking", has not been previously used in studies of X-ray emission from QSOs, and some basic approximate formalism appropriate for samples C and N is derived. The stacking technique is found through Monte Carlo simulations to be largely free of the threshold effects found for survival analysis, and is well suited to (1) deriving the ensemble contribution of complete samples (*e.g.*, sample C) of QSOs to the diffuse X-ray background; and (2) as a double check on the $\alpha_{ox}^{\rm eff}$ value for sample N. With the statistical techniques at hand, it is now possible to proceed to the final phases of this dissertation: the estimation of such quantities for samples C and N.

5. X-RAY EMISSION FROM HIGH REDSHIFT QSOs, AND THE CONTRIBUTION OF QSOs TO THE DIFFUSE X-RAY BACKGROUND

In the previous chapter, I discussed the two statistical approaches that will now be employed to estimate the X-ray emissivities of the newly discovered high redshift QSO samples. These statistical approaches allow this estimate to be made in the presence of X-ray censoring.

For sample C, I estimate from the stacking technique (and survival analysis as well) the contribution of high redshift QSOs to the diffuse X-ray background at 2 keV; the importance of complete samples is emphasized, and in conjunction with the stacking technique (Chapter 4), such complete samples are shown to be potentially powerful estimators of the contribution of QSOs to the X-ray background. Despite the large number of X-ray flux detections and upper limits for QSOs which are currently available in the literature, sample C is only the third largely complete sample of optically selected QSOs to be studied in X-rays (the others are the Braccesi sample, and the unpublished data on the PG sample), and the first such sample at high redshift. It is the first published QSO sample studied with the stacking technique.

For sample N, I estimate the α_{ox} distribution, the mean value $< \alpha_{ox} >$ and $\alpha_{ox}^{\rm eff}$, relying on both survival analysis and stacking. The reader is reminded that in the discussion of Chapter 4, I showed it to be prudent to regard survival analysis estimates of such mean parameters to be *lower limits* on the true values.

Because sample N occupies a narrow region of optical luminosity and redshift space, corrections for any possible dependence of $< \alpha_{ox} >$ on optical luminosity and/or redshift should be quite small, and thus mean parameters can be estimated

in a largely model independent fashion (*i.e.*, without appeal to some specified form for the corrections). Using the sample N data and recent data on the surface density of QSOs, it is shown that QSOs (defined here to be $M_B \leq -23.0$) probably could *not* dominate (contribute > 50%) to the diffuse X-ray background unless there is a dependence of $< \alpha_{ox} >$ on optical luminosity and/or redshift of the sort predicted by the Avni and Tananbaum (1982); *i.e.*, the dependence of $< \alpha_{ox} >$ on l_{2500} and/or redshift found by Avni and Tananbaum is probably ***required*** if QSOs are to dominate the X-ray background. Note that this is the inverse of the usual arguments: previously (*e.g.*, Setti and Woltjer 1979, Zamorani *et al.* 1981) it has been argued from the X-ray data that in order that the diffuse X-ray background not be exceeded, there must be a turnover in the optical surface density of QSOs (*i.e.*, the X-ray data has been used to constrain the optical surface density counts); instead here I show that new optical observations of this turnover in QSO surface density counts constrain the X-ray data. The data from sample N are in excellent agreement with the predictions of the Avni and Tananbaum model.

However, the reader will recall from Chapter 4 that α_{ox} thresholds interacting with survival analysis (joint optical and X-ray thresholds) can give spurious results that qualitatively mimic the relation found by Avni and Tananbaum. Here I will show that, although such effects can happen in principle, they are *not* likely to be the cause of the relation found by Avni and Tananbaum.

Finally, it is argued that in a qualitative sense most of the X-ray background, if it does arise from a superposition of point sources, probably originates from moderate redshift, low to moderate optical luminosity objects.

Throughout the discussion, reference will be made to the intensity of diffuse X-ray background at 2 keV. The spectrum and intensity of the the extragalactic

component of the background are well known only at energies greater than $\sim 1\,\mathrm{keV}$. However, the Einstein IPC, which is the most widely used instrument for determination for QSO X-ray emission, is a relatively soft X-ray imaging device, and hence, to decrease the uncertainties of extrapolation far outside the Einstein waveband (*e.g.*, this makes this uncertainty in α_x more troublesome) the approach generally followed has been to estimate the contribution of QSOs to the diffuse X-ray background at $2\,\mathrm{keV}$. This convention will be continued in the current study.

5.1 The Contribution of $B \leq 19.5$ QSOs to the Diffuse X-Ray Background

The 37 sample C QSOs in Table 3.3.a. have been used to directly estimate an upper limit on the contribution of high redshift QSOs to the diffuse X-ray background. Both survival analysis and stacking can be used to make this upper limit estimate in a very straightforward fashion, with essentially the only assumed parameter being the power law slope in the X-ray (*i.e.*, α_x). As noted earlier, much current data suggest that the spectral slope of QSOs in the X-ray is actually substantially steeper than this value. For the response of the IPC however, this means that using $\alpha_x = 0.5$ is a conservative approach: if α_x is instead 1.2, this reduces the estimate for the monochromatic flux (and hence the contribution to the diffuse X-ray background) by $\sim 40\%$. For the reasons described in Chapter 4, stacking will be the primary method applied to sample C, although survival analysis gives consistent results.

The current approach, using a complete sample, is to be strongly contrasted with many previous estimates of the contribution of QSOs to the diffuse X-ray background. Maccacaro, Gioia, and Stocke (1984) have emphasized the large number of assumptions and parameters needed to compute the contributions of QSOs to the XRB (diffuse X ray background) using the optical luminosity function and

a relationship between $l_{2\,\mathrm{keV}}$ and l_{2500}. This traditionally has been the only way to proceed, since most X-ray observations of QSOs were of rather heterogenous collections of objects, and it was necessary to extrapolate the X-ray properties of these heterogenous objects (perhaps with uncertain corrections) to the QSO population as a whole. Among the assumptions required by this latter approach (see Table 2A of Maccacaro, Gioia, and Stocke 1984) are the following: shape of the optical luminosity function (parameters include the normalization, slope, and L_{max} or L_{min}); shape of the evolution function; maximum redshift to which the model holds; shape (mean and width) of the α_{ox} distribution; dependence of $< \alpha_{ox} >$ on other QSO properties such as redshift, optical luminosity, and radio luminosity; dependence of the width of the α_{ox} distribution on other QSO properties (*e.g.*, z, l_{2500}, l_{radio}); the intensity of the X-ray background at $2\,\mathrm{keV}$; and q_0. Among the ~ 21 parameters listed in that table, only the intensity of the XRB at $2\,\mathrm{keV}$ is required for use with complete samples. Of course, an additional assumed parameter needed (not listed in Maccacaro's table) is the slope of the assumed power law QSO X-ray spectrum. Further, a complete sample is also characterized by a redshift range where it is thought to be complete, the completeness magnitude limit, and a surface density to that completeness limit. Thus, a half-dozen or so parameters or assumptions are involved in using optically *complete* samples of QSOs with X-ray information available; this is certainly at least competitive with the X-ray luminosity function approach emphasized by Maccacaro, Gioia, and Stocke (1984). Thus faint, optically complete samples imaged to faint X-ray flux levels can potentially be very powerful estimators of the contribution of QSOs to the diffuse X-ray background. Again, to risk stating the obvious, the stacking technique (at least in the form described here) cannot be used with X-ray selected samples, since one does not know *a priori* which parts of the image to do the stacking on.

As I have argued earlier there are several reasons to believe that the number derived below for the contribution of sample C-type QSOs to the diffuse X-ray background, should probably be regarded as an *upper limit* on that contribution:

(1) A few ($< 20\%$) lower redshift QSOs may be contaminating the sample: the apparent correlation between $< \alpha_{ox} >$ and optical luminosity (see § 5.2) means that for a given apparent magnitude, these lower redshift objects are likely to have greater X-ray emissivities than their high redshift counterparts.

(2) Random uncertainties in the magnitude distribution of the sample near the completion limit of $B = 19.5$ will probably tend to add extra QSOs to the sample. Imagine there is a typical uncertainty of ± 0.5 magnitudes. Because there are more QSOs at (a true magnitude of) $B = 20$ than at $B = 19.0$, this magnitude uncertainty will tend to add more QSOs at $B = 20.0$ than are excluded at $B = 19.0$.

(3) A great deal of current data (see Chapter 3), suggests that the X-ray slope is steeper than $\alpha_x = 0.5$, and thus the value assumed here actually overestimates the observed flux at 2.0 keV.

(4) The surface densities of X-ray sources at these faint flux levels are such (see Chapter 3) that ~ 1 object included here as a detection is probably just a chance superposition of a high redshift QSO and an unrelated X-ray source.

(5) As pointed out in Chapter 4, for the case of the survival analysis estimate, it is prudent (because of possible α_{ox} threshold effects) to regard parameter estimates as estimates of limits on the true values (in this case an upper limit on the contribution to the XRB).

All five of these uncertainties tend to add spurious extra X-ray photons to the estimates, so that the estimated contribution of sample C-type QSOs to the XRB

should be regarded as an estimated upper limit.

Contamination of the sample by non-QSOs of course would tend to dilute the ensemble average X-ray flux derived for the sample. However, this diluted X-ray flux is then multiplied by an inflated surface density, and these two effects roughly cancel (see discussion in Chapter 2).

Finally, there is the issue of the radio properties of the QSOs in sample C. It is well known that for a given optical luminosity, a radio bright QSO tends to emit $\sim 3\times$ as much in X-rays as does its radio quiet counterpart (*e.g.*, Zamorani *et al.* 1981, Tananbaum *et al.* 1983). Assume that radio bright QSOs are a subset of optically selected QSOs; this certainly seems a reasonable assumption, since radio selected objects do not seem substantially different in their optical properties (*e.g.*, Richstone and Schmidt 1980). Then, on the average, optical selection will pick out the proper fraction of radio bright objects which *must* be included in estimating the contribution of all QSOs to the diffuse X-ray background. Thus, although radio studies of the objects discussed here are currently underway for other reasons, it is not necessary to have this knowledge for the current application.

5.1.1 Survival Analysis of Sample "C"

For a complete sample, one can directly estimate the contribution of QSOs to the XRB merely by estimating the mean X-ray flux of the sample, and in turn multiplying by the surface density of objects in the complete sample. As noted before, this requires only an assumption about the QSO power law X-ray spectrum to convert the broadband count rate (0.5–3.0 keV) into a monochromatic flux at 2 keV in the observer's reference frame. The monochromatic flux at 2 keV is given

by

$$S_{2\,\mathrm{keV}} = \frac{F(0.5-3.0\,\mathrm{keV}}{\nu_{2\,\mathrm{keV}}}(1-\alpha_x)\left[\left(\frac{3.0\,\mathrm{keV}}{2.0\,\mathrm{keV}}\right)^{1-\alpha_x} - \left(\frac{0.5\,\mathrm{keV}}{2.0\,\mathrm{keV}}\right)^{1-\alpha_x}\right] \quad (5.1.1.a)$$

(Note that changing α_x from 0.5 to 1.2 in Eq. 5.1.1.a. reduces the factor in the brackets by $\sim 30\%$. An additional reduction by $\sim 10\%$ enters through the broadband flux term $F(0.5-3.0\,\mathrm{keV})$; this latter change reflects the dependence on the assumed X-ray spectrum of the conversion factor which converts broadband count rates to fluxes (0.5–3.0 keV). For the 37 objects of sample C with X-ray information available, survival analysis gives $< S_{2\,\mathrm{keV}} >= (1.24 \pm 0.10) X 10^{-5}\,\mathrm{keV/sec/cm^2/keV}$ (corresponding to $< F(0.5-3.0\,\mathrm{keV}) >= 3.97 \times 10^{-14}\,\mathrm{erg/sec/cm^2}$ in the broadband). The fractional contribution of such QSOs to the diffuse X-ray background then is

$$f(B \leq 19.5, 1.8 \leq z \leq 3.0) = \frac{I^{\mathrm{QSO}}_{2\,\mathrm{keV}}}{I^{\mathrm{back}}_{2\,\mathrm{keV}}} \approx \frac{n < S_{2\,\mathrm{keV}} >}{I^{\mathrm{back}}_{2\,\mathrm{keV}}} = 0.022 \pm 0.004 \quad (5.1.1.b)$$

where n is the surface density (§ 2.3.2.1.) of the high redshift objects derived for the sample C (3.10 ± 0.49/sq.deg.), and $I^{\mathrm{back}}_{2\,\mathrm{keV}}$ is the intensity of the diffuse X-ray background at 2 keV: $I^{\mathrm{back}}_{2\,\mathrm{keV}} = 5.84 \times 10^{-5}\,\mathrm{keV/sec/cm^2/ster}$ (from Schwartz, 1979). The uncertainties in Eq. 5.1.1.b. include both the uncertainties in the mean flux and that due to Poisson fluctuations in the surface density of QSOs. Note further in this latter regard, that since the discovery grism/grens plates are randomly distributed over the sky, this estimate is not plagued by the possibility of a large positive or negative local fluctuation in the QSO surface density. For the reasons described above in § 5.1, this value is more properly considered an upper limit.

5.1.2 Contribution to the XRB of Sample C QSOs Using the Stacking Approach

One can also address the contribution of such QSOs to the background using the stacking approach outlined in Chapter 4. This stacking technique is much less susceptible to threshold effects than is the survival analysis approach (Chapter 4). Note that in the stacking technique, it is necessary to exclude QSOs for which the detect window is strongly contaminated by a nearby but not physically associated X-ray source (otherwise, one would be stacking X-ray photons clearly not related to the QSO); such exclusions are not necessary (at least for a few isolated cases) in the survival analysis approach. Thus, objects $17272+502$, $17274+503$, and $21556-302$ are excluded from the stacking process due to strong X-ray contamination from a nearby source. Stacking allows a quite natural (in terms of weighting by the variance, etc.) estimation of the ensemble sample mean flux provided that C_i and $(T_i + B_i)/t_i$ are not too different among the various images (Chapter 4). Shown in Table 5.1.2.a are C_i's and values of $(T_i + B_i)/t_i$ for the remaining 34 sample C QSOs. Although in general these terms vary by less than a factor of ~ 2, it is clear from Table 5.1.2.a that the HRI fields do not satisfy such criteria. Thus, Obj. 11, Obj. 15, Obj. 16, and $14149+251$ are also excluded in the stacking approach; 30 sample C QSOs remain viable for stacking. For these 30 objects, the dispersion introduced into calculating the mean flux by the assumption that the values of C_i and $(T_i + B_i)/t_i$ are constant, are, respectively, $\delta < S_{2\,\mathrm{keV}} > / < S_{2\,\mathrm{keV}} > \approx .04$ and .09.

Table 5.1.2.a Stacking Parameters for Sample C X-ray Images

OBJECT	t_i(sec)	$C_i \times 10^{11}$	$(T_i + B_i)/t_i$
Obj. 5	28000	2.50	0.0131
Obj. 6	28000	3.53	0.0115
Obj. 7	12800	4.47	0.0132
Obj. 8	16600	4.21	0.0170
Obj. 10	19900	3.84	0.0161
Obj. 11	96000	24.29	0.0030 HRI
Obj. 12	20500	4.91	0.0147
Obj. 15	45000	33.98	0.0050 HRI
Obj. 16	45000	24.55	0.0044 HRI
Obj. 17	18000	3.38	0.0238
Obj. 19	15600	4.26	0.0140
Obj. 21	12900	4.06	0.0152
08366+654	12800	4.34	0.0122
08388+131	13600	4.22	0.0165
08388+133	13600	3.65	0.0197
08500+283	19100	4.10	0.0151
09038+167	13500	4.39	0.0179
09379+121	14100	3.81	0.0112
09388+117	14100	4.27	0.0131
09392+121	14100	3.81	0.0137
11131+183	16000	4.11	0.0099
11156+180	16000	5.60	0.0110
12071+398	19900	4.26	0.0135
12076+399	19900	4.48	0.0142
12302+120	20300	5.60	0.0348
12354+264	21800	4.69	0.0114
14149+251	22400	75.81	0.0016 HRI
14151+254	22400	3.84	0.0210
16017+184	17100	4.31	0.0110
17272+499	32200	4.20	0.0235
20382-012	15600	4.94	0.0083
21260-150	12000	3.48	0.0177
21342-149	12900	4.51	0.0117
21470-302	11600	8.47	0.0070

In a conservative approach (see discussion in Chapter 3), the total counts (source counts and background counts) are determined from a detect window on each source in a 3′ circle, and the background is estimated using contamination-free regions of a concentric annulus extending from $3 - 5'$ radially about the QSO. The application of the stacking method to the remaining 30 class C QSOs yields the following (see § 4.2.1 for the definition of symbols) for the stacked image:

$$T = 4348 \text{ counts},$$

$$B = 3821 \text{ counts},$$

$$t = 526137. \text{ sec}.$$

Thus, I estimate from the stacked image

$$S = (T - B)/t = 527 \text{ counts}$$

$$\delta S = (T + B)^{1/2} = 90 \text{ counts}$$

$$< s > = S/t = 1.00 \times 10^{-3} \text{ counts/sec}.$$

Using the mean conversion between broadband count rate and fluxes for these fields ($< C >= 4.34 \times 10^{-11}$ erg/sec/cm^2 per count/sec) gives

$$< F(0.5 - 3.0\,\text{keV}) >= 4.34 \times 10^{-14} \text{ erg/sec/cm}^2 \qquad (5.1.2.c)$$

or, for $\alpha_x = 0.5$,

$$S_{2\,\text{keV}} = (9.4 \pm 1.9) \times 10^{-6}\,\text{keV/sec/cm}^2\text{/keV} \qquad (5.1.2.d)$$

where in the last equation I have also included the expected dispersions due to the assumptions about the constancy of the the terms C_i and $(T_i + B_i)/t_i$. Effectively,

this stacked image has a limiting flux of $2.6 < C > B^{1/2} = 1.35 \times 10^{-14}\,\mathrm{erg/sec/cm^2}$ (0.5–3.0 keV). From an extrapolation of the Deep Survey X-ray logN-logS curve of Giacconi *et al.* (1979b), this sensitivity is still far above confusion limits. Thus, for the fractional contribution of class C QSOs to the diffuse X-ray background the stacking technique yields:

$$f(B \leq 19.5,\ 1.8 \leq z \leq 3.0) = 0.016 \pm 0.004 \qquad (5.1.2.e)$$

This value is smaller than (but within 1σ of) the value found using survival statistics (and this is true even when survival analysis is performed on the same 30 objects subjected to the stacking technique). Given the very different approaches, it is comforting (for believing the viability of both approaches) that both these numbers are in even reasonable agreement. As discussed in Chapter 4, there is reason to suspect that survival analysis for samples with significant non-random censoring is appropriate only for estimating limits, and so from this viewpoint it is not unexpected that the stacking technique would be somewhat smaller than the survival analysis value. In either case the value is quite small, and results in part from the low surface density of such high redshift objects, but also from the comparatively low value of X-ray emissivities from these objects (see discussion in the next section).

In summary of the results from the current and previous sections (and recalling from § 2.3.2.1. that the grism/grens selected sample may be $\sim 20\%$ incomplete):

For $B < 19.5$ and $1.8 < z < 3.0$, the fractional contribution of QSOs to the diffuse X-ray background is $< 3\%$. It is to be stressed that this is a reasonably conservative upper limit, and is based on a direct measurement, not dependent on any extrapolations of surface density counts nor on extrapolations of the dependence of α_{ox} on optical luminosity and/or redshift. The only major uncertainty in this

number is the value of the X-ray spectral slope, and the value chosen here is a conservative one.

5.1.3 Contribution of QSOs (of All Redshifts) to $B \leq 19.5$ to the Diffuse X-Ray Background

The "Braccesi faint", or "BF" sample (Formiggini *et al.* 1980, Marshall 1983) consists of 35 UVX selected QSOs in 1.72 sq. deg. and is largely complete for $0 < z < 2.2 (U - B < -0.4)$ and $B < 19.8$. The X-ray properties of this sample have been studied with the IPC and the HRI (Marshall 1983) in exposures of similar limiting X-ray sensitivities to those of the my new grism/grens selected samples. The new grism selected sample investigated here is an excellent complementary sample for comparison and combination with the BF sample. I have applied survival analysis to the 14 BF QSOs which have $B < 19.5$ and $z < 1.8$. The stacking technique is not practical for the BF objects because the actual counts are not published for the non-detections. For the Bracessi objects, I find

$$< S_{2\,\mathrm{keV}} >= (3.4 \pm 1\,4) \times 10^{-5}\,\mathrm{keV/cm^2/sec/keV} \qquad (5.1.3.a)$$

Then to $B < 19.5$, the contribution (more correctly an estimate of an upper limit) to the X-ray background from QSOs in the range $0 < z < 1.8$ is

$$f(B \leq 19.5, 0 \leq z \leq 1.8) = 0.16 \pm 0.08 \qquad (5.1.3.b)$$

Thus, even using the higher survival analysis value (Eq. 5.1.1.b.) for the high redshift QSOs and allowing for $\sim 20\%$ incompleteness in sample C, and 11% in the BF sample, *I estimate the contribution to the XRB from QSOs to $B < 19.5$ and $0 < z < 3.0$ to be*:

$$f(B \leq 19.5, 0 \leq z \leq 3.0) = .20 \pm .08 \qquad (5.1.3.c)$$

Again, this result based on survival analysis of complete samples is more properly considered an estimate of an upper limit on the contribution for the reasons outlined above. Further, there is some current evidence that the surface density of the Bracessi faint sample may well be a positive fluctuation above the mean surface density of QSOs to the same limiting magnitude. In several different directions of the sky, and using color selection criteria, Koo and Kron (Koo 1985) and Marano *et al.* (1984) find only $\sim$ 10 QSOs per square degree to $B = 20$, while there are almost that many to $B = 19.5$ in the BF field. This again suggests that the above estimate is probably more properly viewed as an upper limit.

The surface density of very high redshift QSOs ($z > 3.0$) is the subject of a number of recent and on-going investigations (Osmer 1982, Schneider, Gunn and Schmidt 1983, Koo and Kron 1980, Hazard and McMahon 1985); as noted earlier, plates taken in the course of this dissertation are also being used to search for such high redshift QSOs. However, it seems likely (*e.g.*, Osmer 1982, Hazard and McMahon 1985) that unless QSOs look quite different at very high redshifts than at lower redshifts (*e.g.*, by obscuration by intergalactic dust: Ostriker and Heisler 1984; or different physical conditions: Boldt and Leiter 1984), and have thus escaped selection by current methods, such objects probably have surface densities to $B <$ 19.5 which are no more than $\sim$ 20% of the surface density of QSOs in the redshift range $1.8 \leq z \leq 3.0$ to $B \leq 19.5$. Indeed, in light of the current data, this number seems a quite generous upper limit.

These very high redshift objects are, of course, optically more luminous, for a given apparent magnitude, than their lower redshift counterparts. Because of the apparent dependence of $< \alpha_{ox} >$ on optical luminosity (see § 5.2 below), it therefore seems quite unlikely that $z \geq 3.0$, and $B \leq 19.5$ QSOs contribute more than $\sim 0.4\%$

of the diffuse X-ray background. it Then perhaps a reasonable estimate for (upper limit on) the contribution of all QSOs to $B \leq 19.5$ to the XRB is:

$$f(B \leq 19.5) = 0.21 \pm 0.08 \qquad (5.1.3.d)$$

It is important to realize here that, although $z \geq 1.8$ QSOs comprise ~ 0.28 of the QSOs to $B < 19.5$, they account for (less than) $0.15 f(B \leq 19.5)$. This suggests, and this point will be emphasized again, that lower redshift, lower luminosity objects might be the major contributors to the X-ray background, if indeed the background is comprised of a superposition of point X-ray sources.

To reiterate one previous point, the mean X-ray spectral index may well be closer to $\alpha_x = 1.2$ rather than 0.5 . If the mean spectral slope is this steep, the values above for the contribution to the XRB are overestimates by $\sim 40\%$.

5.2 The Distribution of α_{ox} Values for Sample N QSOs

A number of workers (Reichert *et al.* 1982, Avni and Tananbaum 1982, Zamorani 1983) have found that there apparently is a significant dependence of $< \alpha_{ox} >$ on optical luminosity and/or redshift; the primary dependence seems to be on optical luminosity. Avni and Tananbaum (1982) using a heterogeneous collection of optically selected QSOs and Seyferts (many of them "famous" objects), have determined an empirical relationship between $< \alpha_{ox} >$, l_{2500}, and z (using linear regression techniques appropriate for censored data). Their expression is equivalent to

$$< \alpha_{ox} >= -0.01[\tau(z) - 0.5] + 0.118[\log l_{2500} - 30.5] + 1.50 \qquad (5.2.a)$$

where $\tau(z) = z/(1+z)$ is the fractional lookback time (for $q_0 = 0$).

However, a more recent recalibration of the effective area of the IPC as a function of energy was used for the grism/grens selected samples discussed here, which results

in a systematic offset in α_{ox} for the grism/grens selected sample which is 0.017 units lower in α_{ox} units (*i.e.*, the X-ray fluxes and limit are 11% higher) than the objects for which they derived this relation. Thus, to compare the α_{ox} values for the grism/grens samples of this dissertation, a corrected expression is:

$$< \alpha_{ox} >= -0.01[r(z) - 0.5] + 0.118\,[\log l_{2500} - 30.5] + 1.48 \qquad (5.2.b)$$

Although the primary dependence in Eqs. 5.2.a-b seems to be on optical luminosity, because of (for example) selection biases that correlate optical luminosity with redshift, it is difficult to confidently disentangle the effects of l_{2500} and z on $< \alpha_{ox} >$. Most of the high optical luminosity objects from which this relationship was derived are also at high redshift: one needs to sample a large volume to find high luminosity objects, and in turn these are the only objects bright enough to identify at high redshift. Similarly, most of the low luminosity objects used to derive Eq. 5.2.a are also low redshift objects: low luminosity objects are merely too faint to easily detect at high z.

The relationship of Eq. 5.2.a-b has been given physical motivation (*e.g.*, Tucker 1983 and Netzer 1985; and see discussion below in § 5.4), but as demonstrated in Chapter 4 (and previously suggested by Chanan), α_{ox} threshold effects can conceivably lead to a spurious apparent dependence between $< \alpha_{ox} >$ and l_{2500} (even when such a dependence is not present in the parent distribution) which is qualitatively similar to that of Eq. 5.2.a-b. However, if this dependence is a physical one (and I argue in § 5.4 that this is likely to be the case), quantities such as $< \alpha_{ox} >$, $\alpha_{ox}^{\rm eff}$, and the survivor function for α_{ox} values are immediately interpretable only if determined for a sample of QSOs with a narrow distribution of optical luminosities and redshifts (or in discussing, *e.g.*, the contribution of *complete* samples to the diffuse X-ray background). In Chapter 2, we discussed how grism/grens selection is ideally

suited to obtaining a large sample of such objects, and have consequently defined the sample N.

The dispersion found by Avni and Tananbaum about the mean relation of Eq. 5.2.a-b was ~ 0.2 in units of α_{ox}. From Eq. 5.2.a-b it is readily shown that, the dispersion of $\log(l_{2500})$ values in sample N about the mean (*i.e.*, a dispersion of 0.25 about a mean of $< \log(l_{2500}) >= 31.44$) should introduce an additional uncertainty of < 0.01 in determining the mean $< \alpha_{ox} >$ of the distribution; the small *explicit* redshift dependence in Eq. 5.2.a-b is negligible in this regard. That is, sample N occupies a sufficiently narrow region of optical luminosity and redshift space that it can be used in a largely model independent fashion (*i.e.*, without actually invoking a specific model like that of Eqs. 5.2.a-b in order to make corrections) to directly determine the $< \alpha_{ox} >$ value for QSOs at the mean optical luminosity ($< \log(l_{2500}) >= 31.44$) and mean redshift ($< z >= 2.1$) for sample N. There is currently no other such "narrow" sample of QSOs with X-ray information.

5.2.1 The Survival Analysis of Sample N

For sample N, the survival function, not merely a single parameter like α_{ox} or $\alpha_{ox}^{\rm eff}$ is of interest, and so it will be generally more productive to use survival analysis rather than the stacking technique. Using the Kaplan-Meirer product limit method of survival analysis (see Chapter 4), I have estimated the distribution of α_{ox} values for the sample N QSOs shown in Figure 5.2.1.a. *For sample N the survival analysis estimates for* $< \alpha_{ox} >$ *and* $\alpha_{ox}^{\rm eff}$ *appropriate for* $< \log(l_{2500}) >= 31.44$ *and* $< z >= 2.1$) *are:*

$$< \alpha_{ox} >= 1.58 \pm 0.03 \quad \text{and} \quad \alpha_{ox}^{\rm eff} = 1.50 \pm 0.03. \qquad (5.2.1.b)$$

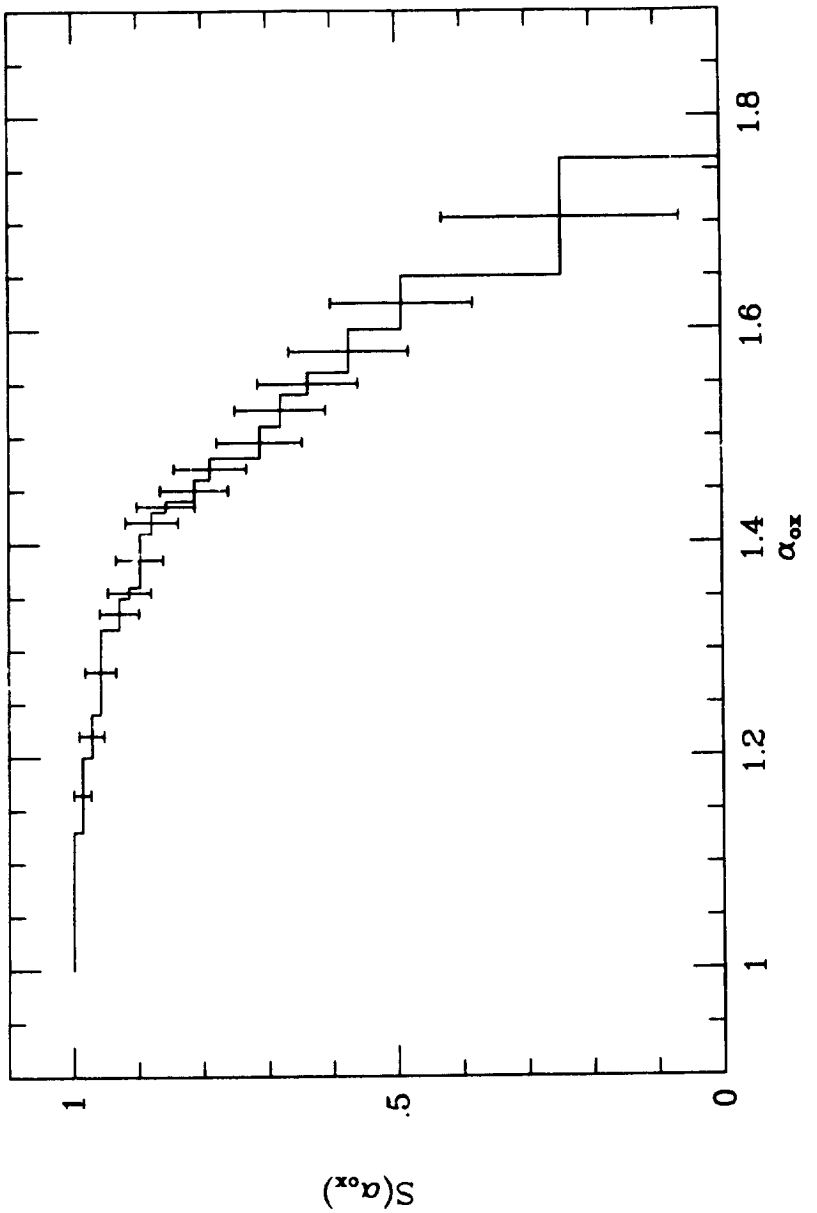

Figure 5.2.1.a. The survivor function for α_{ox} values of QSOs in sample N ($1.8 \leq z \leq 2.5$, $31.0 \leq \log(l_{2500}) < 32$.). The survivor function S(α) describes the probability a QSO will have an α_{ox} value in excess of α.

These high redshift (high luminosity) QSOs are comparatively weak in their relative X-ray emissivities. For example, the X-ray selected QSOs (*e.g.*, Margon, Downes, and Chanan 1985; Gioia *et al.* 1984) as well as radio bright QSO (*e.g.*, Zamorani *et al.* 1981, Tananbaum *et al.* 1983) both have $\alpha_{ox}^{\rm eff} \approx 1.3$; the optically selected high redshift QSOs of sample N have a mean X-ray to optical luminosity ratio which is $\sim 3-4$ times smaller than that for the X-ray selected and radio bright QSOs. (That optically selected QSOs are relatively X-ray underluminous compared with X-ray and radio selected QSOs has been established for quite some time, and is reiterated here for the benefit of the reader new to the field). Note also from the survivor function of Figure 5.2.1.a that $\alpha_{ox}^{\rm eff}$ can be a somewhat misleading parameter: more than 70% of the QSOs in sample N have $l_{2\,\rm keV}/l_{2500}$ ratios which are smaller than the mean value found for sample N, and indeed more the 95% of sample N QSOs have smaller X-ray to optical luminosity ratios than the mean for X-ray and radio selected samples.

For the mean parameters, $< \log(l_{2500}) >= 31.44$ and $< z >= 2.1$, appropriate for the 78 sample N QSOs, the model of Avni and Tananbaum (Eq. 5.2.b) predicts values of $< \alpha_{ox} >= 1.59$, and $\alpha_{ox}^{\rm eff} = 1.47$; $\alpha_{ox}^{\rm eff}$ can be estimated from (*e.g.*, Marshall 1983):

$$\alpha_{ox}^{\rm eff} \approx < \alpha_{ox} > +3[\sigma(\alpha_{ox})]^2 \qquad (5.2.1.c)$$

a relation which is appropriate for a Gaussian distribution of α_{ox} values.

Both values in Eq. 5.2.1.b are within 1σ of the predictions of the Avni and Tananbaum model of Eq. 5.2.b. *Thus, the measurements of* $< \alpha_{ox} >$ *and* $\alpha_{ox}^{\rm eff}$ *for sample N strongly confirm the viability of the relationship found by Avni and Tananbaum for the dependence of* $< \alpha_{ox} >$ *on optical luminosity and/or redshift. Note that the measurements here have made no parametric assumptions about the*

particular parametric form (or even the existence!) of the dependence of α_{ox} on optical luminosity and/or redshift, (i.e., the measurements here are largely model independent confirmations of the Avni and Tananbaum relation). Note also that the measured values of α_{ox} and $\alpha_{ox}^{\rm eff}$ are independent of uncertainties in the cosmological parameters H_0 and q_0. Again, it is important to keep in mind the previous discussions (*e.g.*, Chapter 4, and § 5.1) that survival analysis estimates should probably be more properly considered lower limits on $< \alpha_{ox} >$ and $\alpha_{ox}^{\rm eff}$. This, of course, does *not* substantially diminish the significance of the agreement between the value measured here for sample N and the predictions of the Avni and Tananbaum model: the Avni and Tananbaum model is also based on the same statistical approach.

5.2.2 The Width of the α_{ox} Distribution for Sample N

Franceschini, Gioia, and Maccacaro (1985) and Zamorani (1985) have recently emphasized that (along with the value of $< \alpha_{ox} >$) the intrinsic width of the α_{ox} distribution about the mean relation of 5.2.a-b is an important parameter for understanding the X-ray properties of the QSO population. In particular, the large value (~ 0.2) found by Avni and Tananbaum for the standard deviation of the α_{ox} residuals about the mean dependence on optical luminosity leads to some inconsistencies between X-ray and optically selected samples of QSOs. For example, using the optical luminosity function and the α_{ox} distribution for optically selected QSOs, one can predict the X-ray luminosity function: this predicted X-ray luminosity function can be compared with the appropriate data from X-ray selected sample of QSOs. However, such a prediction using the relation of Eq. 5.2.a-b, with an intrinsic standard deviation about the mean of $\sigma(\alpha_{ox}) \approx 0.2$ (from Avni and Tananbaum 1982), overpredicts by a factor of ~ 3 (Franceschini, Gioia, and Maccacaro 1985) the number of X-ray sources that should have been found in, for example, the X-ray selected

sample known as the Medium Sensitivity Survey (*e.g.*, Gioia *et al.* 1984).

Franceschini *et al.* and Zamorani (1985) suggest that a way out of such discrepancies is to suppose that the intrinsic width of the α_{ox} distribution is smaller than the value estimated by Avni and Tananbaum. Intuitively, this suggestion is easy to understand: if the α_{ox} distribution is not so wide, there are relatively fewer objects which are bright enough in X-rays to have been found in the X-ray selected samples. Franceschini *et al.*, suggest that a value of $\sigma(\alpha_{ox}) \sim 0.14$ could resolve the apparent discrepancy. Franceschini *et al.* and Zamorani (1985) suggest a number of possible external effects that might account for the broadening of the intrinsic distribution, including the following: intrinsic absorption at optical and X-ray wavelengths, optical and X-ray variability, errors in optical and X-ray fluxes, errors in the conversion of fluxes to intrinsic luminosities.

The standard deviation of the α_{ox} residuals about the mean for sample N is in fact found to be $\sigma(\alpha_{ox}) \sim 0.14$, and this is the ***observed*** value before the application of any corrections like those of Eq. 5.2.a-b. Since the values for $< \alpha_{ox} >$ and $\alpha_{ox}^{\rm eff}$ found here for sample N are in good agreement with the model of Eq. 5.2.b, I have further estimated the standard deviation of the intrinsic variance in the α_{ox} distribution for sample N about the mean relation of Eq. 5.2.b; that is, I have further corrected the observed residuals of sample N, assuming the applicability of the Avni and Tananbaum model. Following Avni and Tananbaum, I determine, for each sample N QSO, the value (or limit) on the quantity (see Eq. 5.2.a-b)

$$\alpha_{ox}^{\rm corr} = \alpha_{ox} - 0.118\,(\log l_{2500} - 31.44) \qquad (5.2.2.a)$$

where I have neglected any small *explicit* dependence on redshift. The survivor function for these corrected values of α_{ox} are shown in Figure 5.2.2.a. The corrected values of $< \alpha_{ox} >$ and $\alpha_{ox}^{\rm eff}$ for this corrected distribution are 1.56 ± 0.03 and

1.50 ± 0.03, respectively. As suspected, these values are quite similar to those obtained directly from sample N without any corrections (*i.e.*, 1.58±0.03 1.50±0.03, respectively). Further evidence that the corrections for sample N are not large can be seen in Figure 5.2.2.b, in which I have plotted on the same graph both corrected and uncorrected α_{ox} distributions for sample N.

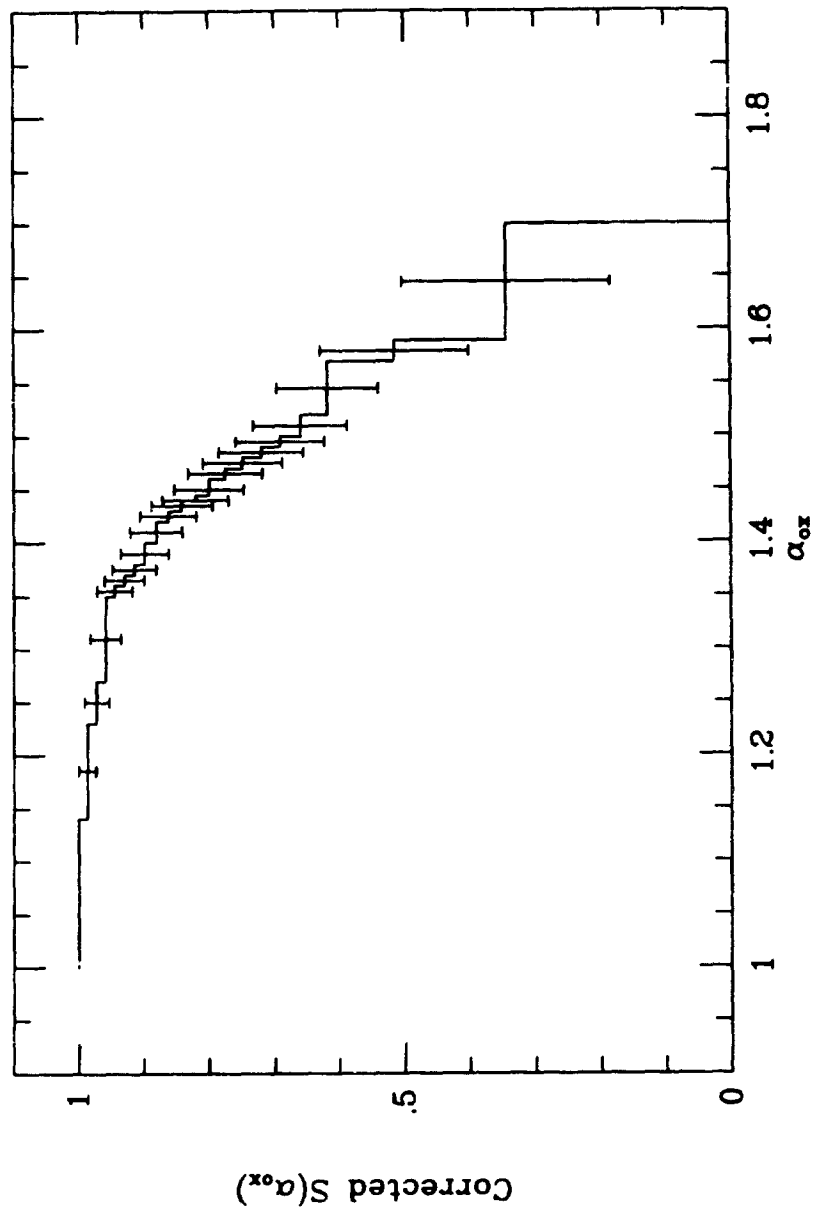

Figure 5.2.2.a. Survivor function for α_{ox} values for sample N with corrections applied for the correlation of α_{ox} and optical luminosity.

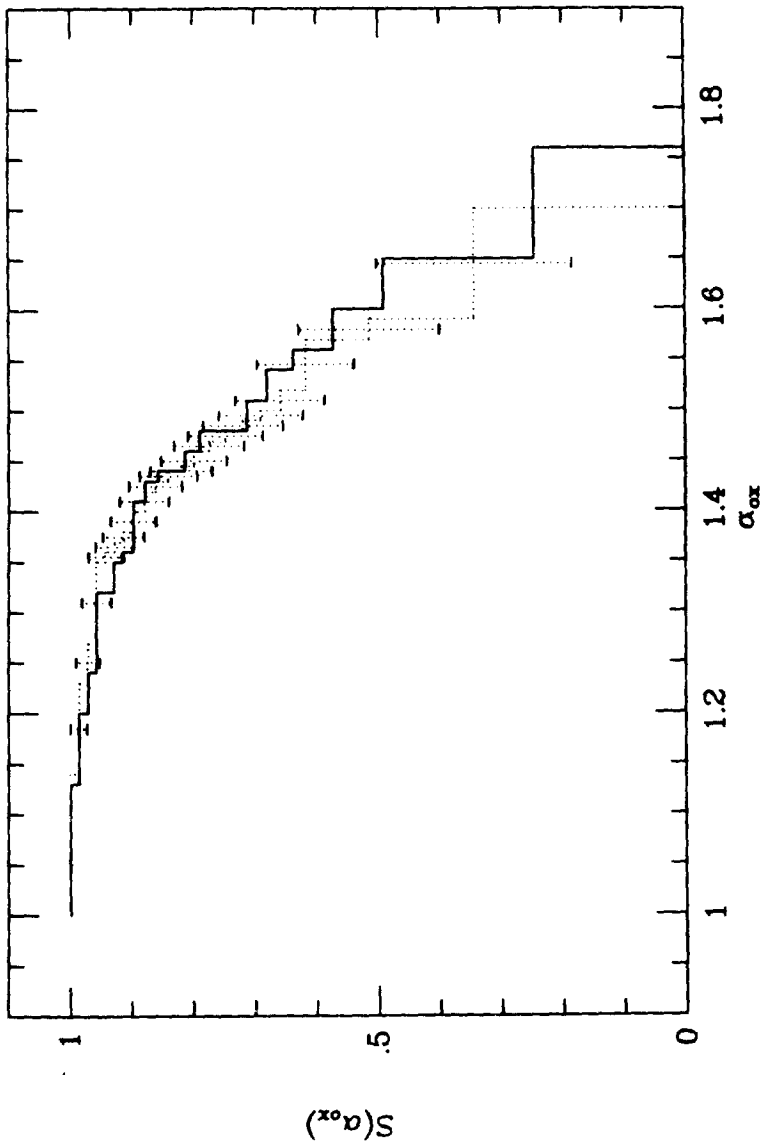

Figure 5.2.2.b. Comparison of survivor functions for α_{ox} values for sample N with and without corrections for optical luminosity dependence. The solid curve shows the distribution without corrections, and the dotted curve shows the distribution with corrections; to avoid confusing the figure, the solid curve is plotted without error bars.

For the corrected values, the standard deviation about the mean dependence of Eq. 5.2.a-b is $\sigma(\alpha_{ox}^{corr}) = 0.12$. Indeed, if it is assumed that the underlying distribution is actually a Gaussian, the relation of Eq. 5.2.1.c can be used to predict an approximate Gaussian width of $\sigma(\alpha_{ox}^{corr}) = 0.14$.

Superficially, these small standard deviations found for sample N (and the corrected sample N) appear quite encouraging in light of the findings of Zamorani and Franceschini *et al.* (1985). However, the results of Chapter 4 on the interaction of non-random α_{ox} censoring and survival analysis must now be recalled. In Chapter 4, I noted that premature threshold truncation of the distribution can spuriously tend to narrow the distribution. Thus, as also pointed out in Franceschini *et al.*, it is really the width of the low side of the α_{ox} distribution which is most relevant. Calculating the contribution to the standard deviation below $< \alpha_{ox} >$ yields 0.13 and 0.11, for, respectively, sample N and the corrected sample N; thus, if the true α_{ox} distribution is approximately Gaussian, the standard deviation in the actual distribution is again likely to be ~ 0.2, in agreement with that found by Avni and Tananbaum. *Thus, although potentially the width of the α_{ox} distribution found here for sample N (and the corrected sample N) are in agreement with the intrinsic value Franceschini et al. suggest is required to resolve the apparent inconsistencies between X-ray selected samples and optically selected samples with X-ray information available, it is also possible that the values found here for sample N are spuriously small due to the interaction of survival analysis and threshold effects.*

As noted by Franceschini *et al.*, an underestimation of the $< \alpha_{ox} >$ for optically selected QSOs might also remove such inconsistencies. In this dissertation, I have described several reasons why it may be more proper to consider survival analysis estimates of $< \alpha_{ox} >$ and α_{ox}^{eff} as lower limits on the actual quantities (*e.g.*, see Chap-

ter 4.), so that perhaps this is a point that deserves further study. In either case, if the intrinsic width of the α_{ox} distribution has been previously overestimated, or if $< \alpha_{ox} >$ has been previously underestimated, earlier estimates on the contribution of QSOs to the diffuse X-ray background will have been overestimates (Zamorani 1985, Franceschini, Gioia, and Maccacaro 1985).

5.2.2.1 Widening of the α_{ox} Distribution Due to Uncertainties in q_0

One source of noise in determining the intrinsic width of the α_{ox} distribution is the uncertainty in the cosmological parameter q_0. This uncertainty as a source of noise has not been stressed by previous workers. Note that while α_{ox} is a parameter determinable independent of cosmology, the righthand side of Eq. 5.2.a-b is *not* cosmology independent; in the current circumstance, cosmological uncertainties enter this relation primarily through the logarithmic term in optical luminosity. Varying H_0 merely propagates through to the quantity $\log(l_{2500})$ in the same systematic fashion for all QSOs, regardless of redshift, and thus only the zero point will change in the relationship of Eq. 5.2.a.-b if H_0 is a value other than 50 (as assumed in the derivation of this relationship). However, this is not the case for the cosmological parameter q_0. For example, for $q_0 = 1$, the luminosities have been overestimated by a *redshift dependent factor* of $(1 + z/2)^2$. For this latter, extreme q_0, a significant redshift dependent dispersion will be added to the mean relation of Eq. 5.2.a-b; the following relation will apply if $q_0 = 1$ instead of $q_0 = 0$ (the small dependence of $< \alpha_{ox} >$ on $r(z)$ which in turn depends on $q_0 = 1$ is neglected):

$$< \alpha_{ox}^{obs} > \approx < \alpha_{ox}^{pred} > + 2 \cdot (0.118) \log(1 + z/2) \qquad (5.2.2.1.a)$$

where $< \alpha_{ox}^{pred} >$ is that value predicted from Eq. 5.2.a-b with $q_0 = 0$. Shown in Table 5.2.2.1.a are some possible examples of the such q_0 effects if the actual value is 1, while the assumed value is 0.

Table 5.2.2.1.a: Dispersion in α_{ox} if $q_0 = 1$

z	$\alpha_{ox}^{obs} - \alpha_{ox}^{pred}$
0.0	0.00
0.5	0.02
1.0	0.04
1.5	0.06
2.0	0.07
2.5	0.08
3.0	0.09
3.5	0.10

Thus, the uncertainty in the precise value of q_0 can add a (redshift dependent) dispersion into the corrected α_{ox} distribution. This broadening is potentially significant for a collection of QSOs with a wide range in redshifts (*e.g.*, the objects used by Avni and Tananbaum in deriving Eq. 5.2.a-b), while the widening will be minimal in samples such as sample N which occupy a narrow redshift range. Thus, if the smaller dispersion found here for sample N is not merely due to threshold effects (and this can only be completely determined via more sensitive X-ray observations with a substantially improved α_{ox} threshold), this widening due to q_0 uncertainties would be a possible explanation for the difference in widths found for sample N and the heterogeneous collection of objects employed by Avni and Tananbaum in the derivation of Eq. 5.2.a-b.

Further, although the relationship of Eq. 5.2.a-b appears to be independent of redshift, this coupling of redshift and optical luminosity through the uncertainty in the cosmological parameter q_0 means that there is indeed a possible redshift evolution of $< \alpha_{ox} >$ hiding in the relationship which is merely obscured by our lack of knowledge of the precise value of q_0. However, the results of the measurement for sample N (again, α_{ox} can be measured independent of q_0) suggest that such q_0 effects are probably small in Eq. 5.2.a-b, and have introduced a dispersion of less than ~ 0.02 into that relationship.

Note that in the ideal world (universe), if one knew somehow that the relationship of Eq. 5.2.a.-b were a correct one, for example, from the physics of the QSO emission process (see § 5.4 for a brief discussion of a physical motivation for this sort of relationship), one could constrain q_0 by analyzing the redshift dependence of the dispersion; of course, as usual there is no *a priori* way to distinguish q_0 effects from evolutionary effects, and given the uncertainties in the relationship of Eq. 5.2.a-b,

in practice this is not of much practical use.

5.2.3 Stacking Estimate of $\alpha_{ox}^{\rm eff}$ for Sample N

Having discussed in some detail the distribution function of α_{ox} values using estimates from survival analysis, I now employ the stacking technique to once again estimate $\alpha_{ox}^{\rm eff}$ for sample N. Note that stacking does not directly yield the distribution function for α_{ox}. As with sample C (see § 5.1.2), there are a number of objects not suitable for inclusion in the stacking process. The appropriate data for the ten QSOs from Kriss and Canizares is not published and so these objects are excluded from stacking. Also, the following six objects from my grism/grens selected sample are excluded because they are in HRI fields (see discussion in § 5.1.2): 00151 + 160. Obj. 11, 12275 + 024, Obj. 15, 14149 + 251, and 15090 − 092. Further, the following five objects are severely contaminated by additional X-ray photons from strong, nearby, but unrelated X-ray sources (again, see discussion in § 5.1.2): 03061+169, 11143+184, 17274+503, 17272+502, 21556 − 202. Additionally, two objects are excluded because they are not imaged to comparable limiting X-ray flux sensitivities: 15100-089 is in a comparatively short X-ray IPC exposure, and 17252+499 is near the the support "ribs" where the IPC has reduced sensitivity. This leaves 54 sample N QSOs suitable for stacking. Stacking yields

$$\alpha_{ox}^{\rm eff} = 1.53 \pm 0.02 \qquad (5.2.3.a)$$

This value is larger than that estimated from survival analysis of the 78 sample N QSOs, but the difference is only "significant" at the 1σ level. Note that this is in keeping with the sense of the discussions of Chapter 4: survival analysis estimates are more properly regarded as lower limits on the true $\alpha_{ox}^{\rm eff}$ in the presence of significant non-random censoring. Of course, at some level this tendency is also introduced through the weighting by optical flux (Eq. 4.3.2.b.) If all objects were at

the same redshift (approximately true for sample N), the objects which are apparently brightest in the optical would also be the objects intrinsically most luminous in the optical, and thus from the dependence of $< \alpha_{ox} >$ on optical luminosity (Eq. 5.2.a-b) these apparently brightest objects would also tend to have higher α_{ox}'s. These notions are actually more strongly confirmed in the present situation than the numbers above would at first suggest, because for the same 54 objects analyzed by stacking, survival analysis yields $\alpha_{ox}^{\rm eff} = 1.48(-0.03, +0.4)$.In any case, the results here from stacking of sample N QSOs are mainly intended to be a useful check on the results from survival analysis, and do give consistent results.

5.3. The Contribution of QSOs to the Diffuse X-ray Background Assuming No Evolution of $\alpha_{ox}^{\rm eff}$

At this point, the direct measurements for sample N have been described and compared with earlier predictions and results. It is of considerable interest to estimate the total contribution of QSOs to the X-ray background. However, to do so involves the introduction of considerable uncertainties, because of the sorts of assumptions and additional parameters needed (*e.g.*, see Maccacaro, Gioia, and Stocke 1984, and the discussion of § 5.1). However, at least the following question can be addressed in a semi-quantitative fashion: Suppose that all QSOs arise from the same parent distribution of α_{ox} values, independent of their optical luminosity and redshift; what would then be their contribution to the XRB? I now show, using current estimates of the optical surface densities of QSOs, that if the survival function (and hence $< \alpha_{ox} >$ and $\alpha_{ox}^{\rm eff}$) of all QSOs were like that found here for sample N, QSOs probably could *not* dominate (contribute > 50%) to the XRB. Thus, if QSOs are to dominate the the background, the sample N data presented here, coupled with current estimates of the surface densities of optical QSOs, suggest that some sort of evolution of $< \alpha_{ox} >$ with optical luminosity and/or redshift is probably *required*.

In order to proceed with this argument, a description of the surface density of optically selected QSOs or a model of the optical luminosity function is required. I prefer to use the surface density counts directly because: (1) parameters for the optical luminosity function and its evolution are, of course, generally estimated using these data anyway (*e.g.*, Schmidt and Green 1983, Marshall 1985), and thus are implicitly tied to the surface density counts; and, (2) most current evolutionary models for the luminosity function are not very successful at reproducing the surface density counts and redshift distributions at very faint magnitudes (*e.g.*, Koo 1985).

The surface density of QSOs, especially at very faint optical magnitudes, is the topic of extensive current research. Setti (1984) compiled the then available surface density information, using information from the following QSO samples: the Bright Quasar sample of Schmidt and Green (1983) (a color selected sample, largely complete to $B \sim 16.0$), the "BFG" sample of Braccesi, Formiggini, and Gandolfi (1970) (a color selected sample largely complete to $B \sim 18.3$), the "BF" sample of Formiggini *et al.* (1980) (a color selected sample largely complete to $B = 19.8$), the Kron and Chiu proper motion selected sample (largely complete to $B \approx 21.1$), and the two-color selected sample of Koo and Kron (1982) (largely complete to $B \approx 22.6$). Setti carefully considered the probable sources of incompleteness in these samples, (*e.g.*, by also using data on high redshift QSOs derived from slitless spectroscopy surveys), and has applied the appropriate corrections to obtain an estimate of the integral counts per square degree for QSOs of *all* absolute magnitudes (no attempt was made to distinguish between "true" QSOs and Seyfert 1 nuclei). Empirically he derives the following relations between surface density counts $n(< B)$

(in units of the number per square degree) and limiting magnitude B; he found that two power laws with a break around $B \sim 20$ could fit the data well:

$$\log n(< B) \approx 1.58 + 0.91(B - 20) \quad \text{for} \quad B \leq 20.1 \qquad (5.3.a)$$

$$\log n(< B) \approx 1.67 + 0.21(B - 20) \quad \text{for} \quad B > 20.1$$

Although the B magnitude of the break is uncertain, I have assumed a sharp break to occur at $B = 20.1$ (where the two relations in 5.3.a yield the same surface density). In fact, there is probably a much smoother transition, and this sharp-break assumption is a conservative one because it probably overestimates the surface density of QSOs at $B \sim 20$ by factors of 2-3. This is a conservative assumption, since in the current application I am interested in an upper limit on the contribution of QSOs to the diffuse X-ray background. Updates on QSOs counts at very faint magnitudes in the samples of Kron and collaborators have been given recently by Koo (1985); these updates indicate that some earlier estimates (at, *e.g.*, $B = 21.1$ and 19.8) used in deriving the relations of Eq. 5.3.a may have been overestimates (see also discussion in 5.1.3). Marano *et al.* (1985) have also found surface densities at $B \sim 20$, which are lower (by a factor of two) than those derived from the BF sample. In the light of these new data, the above model is likely to be an overestimate of the surface densities of faint QSOs. Although derived using only counts to $B \sim 22.6$, this model also agrees well with counts to $B \sim 24$ recently discussed by Hamilton (1984).

From Eqs. 2.4.c-i, it is straightforward to show that a QSO of magnitude B, redshift z, and X-ray to optical luminosity ratio characterized by α_{ox}, has a flux at 2 keV (in the observer's frame) of

$$S_{2\,\mathrm{keV}} = \left(\frac{2500}{4410}\right)^{\alpha_o} (1+z)^{\alpha_o - \alpha_x} 10^{-2.605\alpha_{ox}} 10^{-0.4B} 10^{-19.380} \qquad (5.3.b)$$

In the mean, a random sample of such QSOs will yield a mean flux (per QSO) of

$$< S_{2\,\mathrm{keV}} >= \left(\frac{2500}{4410}\right)^{\alpha_o} (1+z)^{\alpha_o - \alpha_x} 10^{-0.4B} 10^{-19.380} \int_{\mathrm{all}\ \alpha_{ox}} 10^{-2.605\alpha_{ox}} f(\alpha_{ox}) d\alpha_{ox} \qquad (5.3.c)$$

where the integral is just $10^{-2.605\alpha_{ox}^{\mathrm{eff}}}$. The combined intensity from all QSOs (*e.g.*, in units of erg/cm^2/sec/ster/Hz) with magnitudes in the range B_{min} to B_{max} can then be expressed as (*e.g.*, Zamorani *et al.* 1981):

$$I_{2\,\mathrm{keV}}^{\mathrm{QSO}} = \left(\frac{2500}{4410}\right)^{\alpha_o} (1+z_{\mathrm{eff}})^{\alpha_o - \alpha_x} \int_{B_{\mathrm{min}}}^{B_{\mathrm{max}}} 10^{-0.4B} 10^{-19.380} 10^{-2.605\alpha_{ox}^{\mathrm{eff}}} \frac{dn}{dB} dB \qquad (5.3.d)$$

where z_{eff} is a typical redshift of a QSO contributing to the XRB. For the purposes of this study I follow a common optical luminosity criterion (*e.g.*, Schmidt and Green 1983) for distinguishing between Seyferts and QSOs: QSOs are defined here to be have $M_B \leq -23.0$. Then B_{max} is approximately set by the constraint that $M_B(B_{\mathrm{max}}, z_{\mathrm{eff}}) \leq -23.0$. The surface density of QSOs is so low at magnitudes brighter than $B_{\mathrm{min}} = 16.0$, that their contribution to the diffuse X-ray background will be entirely negligible, and so I take $B_{\mathrm{min}} = 16.0$. Note that in making the above approximations, I effectively have assumed that all QSOs are at z_{eff}; the consequences of this assumption will be discussed below.

Taking the survival analysis estimate of $\alpha_{ox}^{\mathrm{eff}} = 1.5$ (more properly a lower limit) for sample N, assuming that $\alpha_{ox}^{\mathrm{eff}}$ is independent of optical luminosity and redshift, and employing the optical surface densities of Eq. 5.3.a (also extrapolated to $B \sim 26$), the fractional contribution of non-evolving (in α_{ox}) QSOs to the XRB at 2 keV (for various values of z_{eff} and in various magnitude intervals), is estimated from Eq. 5.3 a to be as shown in Table 5.3.a.

Table 5.3.a: Fractional Contribution of Non-evolving (in α_{ox}) QSOs to the XRB

z_{eff} =	0.5	1.0	1.5	2.0	2.5	3.0	3.5
(B_{max}) =	(19.87)	(21.77)	(22.99)	(23.90)	(24.64)	(25.27)	(25.81)
ΔB							
16-17	0.0042	0.0049		0.0059		0.0069	
17-18	0.0136	0.0157		0.0192		0.0222	
18-19	0.0440	0.0508		0.0622		0.0719	
19-20	0.1132	0.1644		0.2014		0.2325	
20-21		0.0862		0.1055		0.1218	
21-22		0.0314		0.0509		0.0587	
22-23				0.0328		0.0379	
23-24				0.0195		0.0245	
24-25						0.0158	
25-26						0.0032	
16-B_{max}	0.1749	0.3555	0.4359	0.4974	0.5493	0.5953	0.6371

As noted before, the entries above are calculated assuming all QSOs to be at the various respective values of z_{eff}. Thus, to determine the joint contribution of QSOs to the X-ray background, the entries in Table 5.3.a should be multiplied by the fraction all QSOs, as a function of B, that are actually at $z = z_{eff}$, and then rows and columns of the table should be summed (*i.e.*, the proper calculation is obtained by an double integral over redshift and magnitudes). Unfortunately, especially at very faint magnitudes, these fractions (as functions of z and B) are not well known. Very approximately, however, the BF sample, sample C of the current study, and the very faint samples of Koo (1985), suggest the following values are reasonable: $z_{eff} < 1.5$ to $B < 19.5$, and $z_{eff} < 2.5$ to $B \sim 22.6$. Thus, noting that QSOs fainter than $B = 22.65$ contribute only a few percent to the XRB (see, *e.g.*, column 7 of Table 5.3.a), *I crudely estimate from this table that the contribution of all QSOs to the XRB would be less than 50% if there is no dependence of α_{ox} on optical luminosity and/or redshift of the sort described by Eq. 5.2.a-b. That is, unless lower optical luminosity and/or lower redshift QSOs are relatively more X-ray luminous than the high redshift/high luminosity QSOs of sample N, QSOs ($M_B \leq -23.0$) probably cannot dominate the XRB.* Even in the most optimistic case, with all QSOs at $z = 3.5$ (certainly not a likely situation), the contribution is $< 60\%$.

Thus, the usual arguments can be (at least qualitatively) inverted: The X-ray properties of QSOs, combined with the added constraint that the combined X-ray emission from QSO not exceed the XRB, have previously (*e.g.*, Setti and Woltjer 1979, Zamorani *et al.* 1981) been used to argue that the optical QSO surface density counts must show a turnover at faint optical magnitudes. Here I argue that the recently determined optical counts at faint magnitudes (which indeed confirm such a turnover at $B \sim 20.$), coupled with the X-ray properties of sample N QSOs, at least qualitatively imply that the ratio of X-ray to optical luminosity in QSOs *must*

evolve with optical luminosity and/or redshift if QSOs are to dominate (contribute more than 50%) to the XRB. Note that the reasons enumerated in § 5.1 for believing that the value found above for $\alpha_{ox}^{\rm eff}$ for sample N is more properly regarded as an estimate of a lower limit on the true value, strengthen this conclusion; for example, if one repeats the calculations of Table 5.3.a, but with $\alpha_x = 1.2$, the values in the table are decreased by $\sim 40\%$.

5.4. Is the Dependence of $< \alpha_{ox} >$ on Optical Luminosity a Physical Effect?

In the previous section, I showed that, unless there is some evolution (with optical luminosity and/or redshift) of α_{ox}, objects traditionally classified as QSO ($M_B \leq -23.0$) probably cannot be the dominant contributors to the XRB. However, as much of the earlier discussion has emphasized, there is considerable evidence that such evolution does exist (*e.g.*, Avni and Tananbaum 1981, and other references in § 5.2).

A number of workers (*e.g.*, Tucker 1983, Shull 1983, Netzer 1985) have given physical interpretation for a relationship like that in Eq. 5.2.a-b. For example, Tucker has shown that a thick disk around a black hole accreting at rates near the Eddington limit would be consistent with the sort of dependence of X-ray luminosity on optical luminosity described by Eq. 5.2.a-b. He showed that in such a situation, one might predict a relation between optical and X-ray luminosity of $L_x \propto L_{\rm opt}^{\gamma}$, with γ in the range 0.5–0.8. Accretion substantially below the Eddington limit, or non-thermal Compton synchrotron models would predict a γ of ~ 1.0, however.

Recently Netzer (1985) has also given a possible physical interpretation for the relationship of Eq. 5.2.a-b. He suggests that random geometric orientations (from one QSO to another) of an optically thick (but geometrically thin) disk might give

rise to a range of *apparent* optical luminosities for a given *intrinsic* disk luminosity. There is evidence for such a disk from the "optical bump" seen in QSO continuum spectra (*e.g.*, Malkan and Sargent 1982, Malkan 1983). The X-ray emission is assumed to be more isotropic (for example, it might arise near the very central engine, not in the disk) so that the observed X-ray flux is not strongly affected by the orientation of the thin disk; then for an intrinsic input strict proportionality of $L_x \propto L_{\rm opt}$ (or $\gamma = 1$), a random set of disk orientations (as would be observed in a sample of objects) produces an apparent relation $L_x \propto L_{\rm opt}^{\gamma}$ with $\gamma < 1$. For given intrinsic optical and X-ray luminosities, the QSO viewed with its disk more nearly edge-on will have a lower apparent optical luminosity than a comparable QSO viewed with the disk nearly face-on; but their (observed and intrinsic) X-ray luminosities will be the same. Thus, the optically more luminous (face-on disk) QSOs will seem to have a smaller X-ray to optical emissivity ratio (*i.e.*, a larger α_{ox}).

On the other hand, Chanan (1983) and my investigations in Chapter 4 of this dissertation also show that, at least potentially, non-random α_{ox} threshold effects might mimic the sort of dependence described by Eq. 5.2.a-b. In light of the results of the previous section (that is, that a *physical* relationship is required if QSOs are to dominate the XRB), it is important to establish that the relation of Eq. 5.2.a-b is not due merely to such threshold effects.

Reviewing the results of Chapter 4, for a given redshift, and compared with the low optical luminosity objects, the optically more luminous QSOs will systematically tend to have a more sensitive α_{ox} threshold (for a fixed X-ray flux threshold); thus for QSOs of a given redshift, observation of the high optical luminosity objects will more effectively sample the high α_{ox} portions of the α_{ox} distribution. The systematic

offset in α_{ox} thresholds (for a fixed X-ray flux threshold) between the high and low optical luminosity objects will cause survival analysis to incorrectly presume that the lower optical luminosity objects have systematically lower α_{ox} values, even when both high and low optical luminosity objects arise from the identical parent distribution of α_{ox} values. However, there is also observational selection at work that tends to oppose this sort of spurious threshold effect: most optically luminous QSOs are at high redshift and therefore *apparently* faint; for a fixed X-ray flux threshold, the apparently faint objects will tend to have systematically less sensitive α_{ox} thresholds.

In Figure 5.4.a I have plotted the α_{ox} *thresholds* against optical luminosity for the objects used by Avni and Tananbaum to derive the relation of Eq. 5.2.a. If the relation of Eq. 5.2.a were due mainly to the presence of α_{ox} threshold effects, the plot of Figure 5.4.a would be expected to show that the high optical luminosity objects were systematically surveyed to more sensitive α_{ox} thresholds than the low luminosity objects. There is no evidence for such a pattern in Figure 5.4.a, and thus I conclude that the relationship of Eq. 5.2.a-b is unlikely to be due to such non-random threshold effects. For the objects considered by Avni and Tananbaum in deriving Eq. 5.2.a-b, there is a wide enough range and sufficiently sensitive set of α_{ox} thresholds (many of the objects they include have large apparent brightnesses) that a spurious relation due to threshold effect is unlikely.

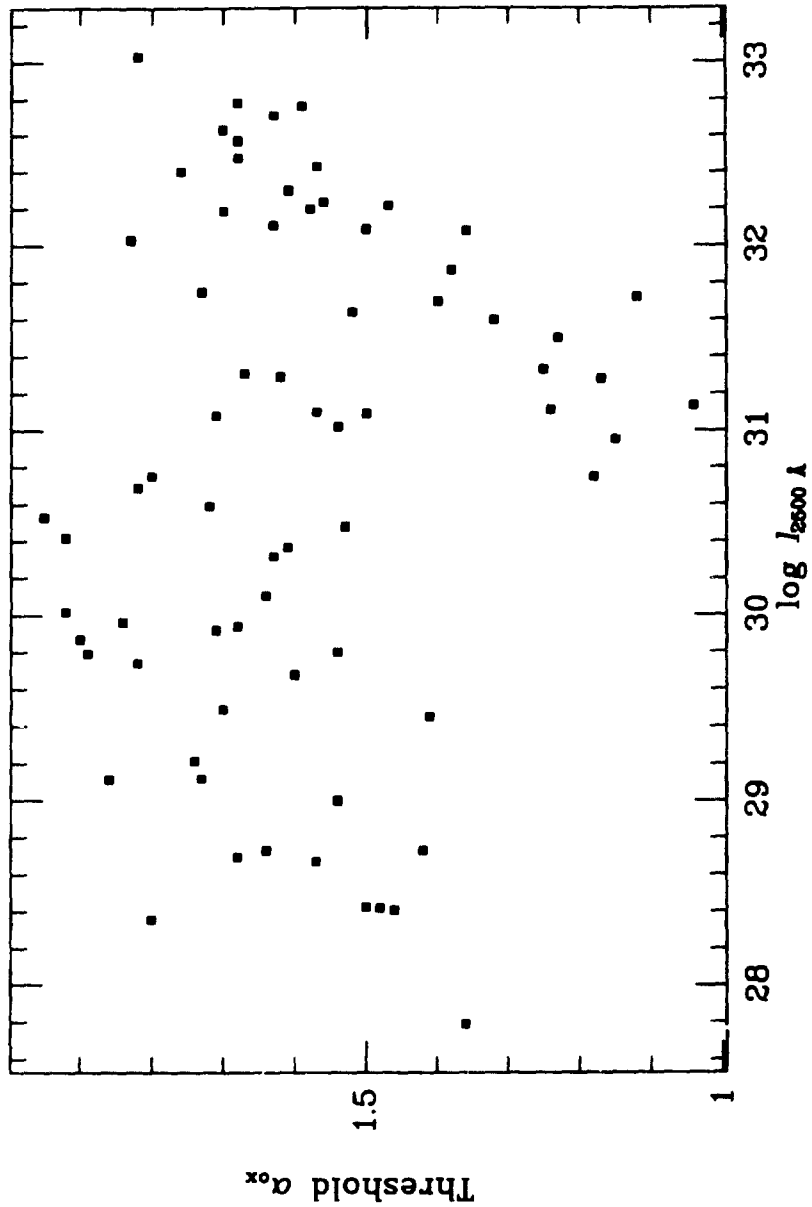

Figure 5.4.a. α_{ox} threshold effects do not appear to be significant in the data used by Avni and Tananbaum to empirically model the dependence of α_{ox} on optical luminosity and/or redshift. If such effects were significant for this sample, a correlation between optical luminosity and α_{ox} thresholds would be expected.

Thus, there are now at least three motivations for believing that the relationship of Eq. 5.2.a-b is likely to be a physical one (*i.e.*, $< \alpha_{ox} >$ is dependent on redshift and/or optical luminosity) rather than a spurious one due to threshold/selection effects: (1) there is no apparent systematic difference in the α_{ox} threshold pattern between low and high optical luminosity objects; (2) the relationship (if due to a dependence on optical luminosity and not on redshift) has plausible physical interpretations; and (3) the results of § 5.3 suggest that such a relationship is probably *required* if QSOs are to dominate the diffuse X-ray background. (It should also be noted that a sample of radio selected objects show a qualitatively similar dependence of $< \alpha_{ox} >$ on optical luminosity: Tananbaum *et al.* 1983).

5.5 The Contribution of QSOs to the Diffuse X-ray Background with Evolution of α_{ox}^{eff}

With some added confidence that the relation of Eq. 5.2.a-b is probably a physical one, I now enter the even more uncertain regime of trying to predict the contribution of all QSOs to the diffuse X-ray background in the presence of such $< \alpha_{ox} >$ evolution. I assume that there is a constant offset between α_{ox}^{eff} and $< \alpha_{ox} >$, so that Eq. 5.2.b (neglecting the small explicit redshift dependence) can be expressed, in terms of α_{ox}^{eff}, as

$$\alpha_{ox}^{eff} = \alpha_{ox}^{eff}(31.44) + 0.118(\log l_{2500} - 31.44) \qquad (5.5.a)$$

where $\alpha_{ox}^{eff}(31.44) = 1.50$ is the value found here for sample N QSOs with $< \log(l_{2500}) >= 31.44$ and $< z >= 2.1$. Using the approach outlined above in § 5.3, but with the optical luminosity dependent α_{ox}^{eff} of Eq. 5.5.a, yields the results in Table 5 5.a (which should be compared with the Table 5.3.a).

Table 5.5.a: Fractional Contribution of Evolving (in α_{ox}) QSOs to the XRB

z_{eff} =	0.5	1.0	1.5	2.0	2.5	3.0	3.5
(B_{max}) =	(19.87)	(21.77)	(22.99)	(23.90)	(24.64)	(25.27)	(25.81)
Δ B							
16-17	0.0059	0.0040		0.0027		0.0021	
17-18	0.0254	0.0171		0.0115		0.0090	
18-19	0.1091	0.0736		0.0493		0.0387	
19-20	0.3632	0.3159		0.2117		0.1661	
20-21		0.2056		0.1378		0.1081	
21-22		0.1061		0.0906		0.0711	
22-23				0.0777		0.0610	
23-24				0.0604		0.0523	
24-25						0.0447	
25-26						0.0108	
16-B_{max}	0.5032	0.7223	0.6863	0.6417	0.6004	0.5639	0.5318
16-19.5	0.2930	0.1975	0.1565	0.1324	0.1159	0.1038	0.0945

There are many uncertainties involved in the preceding calculation, some of which are difficult to quantify and probably systematic (*e.g.*, the uncertainty associated with the parametric *form* of the model for the surface densities of Eq. 5.3.a); nevertheless, some (at least semi-quantitative) approximate information can be gleaned from this Table 5.5.a.

First, note that *if the typical contributor to the X-ray background is at moderate redshifts of* $z_{\rm eff} \sim 1-1.5$, *very substantial contributions* ($\sim 70\%$) *to the diffuse XRB are consistent with the data.* From the data in the BF sample, and that in sample C, $z_{eff} < 1.5$ is certainly reasonable to $z = 19.5$. Further, the results presented in Koo (1985) of spectroscopy of "two-color" selected QSOs to $B \sim 22.5$ also show that $\sim 1/2$ the objects are at redshifts substantially less than $z = 2$. *The additional contributions of (luminous) active galaxies* ($\sim 15\%$), *clusters of galaxies* ($\sim 5\%$), *and low luminosity active galaxies* ($\sim 5\%$), *(e.g., see Fabian 1984, and references therein) can thus yield a consistent picture (to within a few percent!) of the entire XRB arising from the superposition of point X-ray sources.* Note also that the value predicted in Table 5.5.a for the contributions from all QSOs to $B < 19.5$ for the case of $z_{\rm eff} \sim 1$. This is quite consistent with that determined in § 5.1.3 from much more direct considerations of the BF and C (complete) samples. Given all the uncertainties involved in the calculations of the entries in Table 5.5.a, that the possible contribution of QSOs and other point sources to the XRB can come out so close to unity seems somewhat surprising.

However, note again that there are number of reasons to believe that the values in Table 5.5.a may more properly be considered as upper limits on the fractional contributions:

(1) A few ($< 20\%$) of the objects in sample N are probably low redshift QSOs:

the correlation of $< \alpha_{ox} >$ and optical luminosity in Eq. 5.2.a-b means that for a given apparent magnitude, these lower redshift objects are likely to have greater X-ray emissivities than their higher redshift (higher optical luminosity) counterparts. This could cause an overestimation of $\alpha_{ox}^{\rm eff}(31.44)$.

(2) A great deal of current data (Chapter 3) suggests that the actual X-ray slope in QSOs is substantially steeper on the average than the assumed value of $\alpha_x = 0.5$; not only does it then become difficult to reconcile the spectrum of the XRB ($\alpha_x \sim 0.4$) with that from a superposition of QSOs, but the estimated flux contribution from QSOs at 2 keV (in the observer's reference frame) will be overestimated (by $\sim 40\%$ if $\alpha_x = 1.2$ is the true value).

(3) The surface densities of sample N QSOs and X-ray sources at these faint X-ray and optical magnitudes are such that the order of one spurious identification of a high redshift QSO and an unrelated X-ray source is expected. Again, this will tend to cause an overestimation of $\alpha_{ox}^{\rm eff}$.

(4) The results of Chapter 4 on the interactions of survival analysis and α_{ox} thresholds again suggest that it may be more proper to consider $\alpha_{ox}^{\rm eff}(31.44) = 1.50$ to be a lower limit.

(5) The surface densities implied by the empirical model of Eq. 5.3.a may overestimate the surface density of QSOs near the turnover point ($B \sim 20$) by factors of 2 or 3.

Now note from Table 5.5.a that whatever the absolute fraction of the XRB which is due to QSOs, roughly *half the contribution due to QSOs is likely to arise from QSOs at apparent magnitudes brighter than* $B \sim 20$. *Such QSOs are precisely those which have been studied in X-rays in the BF sample (Marshall et al. 1983) for* $z < 2.2$, *and in this dissertation for* $z > 1.8$. Ultimately, the least assumptive

way of getting at the contribution of QSOs to the XRB is to obtain a large fraction of X-ray detections in complete samples. Thus, a very useful (and feasible!) sort of experiment to perform on future more sensitive X-ray satellites (*e.g.*, ROSAT and AXAF) will be to image in X-rays complete samples, (like the BF sample and sample C) which have completeness limits in the range $B = 19 - ?$ ery nearly complete detection fractions (*e.g.*, > 80% to $B \sim 19.5$ in the ROSAT deep surveys: Maccacaro 1984) might be expected and should yield considerable insight into the sort of typical QSO that could potentially contribute substantially to the XRB. Further, at such ROSAT deep survey sensitivities, $\sim$ 50% of the QSOs to $B \sim 21$ should be detected (if the properties of these faint QSOs follow the ideas described in this chapter); the results of Table 5.5.a suggest that under favorable circumstances (say, $z_{\rm eff} \sim 1$), QSOs brighter than $B \sim 21$ may account for as much as $\sim$ 60% of the XRB, and indeed for 85% of the background fraction due to QSOs.

A qualitative inference that follows from the considerations of § 5.3–5.5 is the following: If QSOs are the dominant contributors to the XRB, the typical contributor is probably a low to moderate optical luminosity QSO at moderate redshifts of $z \sim 1 - 1.5$ (*e.g.*, at $z = 1$, a QSO of magnitude $B = 20.1$ has an absolute B magnitude of $Mb = -24.7$). The recent results of Koo and Kron (*e.g.*, Koo 1985), Hazard and McMahon (1985), Schneider, Gunn and Schmidt (1983), and Osmer (1980) on the paucity of high redshift QSOs (scarcity in comparison to that expected from most QSO evolutionary models) is, at least *qualitatively*, in agreement with the sense of this argument. High redshift QSOs apparently have too low a surface density to contribute substantially, and because they have relatively higher optical luminosities, they also have lower X-ray fluxes for a given apparent magnitude than their lower redshift counterparts; while the QSOs to say $z \leq 0.5$ are simply not abundant enough to make a substantial contribution.

5.6 Summary

In summary of the results of this final (and le ngthy) chapter:

(1) For $B < 19.5$ and $1.8 < z < 3.0$, sample C (the complete sample) has been used to show (§ 5.1.2.) that the fractional contribution of such QSOs to the diffuse X-ray background is less than 3%. This small value results in part from the relatively low surface density of such high redshift objects, but also because of their comparatively small X-ray to optical emissivity ratios. It is to be stressed that this value should probably be regarded as an upper limit to the contribution (for a lengthy set of reasons enumerated in § 5.1). Further, this estimate is based on a measurement (survival analysis and stacking giving consistent results) which does not require any extrapolations of the dependence of α_{ox} on optical luminosity and/or redshift. Essentially the only parameters or assumptions required are the X-ray spectral slope and the surface density of sample C-type objects. The latter value is obtained directly from the sample, while the X-ray spectral slope is assumed (conservatively) to be $\alpha_x = 0.5$.

(2) Combining the results for sample C with published X-ray data of the BF sample (*e.g.*, Marshall 1983), and employing survival analysis, I estimate (§ 5.1.3.d) that (an upper limit) to the contribution of all QSOs brighter than $B = 19.5$ to the X-ray background is $21 \pm 8\%$. Again, this estimate relies almost entirely on data from the complete BF sample and sample C, and therefore is also not subject to the vast majority of the assumptions and parameters which are usually required in such an application (*e.g.*, Maccacaro, Gioia, and Stocke 1984); most of the uncertainty in this result enters from the small sample size (14) of appropriate objects in the BF sample.

(3) Because of their apparent dependence on optical luminosity and/or redshift,

the parameters $< \alpha_{ox} >$ and $\alpha_{ox}^{\rm eff}$, as well as the distribution of α_{ox} values, are directly interpretable quantities only if measured in a narrow region of optical luminosity and redshift space. The measurements for sample N (which is by construction such a "narrow" sample) yield $< \alpha_{ox} >= 1.58$, and $\alpha_{ox}^{\rm eff} = 1.50$ for QSOs with $< \log(l_{2500}) >= 31.44$, and $< z >= 2.1$. These values, which were determined here in a model independent fashion (*i.e.*, without the need to make large corrections for the dependence of $< \alpha_{ox} >$ on optical luminosity and/or redshift through a parametric relation such as Eq. 5.2.a-b), are in excellent agreement with the values predicted from the empirical relation derived by Avni and Tananbaum (1982) for the evolution of $< \alpha_{ox} >$ with optical luminosity and/or redshift. Applying the corrections of Eq. 5.2.a-b gives corrected values of $< \alpha_{ox} >= 1.56 \pm 0.03$, and $\alpha_{ox}^{\rm eff} = 1.50 \pm 0.03$ for a distribution of QSOs with $< \log(l_{2500}) >= 31.44$ and $< z >= 2.1$.

(4) The width of the α_{ox} distribution for sample N is found to be smaller than that determined by Avni and Tananbaum for a sample with quite different selection criteria: for sample N I find $\sigma(\alpha_{ox}) = 0.14$ (or 0.12 for the corrected residuals), while Avni and Tananbaum found $\sigma(\alpha_{ox}) \sim 0.2$. It is likely that α_{ox} threshold effects are artificially narrowing the width of the distribution: the half-width of the distribution below $< \alpha_{ox} >$ is of order 0.1 for sample N, and thus, unless the distribution is quite skew, its true full width is probably also $\sigma(\alpha_{ox}) \sim 0.2$, in agreement with the Avni and Tananbaum result. Franceschini, Gioia, and Maccacaro (1985) have suggested that an intrinsic width of $\sigma(\alpha_{ox}) = 0.14$ is required to resolve some apparent discrepancies between the X-ray selected and optically selected sample of QSOs. Thus, although the apparent width found here for the distribution of α_{ox} values for sample N potentially is in agreement

with the value predicted by Franceschini *et al.*, it is also possible that the value found here has been artificially narrowed (§ 5.2.2.) by α_{ox} threshold effects.

(5) Using the value of $\alpha_{ox}^{\rm eff}$ found for sample N, and assuming no dependence on optical luminosity or redshift, it is found (§ 5.3)that QSOs (defined here to be $M_B \leq -23.0$) probably could not dominate the XRB. That is, the current observations of a turnover in the surface density counts of optically faint QSOs can now (with the assumption that QSOs make up the background) be used to constrain the evolution of their relative X-ray luminosities. In particular, I estimate that with no dependence of $< \alpha_{ox} >$ on optical luminosity and/or redshift (so that lower luminosity and/or lower redshift have relatively higher X-ray emissivities) the contribution from all QSO to the XRB is $< 50\%$.

(6) However, if there is a physical dependence of $< \alpha_{ox} >$ on optical luminosity and/or redshift of the sort empirically modeled by Avni and Tananbaum (and I make several arguments that this is likely to be a physical relationship), then QSOs can dominate the background. If the typical contributor to the XRB is a QSO with moderate redshift of 1–1.5, contributions to the XRB of $\sim 70\%$ are found. Coupled with additional contributions of $\sim 15\%$ from luminous active galaxies (such as Seyferts), $\sim 5\%$ from low luminosity active galaxies (for example, starburst galaxies), and $\sim 5\%$ from clusters of galaxies, the total discrete source contribution to the diffuse XRB is found to be very close to unity (within a few percent). There are a number of reasons to believe it prudent to treat this number as an estimate of an upper limit on the contribution to the XRB.

(7) It is shown for the Avni and Tananbaum model and a reasonable (although perhaps over-optimistic) surface density/magnitude relation for optically selected

QSOs, that whatever the absolute contribution of QSOs to the XRB, on the order of one-half arises from QSOs brighter than $B \sim 20$. Thus, the BF sample and the grism/grens selected samples described here are at least partially sampling the sort of QSOs that are the typical contributors to the XRB (if the XRB arises from the superposition of point sources).

(8) Qualitatively, several of the results above tend to suggest that the typical contributor to the XRB may well be a moderate redshift object with moderate to low optical luminosity: the high redshift QSOs apparently have too low a surface density, and because they are more optically luminous, have lower X-ray fluxes for a given apparent magnitude as well. Nearby QSOs ($z < 0.5$) are simply not abundant enough to make a substantial contribution.

BIBLIOGRAPHY

Anderson, S. F., and Margon, B. 1983, in "Quasars and Gravitational Lenses", Proc. of the 24th Liege Ap. Colloq., Universite de Liege, p.68.

Avni, Y., Soltan, A., Tananbaum, H., Zamorani, G. 1980, *Ap. J.*, **238**, 800.

Avni, Y., and Tananbaum, H. 1982, *Ap. J. (Letters)*, **262**, L17.

Boldt, E., and Leiter, D. 1984, 276, 427.

Bowen, I. S., and Vaughan, A. H. 1973, *Publ. Astron. Soc. Pac.*, **85**, 175.

Bowyer, S., Lampton, M., Mack, J., and de Mendonca, F. 1970, *Ap. J. (Letters)*, **161**, L1.

Brown, R. L., and Gould, R. J. 1970, *Phys. Rev. D*, **1**, 2252.

Buchroeder, R. A. 1974, "A Raytrace Study of Prime Focus Grisms and the Like", Report of the Optical Sciences Center, University of Arizona, Tucson, Ariz.

Caillault, J.-P., and Helfand, D. J. 1985, *Ap. J.*, **289**, 279.

Carswell, R. F., and Smith, M. G. 1978, *M.N.R.A.S.*, **185**, 381.

Chanan, G. A. 1983, *Ap. J.*, **275**, 45.

Clowes, R. G. 1981, *M.N.R.A.S.*, **197**, 731.

Crampton, D., Schade, D., and Cowley A. P. 1985, *A. J.*, **90**, 987.

di Francia, G. 1949, *Nuovo Cimento*, **6**, 1.

Elvis, M., and Lawrence, A., 1985, in "Astrophysics of Active Galaxies and Quasars", Proc. of the 7th Santa Cruz Workshop on Astr. and Ap., J. Miller (ed.).

Fabian, A. C. 1981, *Ann. N. Y. Acad. Sci.*, **375**, 235.

Feigelson, E. D., and Nelson, P. I. 1985, *Ap. J.*, **293**, 192.

Field, G. B., and Perrenod, S. C. 1977, *Ap. J.*, **146**, 686.

Formiggini, L., Zitelli, V., Bonoli, F., and Braccesi, A. 1980, *Astr. Ap. Suppl.*, **39**, 129.

Fouere, J. C., *et al.* 1982, IAU Colloq. No. 67, "Instrumentation for Astronomy with Large Optical Telescopes", Ap. and Space Sci. Lib, Vol. 92, C.M. Humphries (ed.), Reidel (1982), p. 143.

Franceschini, A., Gioia, I. M., and Maccacaro, T. 1985, submitted to *Ap. J.*

Gaston, B. 1983, *Ap. J.*, **272**, 411.

Giacconi, R., Gursky, H., Paolini, F. R., and Rossi, B. B. 1962, *Phys. Rev. Letters*, **9**, 439.

Giacconi, R. 1974, in "X-Ray Astronomy", *Ap. and Sp. Sci. Lib. Vol 43.*, eds. R. Giacconi and H. Gursky, Dordrecht:Reidel, p. 1.

Giacconi, R., *et al.* 1979a, *Ap. J.*, **230**, 540.

Giacconi, R., *et al.* 1979b, *Ap. J. (Letters)*, **234**, L1.

Giacconi, R., *et al.* 1981, in "Telescopes for the 1980's", *Ann. Rev. Monograph*, eds. G. Burbidge and A. Hewitt, p. 195.

Gioia, I. M., *et al.* 1984, *Ap. J.*, **283**, 486.

Greenstein, J. L., and Matthews, T. A. 1963, *Nature*, **197**, 1041.

Gursky, H., Giacconi, R., Paolini, F. R., and Rossi, B. B. 1963, *Phys. Rev. Letters*, **11**, 524.

Gursky, H., and Schwartz, D. 1974, in "X-Ray Astronomy", *Ap. and Sp. Sci. Lib.* Vol. 43, R. Giacconi and H. Gursky (eds.), Dordrecht:Reidel, p. 25.

Harnden, Jr., F. R., Fabricant, D. G., Harris, D. E., and Schwartz, J. 1984, "Scientific Specification of the Data Analysis System for the Einstein Observatory (HEAO-2) Imaging Proportional Counter", SAO Special Report 393.

Hayman, P. G., Hazard, C., and Sanitt, N. 1979, *M.N.R.A.S.*, **189**, 853.

Hazard, C., and McMahon, R. 1985, *Nature*, **314**, 238.

Hoag, A. A., and Schroeder, D. J. 1970, *Publ. Astron. Soc. Pac.*, **82**, 1141.

Hoag, A. A., and Smith, M. G. 1977, *Ap. J.*, **217**, 362.

Kalbfleisch, J., and Prentice, R. L. 1980, "The Statistical Analysis of Failure Time Data", New York: Wiley.

Kaplan, E. L., and Meier, P. 1958, *J. Am. Stat. Assoc.*, **53**, 457.

Koo, D. C., and Kron, R. G. 1980, *Pub. Astron. Soc. Pac.*, **92**, 537.

Koo, D. C. 1985, in "Structure and Evolution of Active Galactic Nuclei", Trieste, in press.

Kriss, G. A., and Canizares, C. R. 1985, submitted to *Ap. J.*

Ku, W. H.-M., Helfand, D. J., and Lucy, L. B. 1980, *Nature*, **288**, 323.

Maccacaro, T. 1984, in "X-ray and UV Emission from Active Galactic Nuclei" Conf. Proc. of Max-Planck Institut, W. Brinkmann and J. Trümper (eds.), p. 63.

Maccacaro, T., Gioia, I. M., and Stocke, J. T. 1984, *Ap. J.*, **283**, 486.

Marano, B., Zamorani, G., and Zitelli, V. 1984, *The Messenger*, **38**, 6.

Margon, B., Downes R. A., and Chanan, G. A. 1985, *Ap. J. Suppl.*, **59**, 1.

Marshall, F. E., *et al.* 1980, *Ap. J.*, **235**, 4.

Marshall, H. L. 1983, Ph.D. dissertation, Harvard Univ.

Marshall, H. L., *et al.* 1984, *Ap. J.*, **283**, 50.

Marshall, H. L. 1985, submitted to *Ap. J.*

Netzer, H., *et al.* 1985, *M.N.R.A.S.*, **216**, 63.

Mushotzky, R. F., Marshall, F. E., Boldt, E. A., Holt, S. S., and Serlemitsos, P. J., 1980, *Ap. J.*, **235**, 377.

Osmer, P. S. 1980, *Ap. J. Suppl.*, **42**, 523.

Osmer, P. S. 1982, *Ap. J.*, **253**, 28.

Ostriker, J. P, and Heisler, J. 1984, *Ap. J.*, **278**, 1.

Petre, R., Mushotzky, R. F., Krolick, J. H., and Holt, S. S. 1984, *Ap. J.*, **280**, 499.

Pfleiderer, J., and Krommidas, P. 1982, *M.N.R.A.S.*, **198**, 281.

Reichert, G. A., Mason, K. O., Thorstensen, J. R., and Bowyer, S. 1982, *Ap. J.*, **240**, 347.

Richstone, D. O., and Schmidt, M. 1980, *Ap. J.*, **235**, 361.

Rothschild, R. E., *et al.*, 1983, *Ap. J.*, **269**, 423.

Schmidt, M. 1963, *Nature*, **197**, 1040.

Schmidt, M. 1968, *Ap. J.*, **151**, 393.

Schmidt, M., and Green, R. F. 1983, *Ap. J.*, **352**. 70.

Schmitt, J. H. M. M. 1985, *Ap. J.*, **293**, 178.

Schneider, D., Schmidt, M.. and Gunn, J. 1983, *BAAS*, **15**, 957.

Schwartz, D., and Gursky, H. 19 4, in "X-Ray Astronomy", *Ap. and Sp. Sci. Lib., Vol. 48*, R. Giacconi and H. Gursky (eds.), Dordrecht:Reidel, p. 359.

Schwartz, D. 1979, in "X-ray Astronomy", Proc. IAU/COSPAR Symp., W. A. Baity and L. E. Peterson (eds.), Pergamon Press: New York. p. *.

Setti, G., and Woltjer, L. 1979, *Astr. Ap.*, **76**, L1.

Shafer, R. A. 1983, Ph.D. dissertation, Univ. of Maryland.

Shafer, R. A., and Fabian, A. C. 1983, in "Early Evolution of the Universe and its Present Structure", IAU 104, G. Abell and G. Chincarini (eds.), p. 333.

Shull, J. M. 1983, *Ap. J.*, **264**, 446.

Smith, M. G. 1978, *Vistas in Astronomy*, **22**, 321.

Smith, M. G. 1981, in "Investigating the Universe", ed. F. P. Kahn, Reidel (Dordrecht), p.151.

Smith, M. G. 1982, in "Progress in Cosmology", Oxford International Symposium, ed. A. W. Wolfendale (Dordrecht:Reidel), p.275.

Smith, M. G., 1983, in "Quasars and Gravitational Lenses", Proc. of the 24th Liege Int. Ap. Colloq., (Universite de Liege), p.4.

Sramek, R. A., and Weedman, D. W. 1978, *Ap. J.*, **221**, 468.

Stocke, J. T., *et al.* 1983, *Ap. J.*, **273**, 458.

Tananbaum, H. *et al.* 1979, *Ap. J.(Letters)*, **234**, L9.

Tananbaum, H. *et al.* 1983, *Ap. J.*, **268**, 60.

Tananbaum, H. *et al.* 1985, in preparation.

Tucker, W. H. 1983, *Ap. J.*, **271**, 531.

Vaucher, B., and Weedman, D. W. 1980, *Ap. J.*, **240**, 10.

Veron, P. 1983, in "Quasars and Gravitational Lenses", Proc. of the 24th Liege Int. Ap. Colloq., (Universite de Liege), p.215.

Veron-Cetty, M.-P., and Veron, P., "A Catalogue of Quasars and Active Nuclei (2nd Edition)", ESO Scientific Report No. 4-April 1985

Warwick, R. S., Pye, J. P., and Fabian, A. C. 1980, *M.N.R.A.S.*, **190**, 243.

Weedman, D. W. 1985a, *Ap. J. Suppl.*, **57**, 523.

Weedman, D. W. 1985b, preprint.

Wolter, H. 1952, *Ann. Physik*, **10**, 94.

Worrall, D. M., Mushotzky, R. F., Boldt, E. A., Holt, S. S., and Serlemitsos, P. J. 1979, *Ap. J.*, **232**, 683.

Zamorani, G. *et al.* 1981, *Ap. J.*, **245**, 357.

Zamorani, G. 1983, in "VLBI and Compact Radio Sources", IAU Symp. No. 110, R. Fanti, K. Kellerman, and G. Setti (eds.)

Zamorani, G. 1985, submitted to *Ap. J.*

APPENDIX A: A NOTE ABOUT X-RAY DATA RIGHTS

Although virtually all the Einstein X-ray data used in this dissertation is now in the public domain, access to much of it was generously granted by the respective observers prior to the public release date. In exchange for such access, an agreement was made that the optical coordinates and finding charts for X-ray source identifications not be published in the current dissertation (a similar agreement applies to two QSOs not detected in X-rays as well). In keeping with these agreements, such objects are denoted merely as Obj. 1, Obj. 2, etc. Finding charts, optical coordinates, etc. for these objects will be published at a later date, but are not include within this dissertation.

APPENDIX B: FINDING CHARTS FOR SAMPLE C AND N QSOS

In this appendix, finding charts for most of the sample C and N QSOs are presented. Finding charts are not given for QSOs denoted by "Obj." earlier in the text. See Appendix A for an explanation of this nomenclature. A few of the sample C and N QSOs are previously known QSOs (see Table 2.3.a); for these latter objects new finding charts are not presented here.

Notes to finding charts: 00151+160 is a faint object near end of diffraction spike of bright star on POSS. 02036+150 is the southwest component of faint pair. 09382+117 is 6" northwest of relatively bright star. 12275+024 is the middle object in a triple. 20374-007 is 7" northwest of relatively bright star. 21265-150 is 11" southwest of relatively bright star. 21570-302 is 5" northeast of relatively bright star.

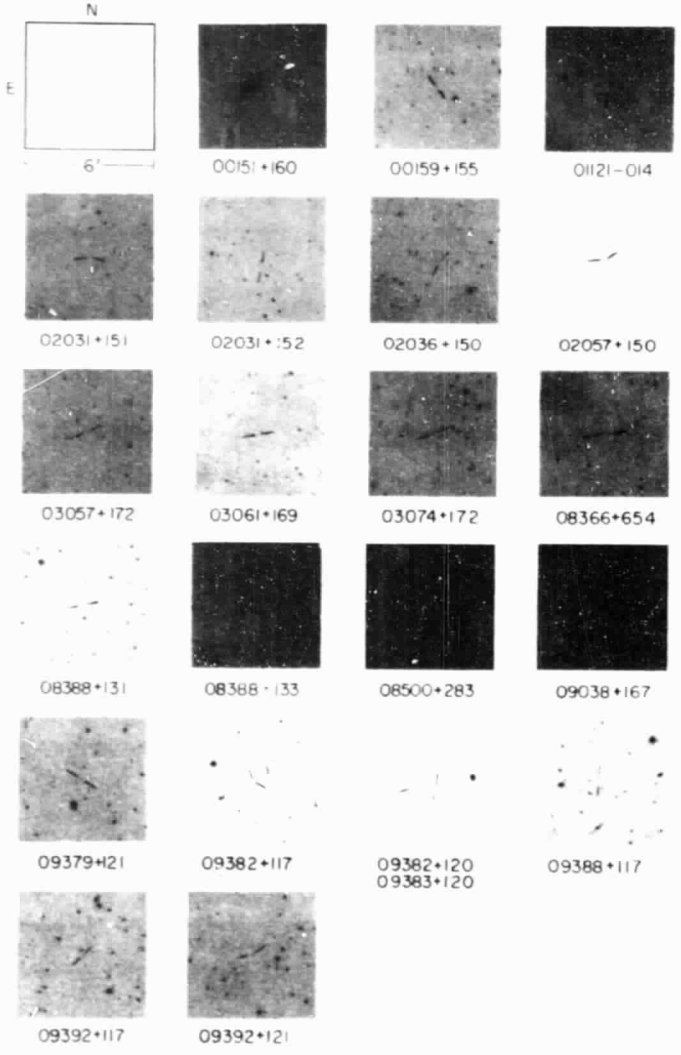

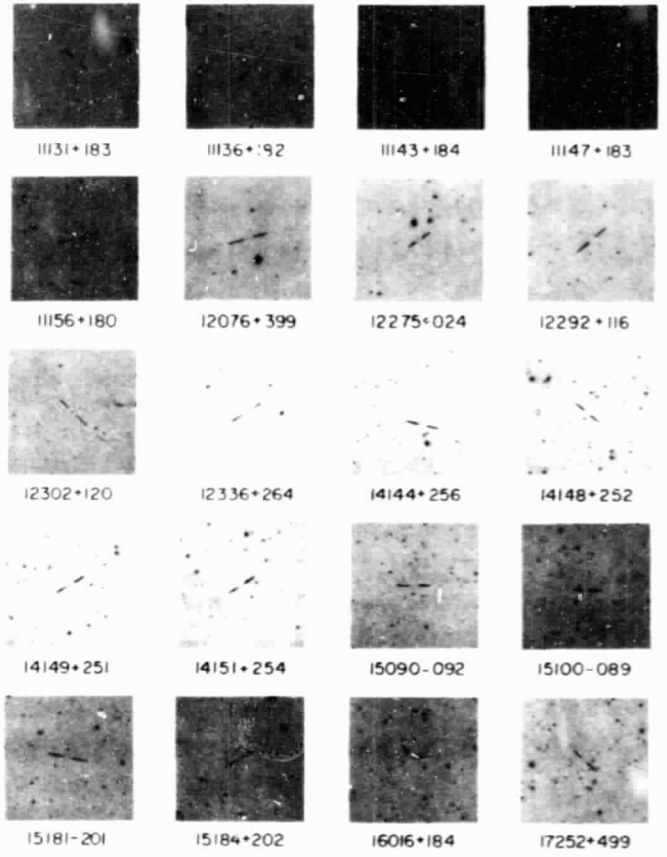

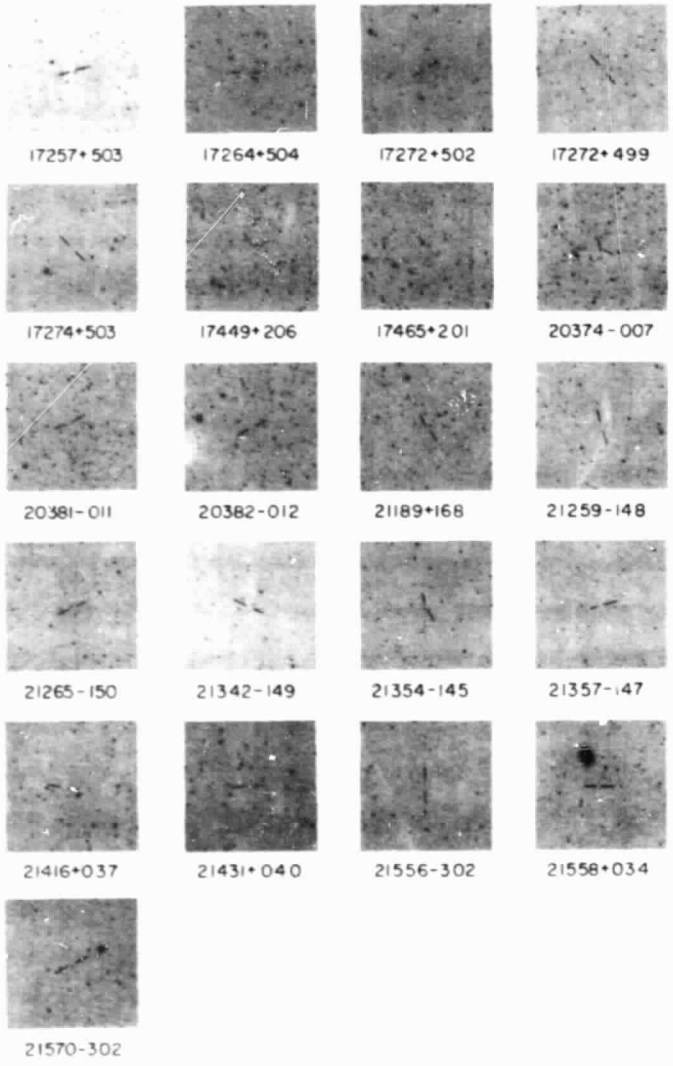

ACKNOWLEDGEMENTS

Foremost among those whom I would like to thank for support of this dissertation is Dr. Bruce Margon. I especially want to thank him for providing me with a lengthy time period in which to concentrate on this research, free from the usual worries of financial support and duties (distractions) of being a graduate student and Research Associate. Throughout our association, he has played very well his many roles as employer, dissertation advisor, teacher, mentor, observing partner, and friend.

I would like also to thank the other members of the Ph. D. supervisory committee Drs. Paul Hodge, Karl-Heinz Bohm, Bruce Balick, and David Bodansky. In serving on my Reading Committee for the dissertation, Drs. Paul Hodge and Karl-Heinz Bohm (and Dr. Margon, of course) provided many useful comments on how to improve the dissertation. With very little advance notice, Dr. David Bodansky generously agreed to fill in for an absent member on the Supervisory committee.

I would like to thank Sandi Larsen for her enormous patience and skill at TEXing (turning VAX 1's and 0's into a printable document) the dissertation, for her friendship, and great brownies.

I obtained much of the optical data for this dissertation as a Visiting Student at Kitt Peak National Observatory (KPNO) and Cerro Tololo Inter-American Observatory (CTIO), National Optical Astronomy Observatories, operated by the Association of Universities for Research in Astronomy, Inc., under contract with the National Science Foundation. Further optical data were obtained as a Visiting Astronomer, Canada-France-Hawaii Telescope (CFHT), operated by the National Research Council of Canada, the Centre National de la Recherche Scientifique of

France and the University of Hawaii. I thank the various Time Allocation Committees at KPNO, CTIO, and CFHT for their generous allotments of telescope time. The staff at these observatories were especially helpful in introducing me to prime focus observing; in this regard Dr. Rene Racine, Bill Schoening, Hal Halbedel, and George Will were especially helpful. Thanks to Dr. Bruce Margon, Dr. Ronald Downes, and Heather Preston for assistance in acquiring some of the optical data. Further,I would like to thank Drs. Greg Bothun, Paula Szkody, and Bruce Balick, and Mike Bolte for generously donating some of their own valuable telescope time to carry out optical observations of some of the QSO candidates studied in this dissertation.

The Einstein staff at the Center for Astrophysics provided me with invaluable assistance in analyzing the X-ray data; special thanks in this regard go to Drs. Frederick Seward, Harvey Tananbaum, Daniel Harris, Frank Harnden. Throughout several extended visits to CfA, I was always made to feel welcome (and not in the way). Thanks to Drs. Isabella Gioia and Tommaso Maccacaro for several discussions on X-ray emission from QSOs, as well as advice on dealing with the Einstein computers. Drs. Tananbaum and Seward were instrumental in allowing me access to CfA X-ray data prior to its public release. Numerous Einstein Guest Observers also generously allowed me access to their data prior to its public release: Drs. Richard Kron, Dr. Paul Boynton, Dr. France Cordova, Dr. Anthony Tyson, Dr. Joseph Cassinelli, Dr. Peter Biermann, Dr. Jerimiah Ostriker, Dr. Blanco, Dr. Guido Chincarini. MIT and Columbia also granted access to their X-ray data. This work has been supported in part by NASA Grant NAG8-433.

I thank Drs. Eric Feigelson and Jurgen Schmitt for discussions on survival analysis.

I also gratefully acknowledge the financial support given me in completing this dissertation by the Achievement Rewards for College Scientists (ARCS) Foundation.

I am indebted to Drs. Bruce Margon, Paul Hodge, and Richard Kron for their assistance in helping me find (gainful?) employment subsequent to the completion of this dissertation.

The day to day life of being a graduate student was made enormously fun by the other graduate students (past and present), and I'm indebted to many of them for providing relaxing distractions at appropriate times. In general, it was their great senses of humor which made things most enjoyable. Special thanks to those at the University of Washington (alphabetical order): Bernard Bates, Don Boggs, Mike Bolte, Dr. Greg Bothun, Dr. Ron Canterna, Dr. Jason Cardelli, Dr. John Deeter, Erik Eason, Paul Eskridge, Dr. Douglas Geisler, Paul Green, Myung Gyoon Lee, Dr. Edward Olszewski, Mario Mateo, Heather Preston, J. P., Charles Proffitt, Simon Radford, Alex Raga, Judy Schultz (honorary Ph. D.), Dr. Evan Skillman, Dr. Verne Smith, Bill Spiesman, Light Sun, Dr. Nicholas Suntzeff (honorary U.W. graduate), Greg Taylor, Scott Temple, Schuyler Van Dyk, Maya Wheelock (honorary graduate student), Pat Whitehill-Bates, and the rest. Also thanks to those (past and present) graduate students at UCLA for introducing me to graduate student life: Dr. Robin Ciardullo, Dr. Ron Downes, Paul Edsel, Dr. Richard Nolthenius, Dr. Phillip Sakimoto, Dr. Allen Shafter, Steven Tomczyck, and Dr. Janet Weiland.

Finally, I would like to thank my family for their support: my parents Mary and Frederic Anderson, and my sister Sherri Guillot have provided the financial and emotional support required to undertake the lengthy study for a Ph. D. Most importantly I want to thank my wife Kathleen, who has been wonderfully under-

standing of my obsession with my work, and who has put up with my many days away from home. Throughout the worst of times, Kathleen has always given me the best of times.